

FMH606 Master's Thesis 2022

Process Technology

# **Performance evaluation of an LNG analyzer by mathematical modeling and experiments in a pilot rig**

Javad Tavakolifaradonbe

Faculty of Technology, Natural sciences and Maritime Sciences  
Campus Porsgrunn

**Course:** FMH606 Master's Thesis, 2022

**Title:** Performance evaluation of an LNG analyzer by mathematical modeling and experiments in a pilot rig

**Number of pages:** 99

**Keywords:** LNG sampler, thermodynamic modeling, Equation of State

**Student:** Javad Tavakolifaradonbe

**Supervisor:** Sumudu Karunaratne, Knut Vågsæther

**External partner:** Moreld Flux

**Summary:**

Moreld Flux is in process of designing and manufacturing a sampling instrument for collecting liquified natural gas (LNG) and sending the sample for further analysis. Therefore, this project is defined to perform a literature study on sampling techniques from process streams, evaluating different equations of states (EoS) and developing procedures to calculate the bubble points, and finally assemble a pilot rig and performed some experiments to validate the developed model on the vaporizer part of the sampling instrument.

In this regard, firstly a comprehensive definition of representative sampling and the condition and benefits of an acceptable representative sample is provided. In the following, an extended literature study is performed on the five most popular sampling techniques in industries, including grab sampling techniques, Adsorption Techniques, Cryogenic techniques, Trapping techniques, Dipping techniques, and tube sampling. For each technique advantages and disadvantages are investigated and examples of their applicability of them are also provided.

This study enlists the four most popular EoS, namely van der Waals, RK, SRK, and PR, and develops a thermodynamic model to calculate the compressibility factor ( $Z$ ) for pure components. Then, a scientifically defined open-source package in python (Phasepy) is applied to develop the models for calculating the phase equilibrium and bubble point of multicomponent mixtures. This study shows that Phasepy can be a reliable package for computing phase equilibria. For this purpose, four binary mixtures (Benzene + Cyclohexane, Benzene + Chlorobenzene, Cyclohexane + Chlorobenzene) and two four-components LNG mixtures are modeled using Phasepy. For comparing the modeling outputs and experimental results, average absolute relative deviation (AARD) and absolute maximum deviation (AMD) are calculated. AMD and AARD for all mixtures are always less than 0.05 (mole fraction) and 3% respectively.

In the case of experimenting, although the facilities have not been provided, based on the literature studied and some standards a sampling procedure for collecting accurate data is prepared. The under-study vaporizer should be equipped with three thermocouples and a Coriolis flow meter is to be used to measure temperatures and flow rate respectively. In this way, a LabVIEW program is provided for real-time measuring temperatures and flow rates using National Instrument modules, including NI 9207 and NI 9211. In addition, simulation on the vaporizer shows that for the flow rate of 2 kg/hr, the outlet temperature of fluid would not be more than 250 K for  $LN_2$ , whereas the Coriolis flowmeter can work in higher temperatures. Therefore, a post-heating part should also be added to the rig. Based on the immersed helically coiled tube into a bath, this study develops a model for calculating the required tube length based on heat exchanger inlet temperature, heat exchanger outlet temperature, bath temperature, tube dimensions, and physical properties of a fluid.

# Preface

This project report is submitted to the University of South-Eastern Norway (USN) for the fulfillment of the requirements for the Master thesis (FMH606). This project work has been carried out under the supervision of Associate Professor Sumudu Karunaratne, and Professor Knut Vågsæther.

The external partner of this project was Moreld Flux. We met online and had discussions about the project. I would like to acknowledge Moreld Flux for providing relevant figures of vaporizer configuration details, information on probe and vaporizer layout and continuation of the project

I am grateful to my supervisors Associate Professor Sumudu Karunaratne, and Professor Knut Vågsæther for their immense guidance, support, and motivation throughout the journey. Moreover, I am deeply indebted to their kindness for believing in me consistently.

Porsgrunn, 16.05.2022

Javad Tavakolifaradonbe

# Contents

<b>1</b>	<b>Introduction .....</b>	<b>9</b>
1.1	Aims and scopes .....	10
1.2	Chapters review .....	11
<b>2</b>	<b>Literature review .....</b>	<b>12</b>
2.1	Design of sampling system .....	12
2.2	Sampling techniques.....	14
2.2.1	<i>Grab sampling</i> .....	15
2.2.2	<i>Adsorption Techniques</i> .....	21
2.2.3	<i>Cryogenic techniques</i> .....	27
2.2.4	<i>Trapping techniques</i> .....	31
2.2.5	<i>Dipping techniques and tube sampling</i> .....	34
<b>3</b>	<b>Material and Methodology .....</b>	<b>36</b>
3.1	Generic Cubic equations of state.....	36
3.2	Mixing rules .....	39
3.3	Natural Gas .....	42
3.4	Sampling requirement .....	43
3.5	The key components of an LNG sampling system .....	44
3.5.1	<i>Sampling probe</i> .....	44
3.5.2	<i>Vaporizer and control devices</i> .....	44
3.5.3	<i>Sample holder and container</i> .....	45
3.6	Sampling condition.....	45
3.6.1	<i>Sampling flow</i> .....	45
3.6.2	<i>Inlet condition</i> .....	46
3.6.3	<i>Vaporization process</i> .....	47
3.7	Specification of the under-study LNG Sampling System .....	48
3.7.1	<i>Probe design operation</i> .....	49
3.7.2	<i>Vaporizer configuration</i> .....	50
3.7.3	<i>Post heating</i> .....	51
3.8	Experiment procedure.....	54
<b>4</b>	<b>Results and Discussion.....</b>	<b>58</b>
4.1	Modeling EoS to calculate fluid phase equilibrium.....	58
4.1.1	<i>Phasepy Package</i> .....	58
4.1.2	<i>SRK modeling</i> .....	70
4.2	LN <sub>2</sub> behavior throughout the Vaporizer.....	72
4.3	Post heating .....	77
4.4	Future Experimental necessity .....	78
<b>5</b>	<b>Conclusion .....</b>	<b>83</b>

# Nomenclature

$\alpha$	Thermal Diffusivity [m/s <sup>2</sup> ]
AARD	Average Absolute Relative Deviation
AMD	Absolute Maximum Deviation
$\beta$	Thermal Expansion Coefficient [1/K]
$\gamma$	Activity Coefficient
$\Phi$	Fugacity Coefficient
$C_s$	Concentration Of Adsorbed Compound [ng/g]
$c_p$	Specific heat [j/kg. K]
$C_w$	Compound Concentration in Flow Stream
$\delta$	Thickness Of Diffusion Boundary Layer
D	Diffusion Coefficient
DGT	Diffusive Gradient in Thin-film
EoS	Equation Of State
g	Gravitational Acceleration
GC	Gas Chromatography
h	Convection Coefficient
k	Thermal Conductivity
$K_p$	Sorption Coefficient [L/g]
LN <sub>2</sub>	Liquified Nitrogen
LNG	Liquified Natural Gas
MESCO	Membrane-Enclosed Sorptive Coating
MHV	Modified Huron-Vidal
$m_s$	Mass Of Adsorbent [g]
NRTL	Non-Random Two-Liquid Model
Nu	Nusselt Number
$\rho$	Density [kg/m <sup>3</sup> ]
P	Pressure
$P_c$	Critical Pressure
PID	Proportional Integral Derivative
POCIS	Polar Organic Chemical Integrative Sampler
Pr	Prandtl Number

PR	Peng-Robinson
$P_s$	Pressure At Standard Condition
P&ID	Pipe And Instrument Diagram
P-H	Pressure-Enthalpy
QA	Quality Assurance
QMR	Quadratic Mixing Rule
Ra	Rayleigh Number
Re	Reynolds Number
RK	Redlich And Kwong
$R_s$	Sampling Rate [L/day]
SGT	Square Gradient Theory
SPMD	Semi-Permeable Membrane Device
SRK	Soave/Redlich/Kwong
T	Temperature
$T_c$	Critical Temperature
$T_r$	Reduced Temperature
$T_s$	Temperature At Standard Condition
$T_{wi}$	Inside Wall Temperature
$T_\infty$	Surrounding Temperature [K]
$\mu$	Viscosity [N.s/m <sup>2</sup> ]
u	Velocity
UNIQUAC	Universal Quasi-Chemical
V	Molar Volume
$V_B$	Process Stream Velocity
vdW	Van Der Waals
$V_f$	Flask Volume
VLE	Vapor Liquid Equilibrium
$V_N$	Velocity In Sampling Nozzle
$V_r$	Volume of Absorbing Solution If Any
$V_s$	Volume of gas at STP
$\omega$	Acentric Factor
W	Sampling Mass Flow Rate [Kg/H]

WS	Wang And Sandler
$x_{fd,r}$	Thermally Fully Developed Internal Length
Z	Compressibility Factor
$Z_c$	Critical Compressibility Factor



# 1 Introduction

To run an operation efficiently, it is required to extract real-time data with representative sampling. Representative sampling is collecting a small amount of the mainstream precisely to identify the characteristics of a batch or process stream. In other words, to monitor the process and control the quality, both to optimize the process and ensure the properties meet commercially required specifications (value of transactions).

By considering the nature of sampled materials and operation conditions, different sampling techniques have been developed appropriate to the required uncertainties of the measurements.

Where a fluid is spatially homogeneous, it may be manually sampled in a tank or from a transfer pipeline. If there are temporal variations in-process quality, then it is more appropriate to sample the process in a flow proportional manner using either online analysis, continuous, or grab sampling techniques. In many cases, where there is a financial transaction related to the quality of transfer of a product, physical samples must be held in case of a dispute.

Grab sampling, adsorption techniques, cryogenic techniques, trapping techniques, and dipping techniques are known as the most popular sampling method and each of them has its advantages and limitations. The uncertainty of the measurement result will depend not only on a small part in recognizing the effect of homogeneity, and time-based changes in the properties being sampled but also on the sample extraction and processing, be this to provide a sample to an analyzer in the field or one in the laboratory. Where there are steps in the process requiring the participation of a human, these add further uncertainties.

By considering the required number of samples, location of samplers, homogeneity of the process, and all aforementioned variables, (including subsequent sample handling, retention, processing, and storage) a sampling technique is consistent when it can take a sample as the representative of the entire process.

## **Process sampling**

sampling should be representative to help engineers, planners, QA, and managers to make reliable decisions about the process. It should not be forgotten that significant commercial value is also associated with the transfer and trade of products both in profit and loss and taxation. Apart from reliability, safety, simplicity, and accuracy should also be considered when you are going to select a sampling technique. An appropriate sampling provides benefits for the process, including

- Provide reliable and accurate results
- Reduce waste and save money through process monitoring, yield improvement, and process optimization
- Ensure the correct payments and taxes are made in regard to the products bought and sold.
- Protect the environment and facilities
- Improve product quality
- Ensure regulatory compliance

## Thermodynamic modeling

To study phase equilibrium thermodynamic models are applied. Model classifications account for equations of state, activity coefficient, empirical, or special system-specific. However, all thermodynamic models are not applicable, and scientists decide to select the model based on the state of the process, information limitation, desired output, etc. Generally, thermodynamic models are developed to predict and understand the behavior of the system.

Because of accuracy, consistency, computational speed, robustness, and predictive ability, thermodynamic modeling based on EoS is more commonly used. However, in the case of calculating phase equilibrium, thermodynamic modeling based on EoS needs more consideration. Indeed, thermodynamics stability and physical reality should also be checked. Nevertheless, the variety of EoS is another challenge that needs to be dealt with. Generally, it is accepted that an EoS does not have ability enough to describe all types of fluids or components. Øivind Wilhelmsen et al. [1] in an extended study investigated the applicability and the consistency of different EoS in diverse cases.

### 1.1 Aims and scopes

Of all fossil fuels (when compared to coal, crude oils, etc.), natural gas is the cleanest and least environmentally damaging to transport or use for the generation of energy or many oil-based products (plastics). Unfortunately, it is impractical to pipe gas under large bodies of water, and to meet worldwide demands, efficient transportation on a global basis is required. Therefore, gas is processed to remove impurities, filtered, and compressed to a liquified state “Liquified Natural Gas” or LNG. LNG is the cryogenic variant of a lean natural gas, held and transported at near atmospheric pressure but temperatures of -160 C to maintain it in a liquid state.

Because of the change in pressure and temperature, the composition of LNG is continuously changing during carriers loading, unloading, and transporting. In addition, two effective parameters on the value of the shipment, namely density and calorific value of the transferred LNG, are calculated based on the average composition of the LNG. Then, an accurate operation for obtaining the composition of the LNG throughout the transportation is required [2].

Indeed, to understand the LNG composition, sampling techniques and analysis methods have taken more attention. In this way, firstly a representative LNG sample should be collected. Then, in following because of the multicomponent inherent of the LNG, the liquid sample should change to the gaseous state without partial vaporization and loss of component to remain still representative [2], [3].

Moreld Flux is developing improvements to the design of a system for sampling and analysis of the LNG. This project is to optimize the sampling system and obtain a representative LNG sample before sending it to a gas chromatography (GC) analyzer or to allow a manual sample or composite samples to be taken as representative of cargo transfers. The vaporizer part of the sampling system is modeled thermodynamically based on SRK EoS. Therefore, instrument performance and insulation requirements can be evaluated. Apart from thermodynamic and

mathematical modeling, some experiments are also to be performed in a pilot rig to compare experimental results and simulation outputs.

In addition, it is to study different sampling techniques from a process stream. The applicability and the limitations of these techniques need to be investigated. As another part of the project, the fundamental necessity for erecting the experimental rig is to be prepared. In this regard, the P&ID of the facility, a sampling procedure, and a measuring program should be provided. Finally, a thermodynamics-based model is to be developed to compare the different EoS in combination with different mixing rules for studying the multicomponent mixtures.

### **1.2 Chapters review**

This study is divided into four parts. In the literature study, the most popular sampling techniques from the process stream are described. The methodology chapter introduces a procedure for calculating phase equilibrium in multicomponent mixtures by applying Peng Robinson and SRK as EoS and quadratic mixing rule and Modified Huron-Vidal First Order mixing rule. The results and discussion chapter is split into two main parts. The first part tries to show the accuracy of the developed model to predict the phase equilibrium for multicomponent mixtures. And the second part describes how much the experimental results are closed to the outputs of the simulation of the vaporizer. Finally, conclusions are drawn in the last chapter.

## 2 Literature review

The gaseous and the liquid process streams are monitored continuously throughout the chemical processes, steam generation plants, refineries, etc. a disturbance in the composition or properties of streams may cause changing the rate of reaction, corrosion, and equipment decomposition, or even affecting on product quality. A poorly designed and operated sampling system prevents the plant from being evaluated in terms of thermodynamical properties and compositions. Then, inconsistent, and erroneous information and fluctuation in concentration unable plant personnel to predict the process chemistry excursion [4], [5].

To solve this problem and make an appropriate decision about the process, the designers need to know the chemical and physical properties of process streams and the compositions. Then, a consistence sampling is required. However, regarding the condition and situation, the sampling method and apparatus may be changed. This chapter is to define the industrial applicable sampling technique and perform a short literature review about what has been done.

### 2.1 Design of sampling system

A sampling conditioning system provides a sampled stream representative of the main process stream to either an analyzer or sampler and then the analysis is performed on the samples. Therefore, to obtain highly accurate results, the sampling system should be designed properly [5].

According to operation conditions, fluid properties, and analytical requirements, an appropriate sampling system can account for the diverse structures and different components. With all this, a well-designed sampling system is made up of:

- Isokinetic sampling nozzle<sup>1</sup>
- Isolation valve
- Sample tubing
- Primary sample cooler
- Secondary sample cooler (conditional, for high-temperature fluid samples)
- Pressure-reduction valves
- Thermal shut off valve
- Backpressure regulator

---

<sup>1</sup> “There is an interesting challenge in the whole concept of "Isokinetic" sampling. Where a product is homogeneous but close to a state where it will change from gas/liquid or vice versa any change in temperature or pressure is likely to cause mis-representativity! If the fluid is non-homogeneous, potentially the effect of non-isokinetic sampling may or may not be important depending on the level of dispersion and dispersion quality of the fluid at the sampling point, the side of the opening relative to the bulk flowrate etc.”, Mark Jiskoot.

- Drain or return

Maybe it can be said that, as the most critical component, the sampling nozzle plays the most significant role in a sampling system. It means this part of the sampling system should be selected and designed rather than other components. Operationally, a well-designed nozzle should be able to tolerate the temperature and pressure fluctuation and the forces caused by the induced vibration and flow. Typically, to reduce the flow effect throughout the sampling, nozzles are designed as a probe with a short-tapered tip or a short radius tube [5].

It was tried in the past to sample a process stream by extracting the fluid from several locations alongside the diameter of the pipeline simultaneously. However, these multi-port nozzles are not recommended because of non-isokinetically operation and vibration failure, even though non-isokinetically sampling can be an applicable operation for uniformly mixed fluids <sup>1</sup>.

Isokinetic sampling is used when extracting a representative sample is performed without affecting on chemical and physical characteristics of samples. Figure 2.1 shows how the isokinetic sampling should be. Indeed, the isokinetic sampling collects a portion of the process stream with the same composition and velocity as the mainstream. Consequently, the collected sample is more representative of the process stream [5].

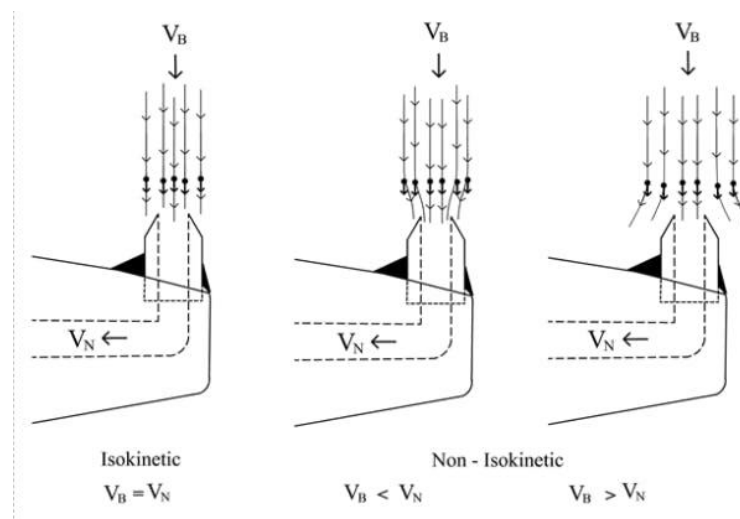


Figure 2.1: Schematic diagram of isokinetic and non-isokinetic sampling nozzle ( $V_B$  = process stream velocity,  $V_N$  = velocity in sampling nozzle) [5].

<sup>1</sup> “Multi-port sampling designs fail, not so much because of vibration or isokinetic issues, but more because the profile can change with process conditions (viscosity/density/comp and flowrates) but interestingly if you have multiple takeoffs, the flow through each takeoff needs to be lower than for one big one and therefore the isokinetic challenge for the individual takeoffs becomes worse!! We found that in water, in oil, etc. an opening in the range 3-6 mm required a lot more care than say a 32mm opening and over that size, isokinetic was not important!” Mark Jiskoot.

Approximately, all fluid leaves an amount of residue throughout the passage of the operational equipment. Consequently, the accuracy of the analysis will be under question. Electrostatic attraction, crystallization and solubility changes, gravitational settling, and hydrodynamic forces are the main mechanism of fluid deposition throughout the process equipment. Then, if the sample in the flowing part is not in equilibrium with the sample at the touched surface, the extracted sample is not representative of the main process stream. Although decreasing the sampler surface area and increasing the sampling velocity reduces the required time to reach equilibrium, it is recommended that the sampling should be a continuous operation [5].

## 2.2 Sampling techniques

“Sampling is the operation of removing a part (of convenient size) from the whole in such manner that the sample represents, within measurable limits of error, the proportion of the quantity on the whole” [4].

The most appropriate sampling method is opted based on the goal of sampling and the required performance of chemical analysis. Generally, the analytic methodologies are more rigorous than sampling procedures. Then the variability of the total result, including analysis error and sampling error, is considered to make an economic balance between sampling procedure and analytical methodologies. For this purpose, multidisciplinary knowledge of materials' nature and condition, analytical methodologies, and sampling tools is required. As it was said priorly, an appropriate sample represents the entire system. So that specialists can approve whether the process stream meets the specification or not [4].

One other important goal of sampling is to specify the unknown material. Although for this purpose sampling impose a cost on the process, and the accuracy cannot be warranted. Why so, the unknown material may not be able to persist in the sampling condition.

Considering that, the collected samples should be representative of the mainstream at the time of sampling, enough samples should be extracted. In addition, the sample must be analyzed subsequently after sampling as much as possible. It is because of some reasons:

- Preventing deposition of the sample into the walls of the container
- Preventing the probable leakage
- Preventing possible chemical reaction

Indeed, reducing the time interval preserves the sample from any possible changes from the original state. This chapter is to describe the sampling technique by considering process streams.

### 2.2.1 Grab sampling

Grab sampling is utilized when there is not any necessity for process monitoring and precise sampling. This method is appropriate for sampling the air, using inflatable plastic bags, evacuated bulbs, or hypodermic syringes. These tools can be applied in dried form or with an absorbing solution. For example, this technique is used to collect the halogenated hydrocarbon in the air.

Different investigations have studied the key factor for collecting a representative sample. The surface area of the bag, concentration, relative humidity, physical and chemical features of the bag, temperature, and existing reactive components in the sample are the significant factor for grab sampling. Grab sampling can be applied for gaseous and liquid streams.

In the case of the gaseous flow stream, there are two well-known samplings set up based on the principle of grab sampling, namely evacuated flask, and flexible bag. Figure 2.2 depicts the schematic of a simple evacuated flask. In this manner, an evacuated flask is connected to the process stream and the volume of the collected gaseous sample can be determined by measuring the pressure and the temperature. Equation (2.1) shows how to calculate the volume based on the ideal gas law.

$$V_s = (V_f - V_r) \left( \frac{T_s}{P_s} \right) \left( \frac{P_i}{T_i} \right) - \left( \frac{P_f}{T_f} \right) \quad (2.1)$$

- $V_s$  = volume of gas at STP
- $V_f$  = flask volume
- $V_r$  = volume of absorbing solution if any
- $T_s$  = Temperature at standard condition (273 K)
- $P_s$  = pressure at standard condition
- $P_i$  = initial pressure in the flask
- $P_f$  = final pressure in the flask
- $T_i$  = initial temperature in the flask (K)
- $T_f$  = final temperature in the flask (K)

Absorbent liquid can also be used in the case of analyzing specific gas. Indeed, the gaseous sample is dissolved into a liquid absorbent and then will be preserved for additional chemical analysis.

A flexible bag can also be used for the grab sampling technique, as it is shown in Figure 2.3. In this case, the created vacuum inside the rigid box causes the flexible bag to be inflated. In addition, a rigid box can also act as a protection for flexible bags during transportation. As an engineering modification, a flexible bag can be enclosed with water.

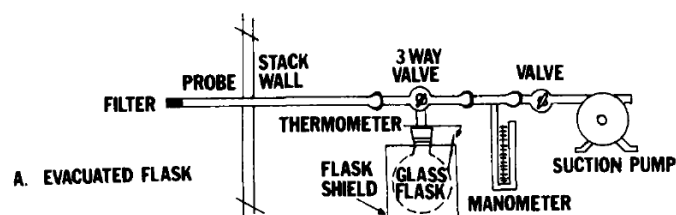


Figure 2.2: Schematic diagram grab sampling with evacuated flask [4].

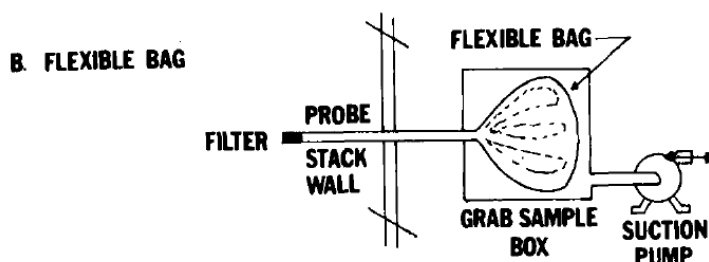


Figure 2.3: Schematic diagram grab sampling with flexible bag [4].

Gas displacement is another type of grab sampling for gaseous streams. The sampler can be made of metal or glass according to the needs. For example, in the case of corrosive gases, metal containers are not good choices, or ferrous containers have the potential to be consumed in the vicinity of oxygen. For gas displacement, Figure 2.4, it must be ensured that the original fluid of the container is replaced by the gas to be sampled. Therefore, an aspirating device should be employed, for example, a double-acting rubber bulb aspirator or a double-acting foot pump.

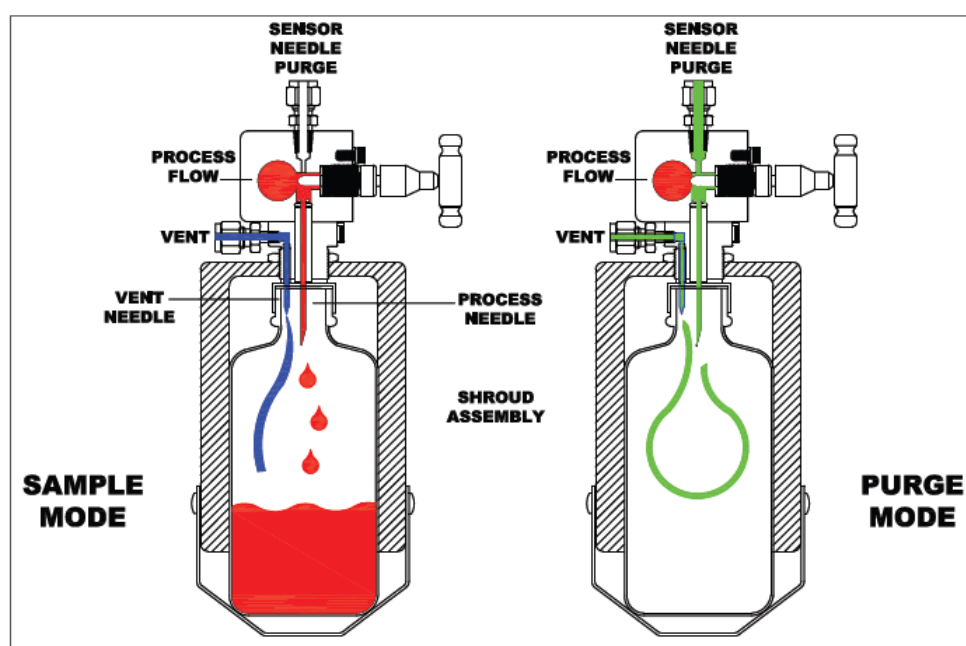


Figure 2.4: Purging and sampling process throughout a container [6].



Through the bubble-acting rubber bulb (as shown in Figure 2.5) rubber bulb removes the original gas from the sample container and admits the sample. This operation should be repeated several times to fill the container with the purposed gaseous sample. In addition, always before sampling, it should be tested that the container does not leak.

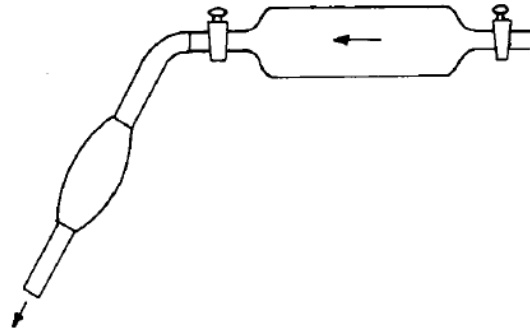


Figure 2.5: Bubble-acting rubber bulb [4].

When grab sampling is utilized for a liquid process stream, the point of sampling and the condition of liquid flow would be important. In this case, grab sampling is classified into three main groups, including composite sampling, continuous sampling, and stack sampling.

Composite sampling refers to when a set of individual grabbed samples are combined. This manner of sampling is not recommended for biological processes. Mainly composite sampling is used when an average value of process stream characteristics is required. Then, for the flow carrying unstable and volatile components, composite sampling is not suited.

Mainly, continuous sampling is applied for chemical, physical and radiological analysis. When it is required to collect a sample from different locations of a process stream, continuous sampling is performed and the taken samples are mixed before analysis. This technique is recommended when the process stream is inhomogeneous. Why throughout the inhomogeneous stream ununiform features distribution imposes some errors in analysis. Although continuous sampling outputs accurate analytical results, the complexity of the system and expensive facilities can be defined as the main drawbacks [4], [7].

Stack sampling usually is implemented to determine the effectiveness of collection equipment or when the quality of a source of material needs to be monitored. Generally, stack sampling is required when:

- To recognize the predominant source in a flowing stream

- To determine how much the regulations have complied
- To collect information for deciding on control equipment
- To evaluate the effectiveness of a control equipment
- To evaluate the results of a process optimization at modification
- To prepare appropriate evidence

This type of sampling is mainly applied for environmental pollutant measurement. And the concentration, the fluid flow rate, and the mass rate are the three most important parameters that need to be considered to prepare an acceptable sample [4], [7].

Grab sampling is being applied in the industrial process stream. Then the scientists are trying to provide a sophisticated procedure for accurate and efficient grab sampling. In addition, regarding the operational condition of the facilities, a safely grab sampling is another issue that has been investigated [4].

E. W. McAllister in the Pipeline rules of thumb handbook [7] describes that grab samplers are utilized to provide a representative of a stream. So that, a small volume from the process stream within a time interval is taken regularly. This book believes a process stream is represented if the sample accounts for 10000 grabs with a volume of 1 cc, though the frequency of sampling should also be considered. He suggests that frequency can be set by using the flowmeters' signals. And by considering the features of the process, the main flow stream or a by-pass loop can be selected for installing the container. More importantly, this book recommends utilizing supplementary devices like jet mixture, pump, etc. to provide a homogenous sample stream and improve the accuracy and the performance. Continuous monitoring is also described shortly in the Pipeline rules of thumb handbook, using a fast loop sampling system shown in Figure 2.6.

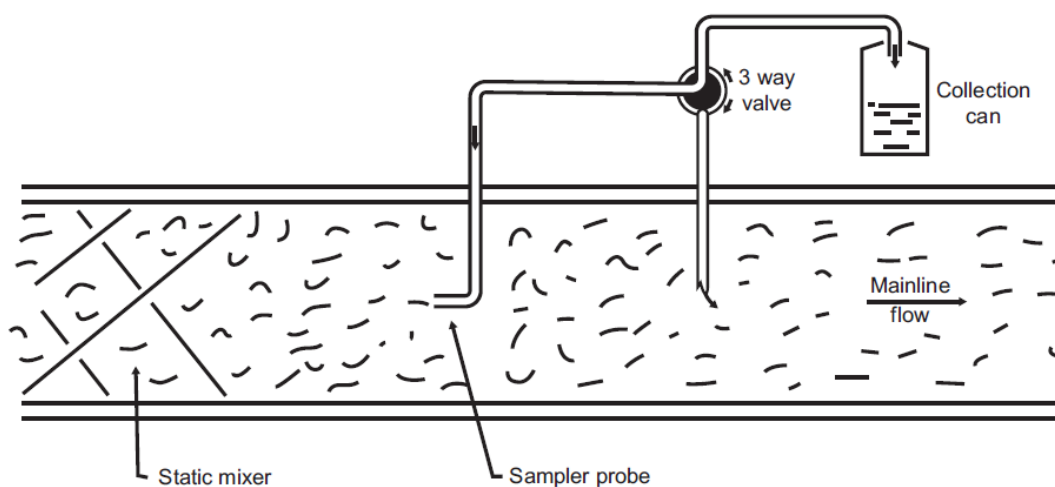


Figure 2.6: Fast loop pipeline sampling system [7].

It is the main advantage of the fast loop sampler that the sample characteristics are less affected by perturbation of the main process stream and the sample is being extracted continuously. Fast loop sampling can be achieved using a pump Figure 2.7, or a control valve Figure 2.8. However different companies are working to design the best layout for their grab sampling apparatus.

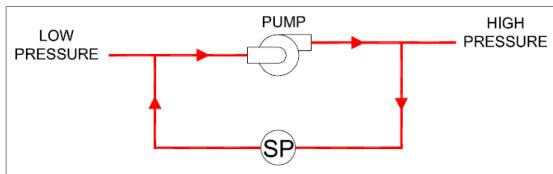


Figure 2.7: Fast loop sampling using a pump [6].

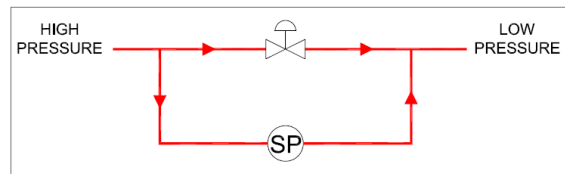


Figure 2.8: Fast loop sampling using a control valve [6].

Sensor Engineering company has classified closed-loop grab sampling system based on the vapor pressure of the fluid flow and line pressure [6].

**Fluid with a vapor pressure less than 19 psi and line pressure less than 175 psi:** this layout accounts for the needle system, sample valve, and cap for ventilation. Mainly Sensor recommends this system for process with temperature and pressure of 350 °F and 175 psi respectively. A nitrogen purging system with a pressure of 3-5 psi is also provided for fleeing from straw effects (Figure 2.9).

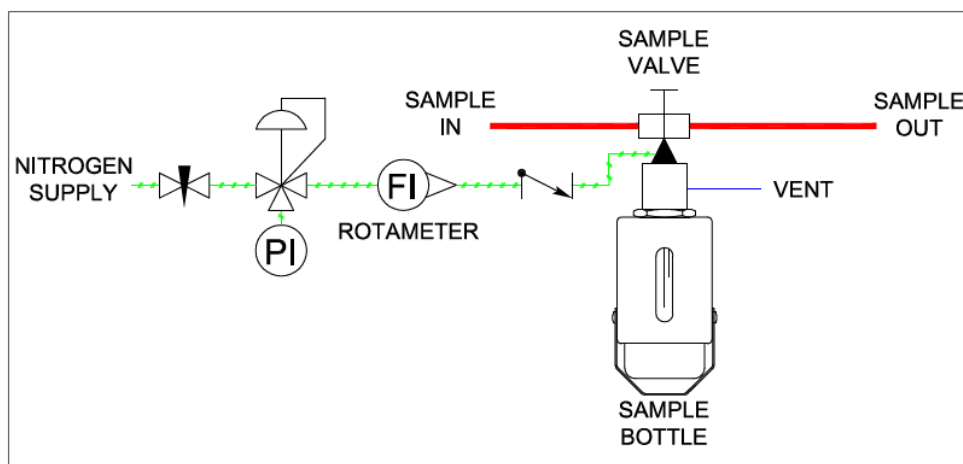


Figure 2.9: Sampling system for Fluid with a vapor pressure less than 19 psi and line pressure less than 175 psi [6].

**Fluid with a vapor pressure of less than 19 psi and line pressure of more than 175 psi:** This layout provides a safer sampling system. Indeed, with increasing the line pressure, the risk of potential danger is raised especially in case of a hazardous flowing flow. To reduce the risk of the high-pressure condition, this system firstly traps a fixed volume sample of the main process into a vessel. Then, the sample is blown into the main container (Figure 2.10).

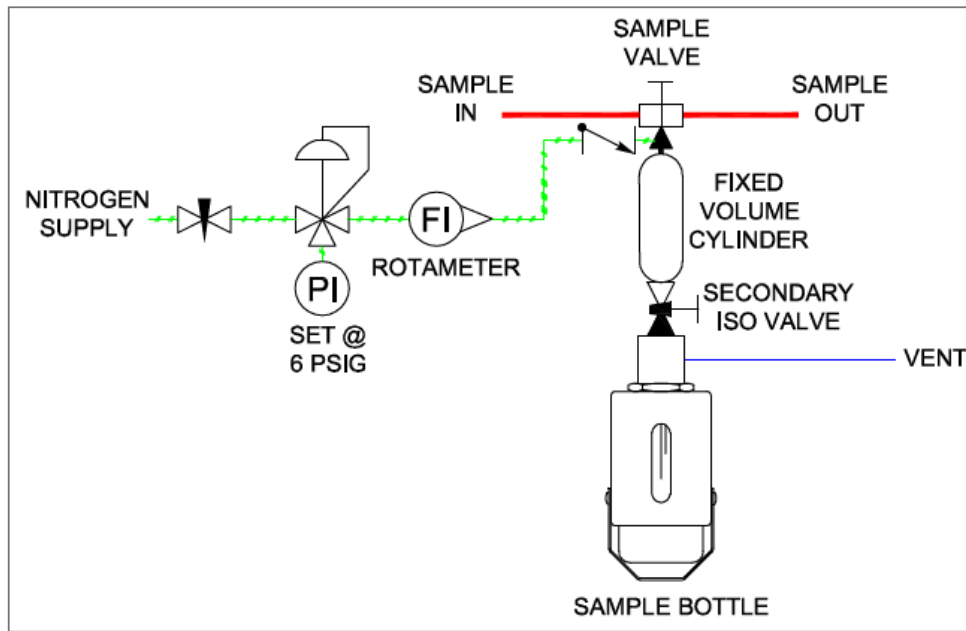


Figure 2.10: Sampling system for Fluid with a vapor pressure of less than 19 psi and line pressure of more than 175 psi [6].

**Fluid with vapor pressure more than 19 psi:** typically to maintain the operation condition, the fluid with high vapor pressure is trapped in the cylinders with 20% space. Then, in the vicinity of heat, the sample expands, and ventilation flares are also considered. However, for multicomponent mixture a vapor recovery system is taken into account, why in this situation the vaporization of some components might be more substantial than others (Figure 2.11).

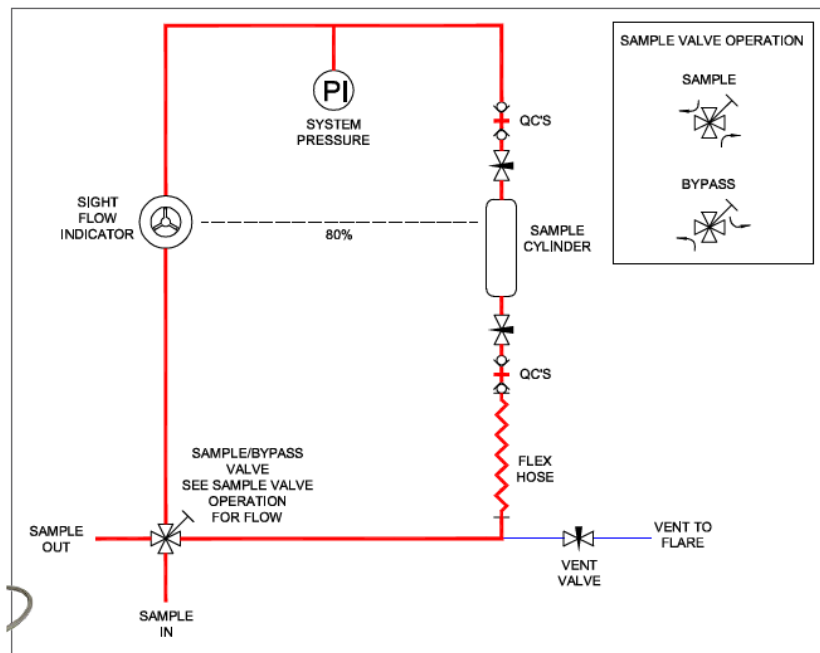


Figure 2.11: Sampling system for Fluid with a vapor pressure of more than 19 psi [6].

Some scientific studies gave to evaluate the performance of the grab sampling technique or provide information about its applicability. Sharvari et al. recommended grab sampling for collecting industrial emitted or generated gas throughout the different operational conditions. They also studied the consistency of the material of storage [8].

Another study compared the grab sampling and passive sampling methods regarding their ability in detecting anticancer drugs in wastewater effluent. Their results showed, that although grab sampling was not managed to detect all 6-target pollutants, this technique is more able to tolerate the fluctuation of water flow [9].

Marion Bernard et al. performed a scientific longtime investigation. They combined grab sampling and Polar Organic Chemical Integrative Sampler (POCIS) to evaluate pesticide pollution in the large-scale watershed. Finally, they concluded that, because of the tolerability of the grab sampling, a combination of POCIS and grab sampling provides better results in comparison with using them individually [10].

### 2.2.2 Adsorption Techniques

The industries utilize adsorbents to separate a part of streams. However, a selective adsorbent to isolate a specific part of the process flow stream has not been developed yet commercially. Then, laboratories may face some difficulties throughout the chemical analysis. Efficiency and price are two important factors that should be taken into account to choosing a decent industrial adsorbent. These days activated carbon, alumina, silica, elites, porous polymers, ion-exchange resins, charcoal, etc. are more commonly used industrial adsorbents. The sample is passed over the adsorbent. In the following, the trapped material will be removed by increasing the temperature or using a consistent solvent for analysis.

As for drawbacks, the adsorbents may be inactivated in the vicinity of moisture. In addition, sometimes isomerization of adsorbent or reaction at a higher temperature may alter the nature of the samples.

Typically, gases are more willing to seat on the surface of solid materials at a lower temperature. While the surface of the solids is defined into two parts interior surface and exterior surface. By performing some modification on the solid materials, namely activation processes, the active surface of solid material can be raised. To select an efficient adsorbent for sampling throughout a process stream, the surface area of the adsorbent and the selectivity of the adsorbent into polar or non-polar materials should be considered. Moreover, the feasibility of retention processes for recovering the samples shall also be evaluated. In this way, many studies have tried to clarify the suitability of the adsorbents for different materials. For example, activated carbon is recommended for organic gases and vapor, and multicomponent extraction or silica gel is a more appropriate adsorbent in case of selectivity. In some other studies, scientists have developed some processes for efficient and selective sample desorption.

Regarding activated carbon adsorbents, there are some general schemes e.g.

1. Gases with boiling and critical temperature less than  $-150\text{ }^{\circ}\text{C}$  and  $-50\text{ }^{\circ}\text{C}$  respectively, hardly can be adsorbed at ordinary temperatures.
2. Gases and vapors with boiling temperatures between  $-100\text{ }^{\circ}\text{C}$  and  $0^{\circ}\text{C}$  and critical temperatures from  $0^{\circ}\text{C}$  to  $120\text{ }^{\circ}\text{C}$  mildly can be adsorbed at ambient temperatures.

Heavier gases and vapors with boiling temperatures more than  $0^{\circ}\text{C}$  can easily be adsorbed or recovered at ambient temperatures.

Regarding retaining the trapped sample from the adsorbent bed, the industries need to develop a decent process. Although adsorption has been known as an inexpensive and simple way of sampling, the following retaining processes make it more complicated. Hydrolysis, isomerization, and even chemical changes are included among the difficulties throughout the recovery processes.

It is worth saying that adsorption sampling techniques are more desirable for gases rather than liquids. In limited cases, the liquid flow stream can be sampled by the adsorption technique directly or indirectly. For the direct approach, the fluid flow is passed throughout an adsorbent bed and the indirect approach refers to the separation of the component of interest firstly using a stripper and then collecting the gas stream will be passed throughout an adsorbent bed.

### **Chemical reaction techniques**

A sampling technique based on chemical reaction is recommended when the desired component cannot be detected readily using chromatographic methods. Then a spectroscopic method should be considered as the final step of the Sampling technique based on the chemical reaction. For example, Kitagawa gas detector tubes, the Dräger analyzer tubes, the Gastec detector Tubes, etc. are among the well-known Sampling technique based on the chemical reaction.

By leading gas to the reaction with a liquid chemically, adsorption efficiency can be increased in comparison with purely physical adsorption. In addition, applying a chemical reaction before adsorption results in easily retaining. For example, sampling from an ethylene stream is performed throughout an adsorption process using charcoal, while adsorbed ethylene cannot be recovered easily. As a solution, by impregnating the ethylene with bromide, retaining the ethylene dibromide will be more easily. On the other hand, the surface of the adsorbent can be modified by a chemical reaction. For instance, hydrogen sulfide has more tendency to be adsorbed on the surface of impregnated charcoal with lead acetate. With all this, the chemical modification may force the industries to employ ion-exchange chromatography instead of gas chromatography.

The adsorption sampling technique mainly is used for fluid flow streams. In this way, there have been a lot of efforts to classify adsorbents based on the nature of the fluid flow. In addition, many scientists are trying to study the effect of operational conditions on adsorption and also modify the adsorption sampling technique to selective adsorbing. Additionally, when the adsorbed or absorbed sample is collected, modifications are arisen to prepare the sample for further analysis. To do that, knowing the mechanism of adsorption-based sampling is crucial.

Based on a publication by Alvarez et al. adsorption-based sampling is divided into three steps, namely linear, curvilinear, and equilibrium partitioning, as shown in Figure 2.12. In the first step, it is supposed that the adsorbent is an infinite sink. In addition, accumulation is performed by fulfilling the first-order one-component model including the kinetics between adsorbent and flow stream (Equation (2.2)) [11].

$$C_s = K_p C_w \left[ 1 - \exp\left(-\frac{R_s t}{m_s K_p}\right) \right] \quad (2.2)$$

- $C_s$  = concentration of adsorbed compound [ng/g]
- $K_p$  = sorption coefficient [L/g]
- $C_w$  = compound concentration in flow stream [ng/L]
- $R_s$  = sampling rate [L/day]
- $t$  = time [day]
- $m_s$  = mass of adsorbent [g]

There are different methodologies to calculate the rate of adsorption. Calibration of the adsorbent is the most reliable approach [12].

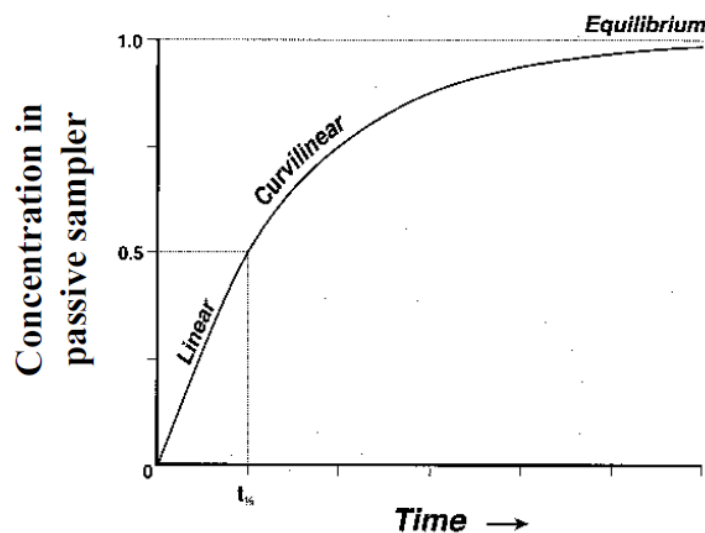


Figure 2.12: Three steps for passive sampling, linear, curvilinear, and equilibrium partitioning, based on first-order kinetics for accumulation [11].

For process streams with organic or inorganic components, adsorption-based sampling can be efficient. For inorganic flow streams, Diffusive Gradient in Thin-film (DGT) or Chemcatcher has been developed [13]. However, for organic compounds, more passive sampling is commercialized, including POCIS (Polar Organic Chemical Integrative Sampler), SPMD (Semi-Permeable Membrane Device), and MESCO (Membrane-Enclosed Sorptive Coating) [13], [14].

Cai et al. [15] studied the Diffusive Gradient in Thin-film intensively. Figure 2.13 presents the proposed mechanism for DGT by the authors.

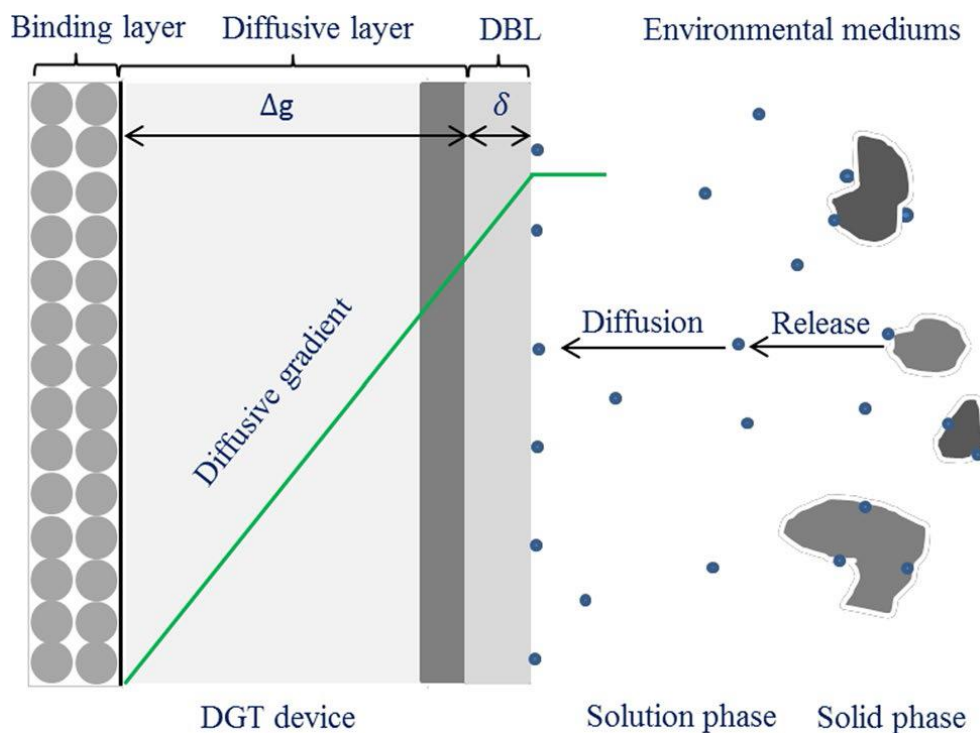


Figure 2.13: Proposed mechanism for DGT by Cai et al. [15].

Typically, DGT possesses a binding and a diffusive layer. A gradient of concentration exists inside the diffusive layer, because of the movement of the targeted compounds throughout this layer. Then the Fick's first law, Equation (2.3) can justify the diffusion during the development:

$$C_{DGT} = \frac{M(\Delta g + \delta)}{DA t} \quad (2.3)$$

- $C_{DGT}$  = average concentration
- $\Delta g$  = thickness of diffusion layer
- $A$  = exposed surface
- $D$  = diffusion coefficient
- $\delta$  = thickness of diffusion boundary layer
- $t$  = development time



Cai et al. also studied the different configurations for DGTs. The piston-type DGTs consist of two parts generally, a DGT piston and a DGT cap (Figures 2.14 and 2.15). DGT accounts for the binding gel, diffusive gel, and filter membrane, and the DGT cap is used to fix the compartments of the DGT piston. Indeed, throughout the sampling filter membrane is exposed to the stream. In addition, for selective adsorption sampling, this study investigated the binding agents applicable in the DGT sampler.

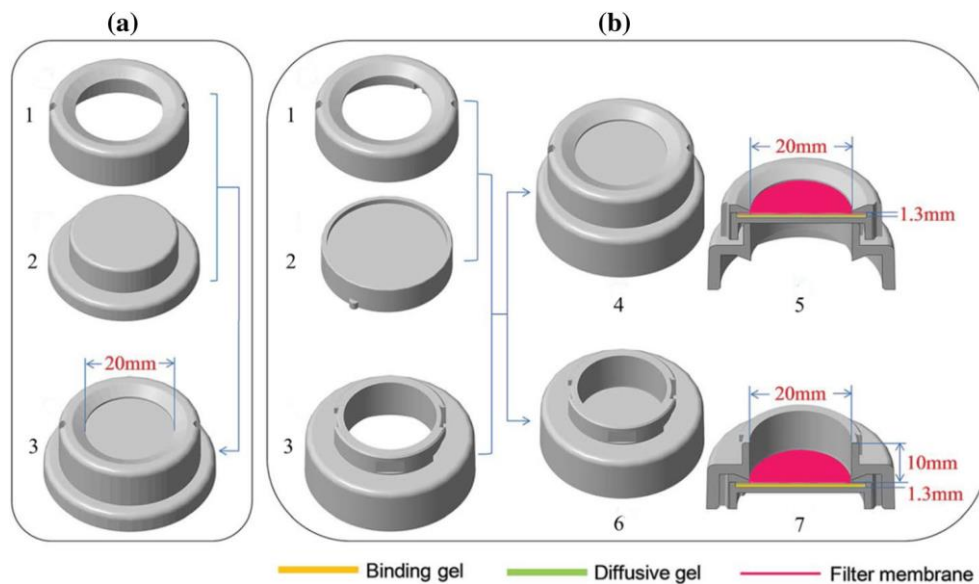


Figure: 2.14: DGT structure, a) dual-mode DGT. b1) Cap, b2) Recessed base, b3) Hollow base. b4 and 6) assembled type, b5 and 7) sectional drawing [15].

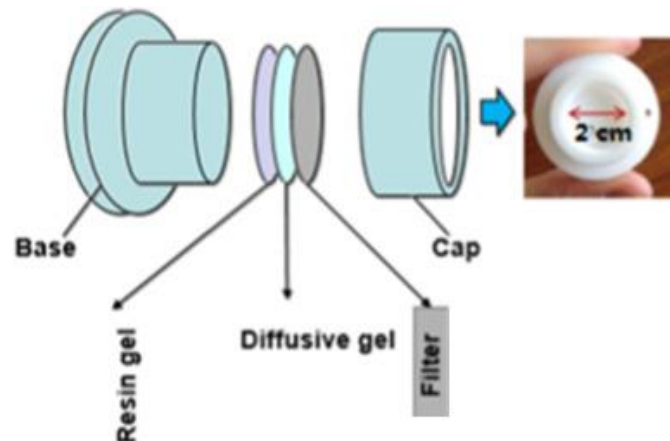


Figure 2.15: Different parts of the DGT sampler separately [16].

POCIS samplers are also studied extensively [17]–[19]. Klaudia Godlewska et al. [20] excused different articles about POCIS configurations and chemical reactions. As a typical structure, the authors presented Figure 2.16 for POCIS samplers, including three parts, sorbent, polyethersulfone membranes, and two stainless steel rings. polyethersulfone is indeed a semi-

porous membrane and is located between the sorbent and the stream. In addition, the porous feature of this membrane deters the sampling from the accumulation of solid particles [19].

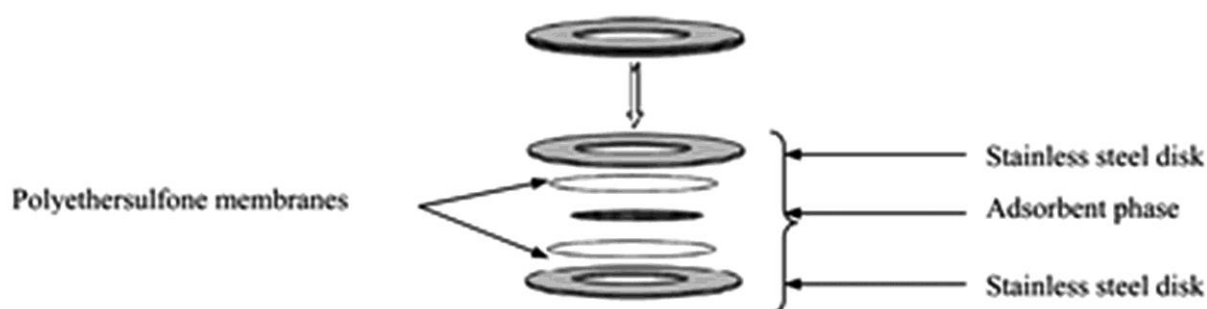


Figure 2.16: Schematic Diagram describing different parts of POCIS [20].

Apart from the mechanism and important parameters during the adsorption-based sampling, the layout of the sampler is also investigated by scientists. Adeline Charriau et al. [13] investigated 4 different exposing systems as it is shown in Figure 2.17. Based on their well-performed study, flow on exposure layout is the most commonly used Chemcatcher, and the artificial stream is mainly developed to study the influence of biofouling on sampling rate. In addition, this paper provided some information about the required time for catching equilibrium in the different exposing systems and talked about calibration methodology based on the type of adsorption-based sampler.

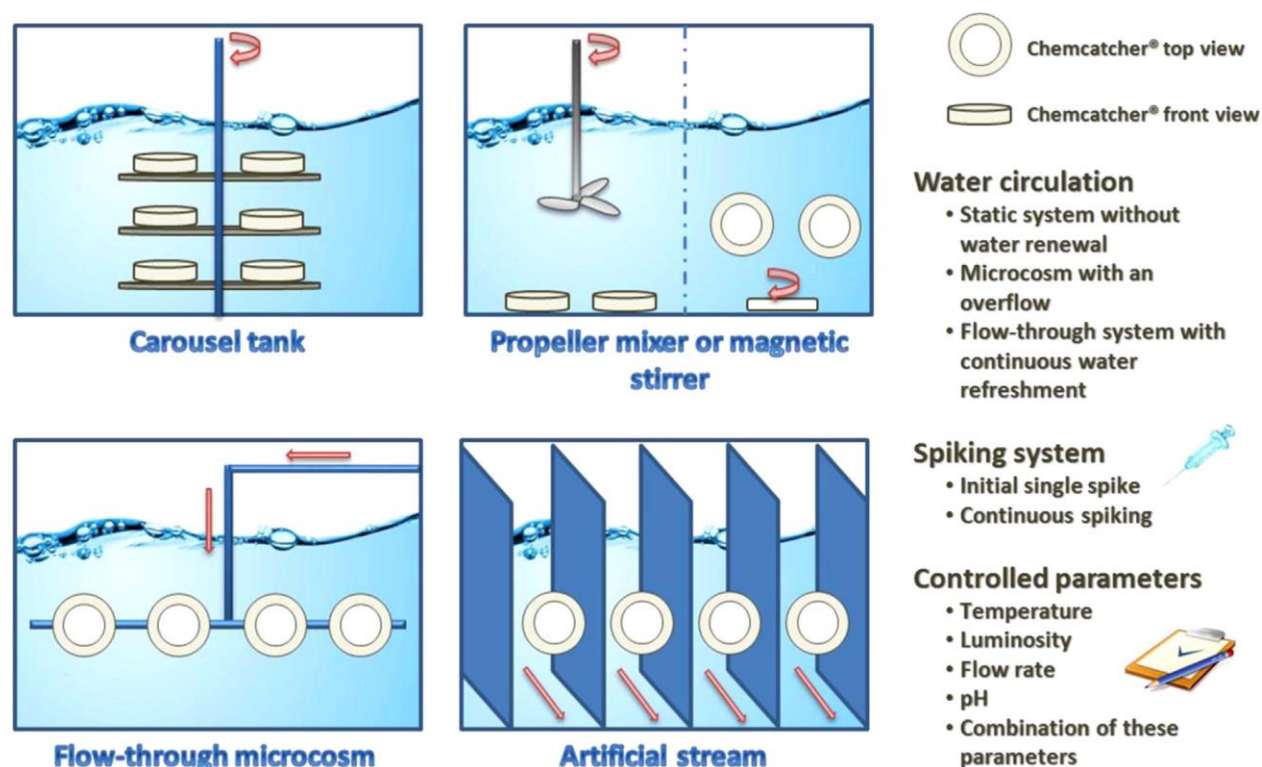


Figure 2.17: Exposure layout by Adeline Charriau et al. [13].

### 2.2.3 Cryogenic techniques

From the process point of view, condensation gases and vapors at low temperatures are more advantageous techniques rather than other concentration techniques. Indeed, the collected sample does not need additional processes for retention and is immediately available for analysis. In addition, sampled gases and vapors can be preserved more reliably. However, forming condensation mist can be considered the most significant drawback for cryogenic processes. These formed aerosols have so that quantity to reduce the efficiency of collection equipment, though equipping the cold trap with a simple filter like a glass wool plug can deal with such losses. Now the efficiency is acceptable to the extent that, accumulated aerosols increase the resistance of the equipment to flow.

Refrigerants are in priority if those materials can hold a constant temperature during a phase change (Table 2.1). Slushes can also be used as a refrigerant for intermediate temperatures (Table 2.2). Stirring liquid nitrogen with a solvent in a Dewar flask converts the system into slush. However, for low sampling rates, liquid nitrogen may trap unwanted components and then make the samples less stable. To solve this problem, a series of trapping with decreasing temperature progressively is recommended. Then sampling is completed, if the last step is empty. With all this, cryogenic sampling should follow a specific procedure based on the purposed sample.

Table 2.1: More common refrigerants [4].

Refrigerants	Temperature (°C)
$N_2(\text{liquid}) \rightleftharpoons N_2(\text{gas})$	-195.5
$O_2(\text{liquid}) \rightleftharpoons O_2(\text{gas})$	-183
$\text{Air}(\text{liquid}) \rightleftharpoons \text{Air}(\text{gas})$	-147
$CS_2(\text{solid}) \rightleftharpoons CS_2(\text{liquid})$	-118.5
$CO_2(\text{liquid}) \rightleftharpoons CO_2(\text{gas})$	-78.5
$NH_3(\text{liquid}) \rightleftharpoons NH_3(\text{gas})$	-33.4
Ice water-salt	-16
$H_2O(\text{solid}) \rightleftharpoons H_2O(\text{liquid})$	0

Cryogenic sampling is limited to collecting samples with low partial pressure. Therefore, the scientists prefer this technique to sample high volatile components from the pressurized systems. In this way, sampling is performed with a needle valve and then transferred into an evacuated methanol-carbon dioxide container for condensation. In the following, thermal equilibrium will be achieved by relieving the vacuum.

Table 2.2: Cold bath slushes [4].

Refrigerants	Temperature (°C)
Carbon tetrachloride slush	-23
Chlorobenzene slush	-45

Chloroform slush	-64
Ethyl acetate slush	-84
Toluene slush	-95
Methylcyclohexane slush	-126
n-Pentane slush	-130
Isopentane slush	-160

To perceive the constraints of the cryogenic sampling system, it is required to discuss thermodynamics fundamentals. In this way, the temperature-entropy diagram of cryogenic fluid should be studied like in Figure 2.18. Indeed, the T-S diagram provides information about transferred heat within the phase changing. Cryogenic point is shown with point C. line DE depicts a binary phase (Liquid-gas) with constant pressure and temperature, while E point is for the saturated liquid and D presents the saturated vapor. The required energy to move from E to D is equal to heat vaporization for fluid. By going from E to F, vapor pressure decreases, and eventually, a solid phase appears. At point F three phases of gas, liquid, and solid are in equilibrium and the system is in triple point thermodynamically. Now if the system is to go to a cryogenic state, the system should be located under point F. It means, the required heat to cryogen a gaseous system is as much as moving from the H point to the G point [21].

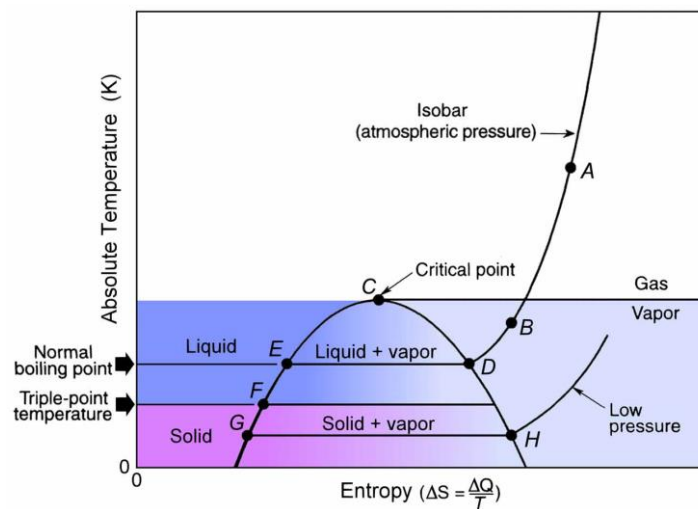


Figure 2.18: T-S diagram for a cryogenic fluid [21].

Additionally, the boiling point of refrigerants at the operational pressure and temperature need also to be considered.

A cryogenic sampler as shown in Figure 2.19 mainly is made of an insulated stainless-steel container with a narrow neck. While a sample is taken, the sampler is immersed completely into a refrigerant at a specified temperature. While the collected sample is liquified, because of reducing the volume a negative pressure gradient is produced between the process stream and

inside the sampler. Therefore, an inherent flow is established from the mainstream to the container throughout the orifice as long as there is a negative pressure gradient [22].

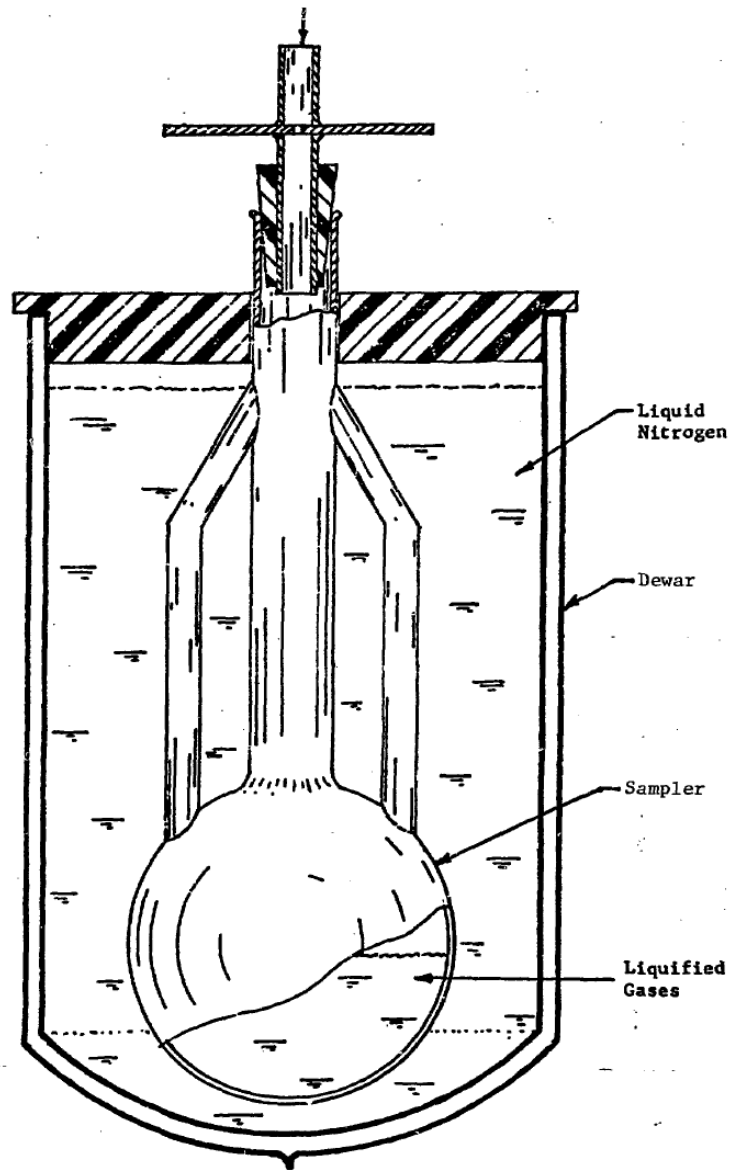


Figure 2.19: Schematic of cryogenic sampler during sampling [22].

Two main cons of cryogenic sampling are that firstly cryogenic sampling is a time-consuming process. Moreover, for multi-component mixture with a wide range of critical temperatures, sampling performance may be affected, though cryogenic inherently is a cleaner technology [21], [22].

Mainly the scientists try to develop a new method or a new device for cryogenic gas sampling. Throughout United State Patent No: US3123982A, Ross M. et al. [23] claimed that:

*'As an illustration of the utility of our invention, the greatly increased use of cryogenic fluids for military purposes has created the requirement for control of the purity of these fluids. The principal problem in obtaining satisfactory control has been the lack of a suitable method and device for obtaining and analyzing the fluids without significant alteration of the impurity level, or the introduction of new impurities into the samples taken'* [23]

In following their invented method and device remove the boiling off of gas from the final sample substantially after collecting a sample. The described device is shown in Figure 2.20. Ref [23] describes all parts of this device separately.

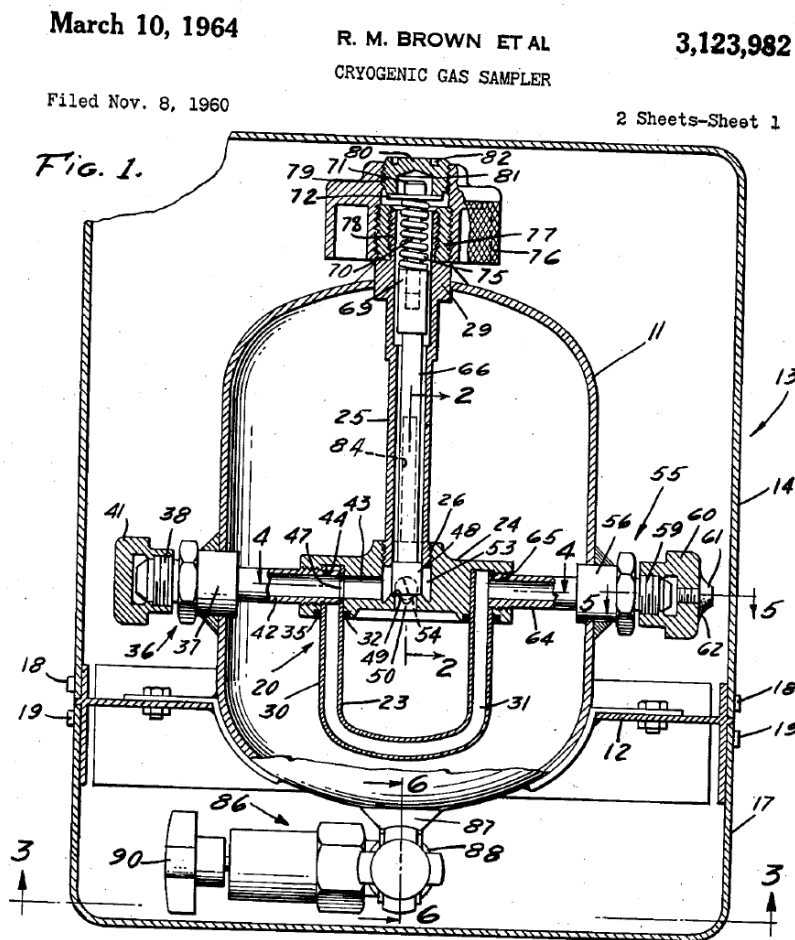


Figure 2.20: schematic diagram of cryogenic gas sampler United State Patent No: US3123982A [23].

In a similar patent, Pellerin et al. [24] developed a device for cryogenic liquid sampling as shown in Figure 2.21. They tried to improve the purity of the collected sample. Indeed,

*'A particular difficulty arises in obtaining a gas sample, which has the same molar concentration of trace contaminants as the cryogenic liquid being sampled'* [24].

By setting a new arrangement and optimizing the operational condition the authors solved the mentioned problem as it is described in ref [24].

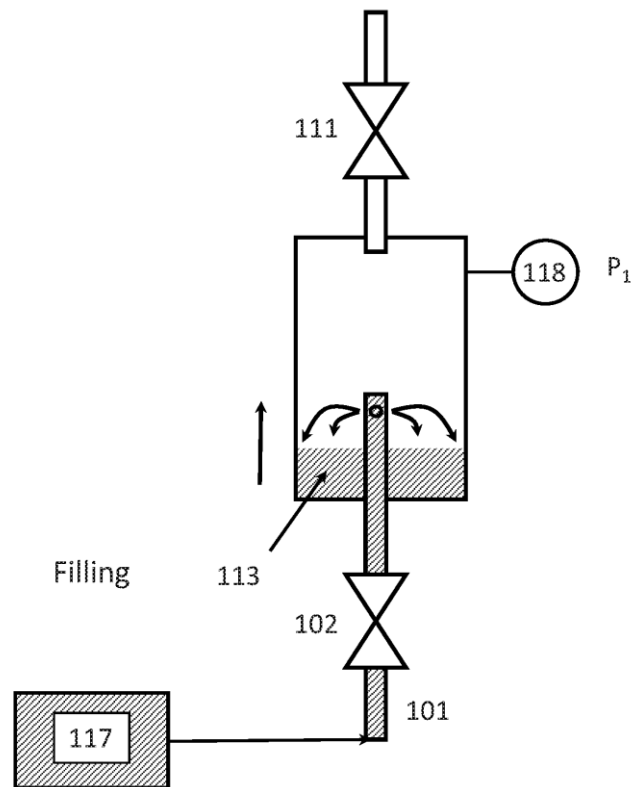


Figure 2.21: Schematic diagram of a cryogenic liquid sampler with Pellerin et al. [24].

#### 2.2.4 Trapping techniques

A set of bubble traps accompanied by fritted disk, bubbler, or diffuser are the main components of a sampling system based on the trapping technique. An external drive force like pumping is required to operate the system and move the samples through the trap. In addition, based on the sampling system requirements, the uniform performance and the capacity of gas pumps can be varied. Although mechanical pumps are desired for longtime sampling operation, induction motors are recommended because these motors perform uniformly even if the line load varied.

Hand pumps can be utilized when the required volume is small and there are not any limitations on variation gas flow. While process streams are supplied adequately in constant pressure, an aspirator can be applied. While aspirators or pumps are pulling the samples and compensating for the downstream reduced pressure, it is better to also predict a flow meter (either rate or volume meters). However, siphons should be used with a bit amount of sampling or low

sampling rates (supplement: to keep the flow uniform while the liquid level is falling, it is better to extend the inlet tube of the siphon to the bottom).

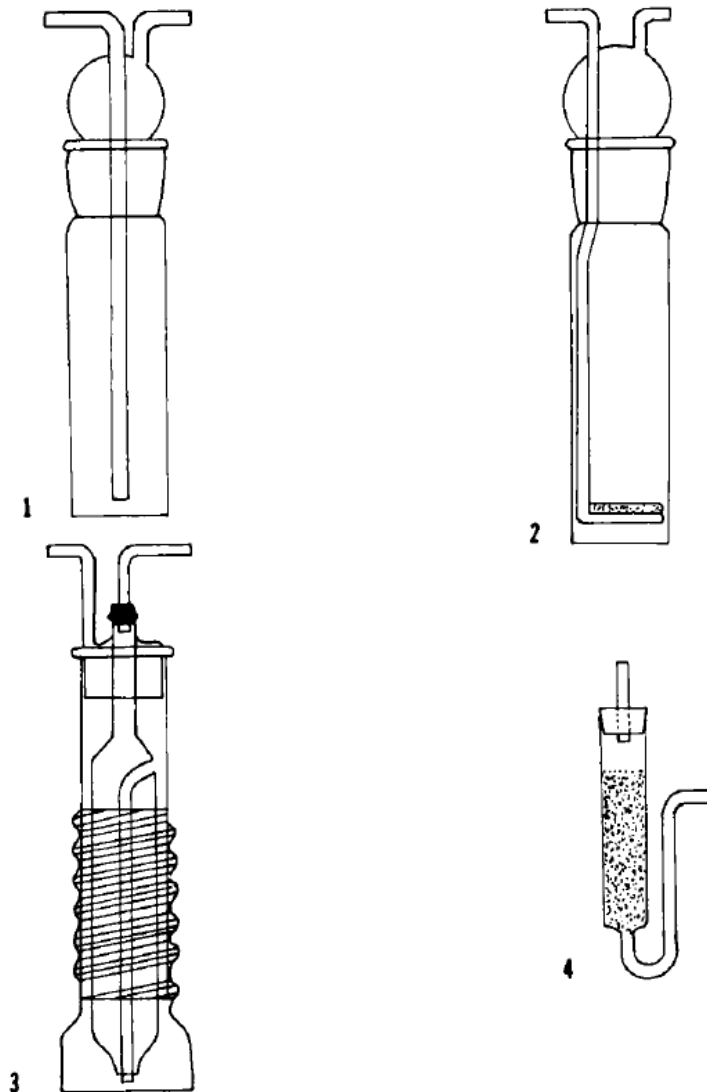


Figure 2.22: Different types of trapping absorbers. 1) simple bubbler, 2) diffuser, 3) spiral type, 4) packed bed tower [4].

Trapping absorbers (Figure 2.22) are mainly classified into four groups:

- (1) Simple absorber: with a capacity of 5 – 100 ml can sample the process stream with a volume rate of 2-3000 ml/min. They are designed simply, and while there is not any plugging, a short time contact occurs within the sampling.
- (2) Diffuser: with an absorbent capacity of 1-100 ml, can collect the sample at a rate of 500-10000 ml/min. although diffuser bubblers need to be plugged in, they are easy to use and provide appropriate gas-liquid time contact.



- (3) Spiral absorber: with a capacity of 10-100 ml and a capacity flow rate of 40-500 ml/min they do not have enough efficiency for low flow rate sampling.
- (4) Packed-bed tower: with an absorbent capacity of 5-50 ml and sampling capacity of 500-2000 ml/min. these absorbers are desired for low flow rate sampling, though the sampling rate may be varied with resistance.

Sometimes it is better to lengthen the tube connection between the sampler and flow streams. The tubing also needs to satisfy some specifications. Firstly, the tube should be as much as thick to not impose extra resistance on the flow stream. In addition, the connection tube should tolerate operational conditions like temperature. The tube should also be inert in front of sample components. Because of that, a specified kind of material is not always usable.

From a layout point of view, the samplers should be arranged in series and flow meters are followed by pressure gauges. This arrangement gives a chance to correct the flow condition immediately for acceptable accuracy. Measuring the pressure also notifies the sampling system in case of increasing flow resistance in the absorber. In most cases, because of the type of process stream, equipping the absorber with filters is required. The filters also need to observe a set of minimum requirements.

Many studies have tried to work on the applicability of the filters. Ahead of the sampler should be equipped with filters. The filters need to be nonreactive and nonabsorbing. Mainly, dry fibrous glass, cellulose paper, and porous plastic fulfill the requirements. However cellulose paper and siliceous material must not be applied to a stream containing hydrogen fluoride, and nonreactive plastics are recommended in this case. indeed, because of the destructive effect of particulate material on chemical analysis, the technology of filters has been developed.

There are so many studies that have tried to improve equipment for trap-based preconcentration or applicability of this technique for different compounds [25]–[29]. In a well-performed study, Hongwan Li et al. [30] used a Needle trap valve for sampling semivolatile organic compounds. Through this study, sorbent was packed in the valve for sampling from a pump. In addition, the authors try to evaluate the effect of some operational conditions like humidity and temperature on the performance of the methodology. Figure 2.23 depicts the schematic configuration of the utilized device. All the configuration of the valve is described in this study, and they applied helium for desorbing and moving the collected sample into GC for further analysis. By describing the operational condition, before, during, and after sampling, the authors investigated the repeatability, sensitivity analysis, and reproducibility of the method. The results showed that increasing the sampling temperature and volume increases the performance of the operation. However, humidity does not influence eye-catching. Finally, Hongwan Li et al. recommended the Needle trap valve for sampling SVOCs (Fig. 2.22) because of its simplicity, efficiency, and reusability of the method.

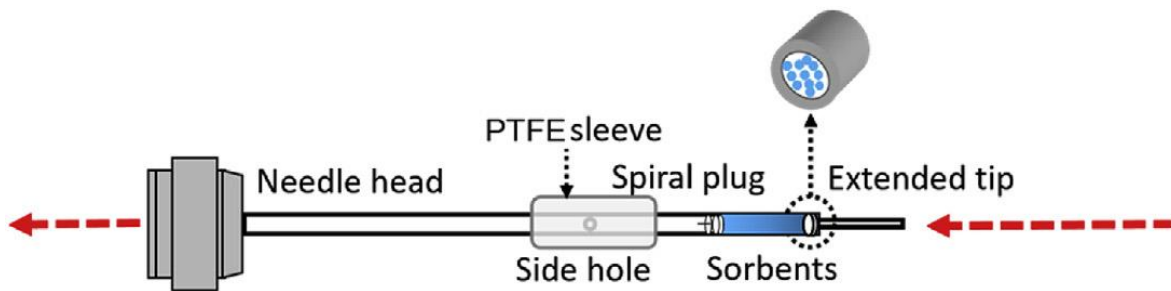


Figure 2.23: Schematic diagram of Needle trap valve for sampling SVOCs [30].

E. Schaller et al. [31] compared Purge-and-Trap and solid-phase microextraction (SPME). They concluded the two preconcentration methods are not satisfying to collect small molecular mass compounds. However, SPME can extract more compounds in higher concentrations. In addition, the SPME technique is easier and more compatible with an auto-sampler rather than Purge-and-Trap techniques.

Another well-established investigation automated GC with cryogenic and sorbent trap approaches. Jia-LinWang et al. [32] showed that sorbent trap and cryogenic approach have the close efficiency regarding sampling C3 to C10, though C2 cannot be sampled with sorbent trap adequately. With all this, they recommended a sorbent trap for sampling streams containing high concentrations of CO<sub>2</sub> and water.

### 2.2.5 Dipping techniques and tube sampling

To sample liquid and semi-liquid through the pipes with an open end, a dipping technique is desired. For example, filling apparatus and pipelines or transfer pipelines with diameters less than 2 in. are classified in this group. Typically, the dipper is constructed of a flared bowl and a convenient handle. In addition, the dipper material should be inert chemically to the samples. Based on the flow stream an adequate capacity for the dipper should also be considered.

A full cross-section of a free-flowing stream is sampled by inserting the dipper into it. Usually, 0.1 volume percentage of a process stream should be sampled by dipper for assurance regarding accuracy. In the following, the collected sample should be transferred into a dry and clean holder container quickly. When sampling is accomplished holder container should be closed and transferred to the laboratory. Given that, the dipper technique is utilized for free flow, the collected samples should not be considered representative of the process stream. In addition, for deep free flow, dipping should not be used for the sampling [33].

In the following, it is tried to describe briefly general procedures throughout the dipper sampling technique. For sampling drums and barrels a large tube with a capacity of 0.5-1 L is

inserted to reach  $\frac{1}{4}$  in of the bottom. Sampling should be taken from the open hung hole uprightly and while the container stands. For a container with a capacity of less than 18 L, whole the container should be considered as the sample. If the number of the small containers is large, the selection of drums can be done with an agreement like Table 2.3 [33].

Table 2.3: Minimum required sample for a set of containers [33].

Number of containers	Number of required samples	Number of containers	Number of required samples
1-3	All	1001-1331	11
4-64	4	1332-1728	12
65-125	5	1729-2197	13
126-216	6	2198-2744	14
217-343	7	2745-3375	15
344-512	8	3376-4096	16
5123-729	9	4097-4913	17
730-1000	10	6860-...	20

## 3 Material and Methodology

In the 19<sup>th</sup> century, scientists tried to investigate and predict the behavior of gases. Then a conservation law of energy and equivalent quantities like pressure discovered that the multiplication of pressure and volume of gas throughout an isothermal compression is constant. In the following, Gray and Lussac related this constant value to the absolute temperature and finally, the first equation of the state of the ideal gas was derived, Equation (3.1) [34], [35].

$$PV = RT \quad (3.1)$$

P, V, and T show the pressure, molar volume, and temperature of the gas respectively. And R as a correlation between pressure and temperature of the gas was derived from the specific heat at constant pressure and volume [34].

While the technology was being progressed, the scientists observed more deviation from ideal gas EoS for higher pressure and lower temperature, indeed, by increasing the molecular interaction. Therefore, statistical thermodynamics was enlisted to consider intermolecular interactions [35], [36].

$$\frac{PV}{RT} = Z \quad (3.2)$$

$$Z = 1 + \frac{B(T)}{V} + \frac{C(T)}{V^2} + \frac{D(T)}{V^3} + \dots \quad (3.3)$$

$$Z = 1 + B(T)P + C(T)P^2 + D(T)P^3 + \dots \quad (3.4)$$

Throughout Equation (3.2), (3.3), and (3.4);  $B$ ,  $C$ , and  $D$  are defined as the temperature-dependent virial coefficients, and  $Z$  represents the compressibility factor. In other words,  $Z$  shows the deviation of real gas molar volume from ideal gas molar volume.

Although to study the PVT behavior of gases a correlation with applicability in a wide range of pressure and temperature is required, it should not be complicated numerically and analytically. Consequently, with considering a compromise between simplicity and applicability, a cubic equation of states emerged [37].

This chapter is going to talk about cubic equations of state, relevant modification, and their applicability throughout a sampling operation.

### 3.1 Generic Cubic equations of state

#### Van der Waals

The first version of cubic EoS was proposed by van der Waals, Equation (3.5), in 1897 [34]:

$$P = \frac{RT}{P-V} + \frac{a}{V^2} \quad (3.5)$$

Where positive constants  $a$  and  $b$  are exclusive for each component.  $\frac{a}{V^2}$  is to justify intermolecular attractive forces and  $b$  is related to the size of the molecules. In addition, these constants are related to the critical pressure and temperature respectively. Van der Waals formulated the phase equilibrium before and separation phases after the critical point. In the following Clausius proved that the intermolecular attractive parameter shall be dependent on temperature. Moreover, by taking into account the sedentary of the molecules at a lower temperature, Clausius derived the Equation (3.6) which is indeed in following of van der Waals EoS [35], [37].

$$P = \frac{RT}{P-V} - \frac{a/T}{(V+c)^2} \quad (3.6)$$

Due to the unsustainable critical compressibility factor, three empirical parameter including  $a$ ,  $b$ , and  $c$  is subjected to this correlation.

### The Redlich-Kwong

Although more than 200 EoS were published by 1949, Redlich and Kwong made effort to deal with the limitations and revive the van der Waals EoS for high- and low-density fluids. They proposed Equation (3.7) EoS [35], [37]:

$$P = \frac{RT}{V-b} - \frac{a_c \alpha(T)}{V(V+b)} \quad (3.7)$$

Where:

$$\alpha(T) = \frac{a}{T^{0.5}} \quad (3.8)$$

$$a_c = \frac{\Omega_a R^2 T_c^{2.5}}{P_c} \quad (3.9)$$

$$b = \frac{\Omega_b R T_c}{P_c} \quad (3.10)$$

$$\Omega_a = 0.4278 \quad \text{and} \quad \Omega_b = 0.0867$$

Although RK EoS does not possess a considerable background theoretically, this model provides acceptable results. It is worth saying that Redlich and Kwong developed their equation just for gasses. By 1980, RK EoS was the most known equation and more than 150 study was performed to modify the RK equation [37].

### Soave/Redlich/Kwong EoS

In 1963, Wilson [38] published an article. The author strived to generalize the RK EoS. Indeed, by introducing the acentric factor ( $\omega$ ), Wilson. investigated different behavior of fluids at the same reduced pressure and reduced temperature. Although Wilson's attempts were not seen, Soave applied this approach and presented a new version of RK EoS by keeping the RK volume functionality and redefining  $\alpha$  as a function of reduced temperature and acentric factor in Equation (3.11) [35].

$$\alpha = \alpha(T_r, \omega) \quad (3.11)$$

$$P = \frac{RT}{V-b} - \frac{a_c \alpha(T_r, \omega)}{V(V+b)} \quad (3.12)$$

$$a_c = \frac{0.42747R^2T_c^{2.5}}{P_c} \quad (3.13)$$

$$b = \frac{0.08664RT_c}{P_c} \quad (3.14)$$

$$\alpha(T_r, \omega) = [1 + (0.480 + 1.574\omega - 0.176\omega^2)(1 - T_r^{0.5})]^2 \quad (3.15)$$

The SRK now is the most popular EoS in hydrocarbon-related industries, and by raising the importance of the optimization of processes, SRK equations have satisfied the requirements in optimization algorithms [37].

### Peng-Robinson

Successfully SRK model led scientists to improve the ability of models in predicting the thermodynamics-related properties, by defining a new temperature model  $\alpha(T_r, \omega)$  and modifying volume dependency of pressure-related terms. Peng and Robinson calculated  $\alpha(T_r, \omega)$  again and modified SRK EoS. This new EoS provides better outcomes for liquid volumes and predicts vapor-liquid equilibrium for mixtures more accurately [34], [35]. PR EoS is as Equation (3.16):

$$P = \frac{RT}{V-b} - \frac{a_c \alpha(T_r, \omega)}{V(V+b)+b(V-b)} \quad (3.16)$$

$$a_c = \frac{0.45724R^2T_c^{2.5}}{P_c} \quad (3.17)$$

$$b = \frac{0.07780RT_c}{P_c} \quad (3.18)$$

$$\alpha(T_r, \omega) = [1 + (0.37464 + 1.54226 - 0.26992\omega^2)(1 - T_r^{0.5})]^2 \quad (3.19)$$

These days, most of research, optimizations, and simulations are using PR and SRK EoS for calculating VLE and interfacial properties, pure fluid, and complex multicomponent mixtures

both. In addition, new modifications to EoS models have focused on recalculating a better  $\alpha(T_r, \omega)$  to increase prediction accuracy. Table 3.1 depicts the most famous expressions for  $\alpha(T_r, \omega)$ .

Table 3.1: List of well-known modifications on  $\alpha(T_r, \omega)$  [37].

Expression for $\alpha(T_r, \omega)$	Author(s)
$1/T_r^{0.5}$	Redlich and Kwong [39]
$T_r(1 + mT_r^{-1})$	Wilson [38]
$\frac{m}{T_r} + \frac{n}{T_r^2}$	Barner et al. [40]
$[1 + m(1 - T_r)]^2$	Soave [41]
$[1 + m(1 + T_r^{-0.5})]^2$	Usdin and McAuliffe [42]
$1 + (1 - T_r)(m + n/T_r)$	Soave [43]
$\exp[C(1 - T_r^m)]$	Heyen [44]
$[1 + m(1 - T_r^{0.5}) + n\sqrt{1 - T_r/0.7}]^2$	Raimondi [45]
$m_1 + m_2/T_r + m_3/T_r^2$	Ishikawa et al. [46]
$[1 + m(1 + T_r) - p(1 - T_r)(0.7 - T_r)]^2$	Mathias [47]
$1 + m(1 - T_r^{0.5}) + m(1 - T_r^{0.5})^2 + m(1 - T_r^{0.5})^3$	Mathias and Copeman [48]
$[1 + m(1 - T_r)]^2/T_r$	Bazua [49]
$m_1 + m_2/T_r + m_3/T_r^2 + m_4/T_r^3$	Adachi and Lu [50]
$1 + m(1 - T_r) + m_2(\sqrt{T_r} - 1)$	Gibbons and Laughton [51]
$[1 + m(1 + T_r^n)]^2$	Kabadi and Danner [52]
$[1 + m(1 - \sqrt{T_r}) - n(1 - T_r)(0.7 - T_r)]^2$	Stryjek and Vera [53]
$1 + m(1 - \sqrt{T_r})^2 - n(T_r - 0.6)^2$	Adachi and Sugie [54]
$[1 + m(1 - \sqrt{T_r}) - p(1 - T_r)(q - T_r)]^2$	Du and Guov [55]
$[1 - m(1 + \theta_r^{0.5})]^2 \theta = (T - T_{pt})/(T_c - T_{pt})$	Nasrifar Moshafeghian [56]

## 3.2 Mixing rules

Theoretically, mixing rules have been developed to connect multicomponent mixture parameters to pure fluid parameters [35]. Mostly, classical van der Waals mixing rules are applied as Equation (3.20):

$$a = \sum \sum x_i x_j a_{ij} \quad (3.20)$$

$$b = \sum \sum x_i x_j b_{ij} \quad (3.21)$$

$$c = \sum \sum x_i x_j c_{ij} \quad (3.22)$$

The volume parameters,  $b_{ij}$  and  $c_{ij}$ , are calculated with arithmetic mean and for force parameter,  $a_{ij}$  the geometric mean is utilized. Therefore, phase equilibrium can be correlated more accurately [35].

$$a_{ij} = \sqrt{a_i a_j} (1 - k_{ij}) \quad (3.23)$$

$$b_{ij} = \frac{1}{2} (b_i + b_j) (1 - \beta_{ij}) \quad (3.24)$$

$$c_{ij} = \frac{1}{2} (c_i + c_j) (1 - \delta_{ij}) \quad (3.25)$$

Although these modifications can keep the concentration-related affinity of the parameters, a better modification is required for complex cases like supercritical fluid processes.  $k_{ij}$ ,  $\beta_{ij}$ , and  $\delta_{ij}$  are known as the interaction coefficients between components  $i$  and  $j$ . moreover, regression analysis of real data or predictive correlations is applied to calculate these interaction coefficients. Some other studies have tried to understand the logic behind the binary interaction coefficient and pure species properties [37].

Graboski and Daubert [57], considered solubility factors to correlate the SRK interaction coefficient. Arai and Nishiumi [58], achieved an empirical correlation between PR interaction coefficients, acentric factors, and critical volumes. Some other studies tried to associate critical temperature, critical pressure, critical compressibility factor, molecular parameters, etc. to EoS parameters. However, none of the proposed correlations are comprehensive. Then, regression analysis is still the preferred approach to calculate EoS parameters. In the following, the best-known mixing rules are to be studied in detail [59].

### Nonquadratic mixing rules

Mainly, it is enough to apply quadratic mixing rules to correlate phases equilibrium. For more complex mixtures, a second interaction coefficient was introduced by Panagiotopoulos et al. [60] in Equation (3.26).

$$a_{ij} = \sqrt{a_i a_j} (1 - k_{ij} + (k_{ij} - k_{ji}) x_i) \quad (3.26)$$

$$k_{ji} \neq k_{ij}$$

In the following, researchers combined quadratic and nonquadratic mixing rules both as ‘general nonquadratic missing rule’, with  $k_{ij} = \delta_i x_i + \delta_j x_j$ . Although further studies showed



that this model can not be applied generally, for binary systems, the general nonquadratic mixing rule is sufficient with acceptable accuracy [37], [59].

### Gibbs free energy models

EoS + Gibbs free energy models have been nominated as the most appropriate model for complex mixtures. Although Orbey and Sandler [61] described the principal concepts of this methodology well-extended, it is out of the context of this study.

Wang and Sandler [36] developed a mixing rule based on Gibbs free energy. By satisfying the quadratic concentration dependency, the WS mixing rule can be applied for two-parameter EoS. In addition, WS mixing is consistent in statistical mechanics [37].

$$b_m = \sum \sum x_i x_j \left( b - \frac{a}{RT} \right)_{ij} / \left( 1 - \sum \frac{x_i a_i}{b_i RT} - A_\infty^E(x) / \Omega RT \right) \quad (3.27)$$

$$a_m = b_m \sum x_i a_i / b_i + A_\infty^E(x) / \Omega \quad (3.28)$$

$$(b - a/RT)_{ij} = (b_i + b_j) / 2 - (a_i a_j)^{0.5} (1 - k_{ij}) / RT \quad (3.29)$$

Some studies applied some better modifications to WS mixing rules and showed that the WS mixing rule is an appropriate model for the asymmetric system and critical conditions can also be predicted in this way. In addition, combination of WS as a mixing rule and NRTL (Non-random two-liquid model) as an activity coefficient model and WS and UNIQUAC (universal quasi-chemical) are recommended for polar and nonpolar mixtures and polar and strongly polar mixtures respectively. Some other studies have tried to separate Gibbs free energy to achieve a more acceptable physical meaning and others extended existing EoS to three parameters for more accurate results. Table 3.2 describes some mixing rules with two constants EoS [59].

Table 3.2: Mixing rules with two constants EoS [37].

Mixing or combining rule	Formulas
Van der Waals One parameter: $k_{ij}$ Two parameters: $k_{ij}, k_{ji}$	$a = \sum \sum x_i x_j a_{ij} \quad b = \sum \sum x_i x_j b_{ij}$ $a_{ij} = \sqrt{a_i a_j} (1 - k_{ij})$ $b_{ij} = \frac{1}{2} (b_i + b_j) (1 - \beta_{ij})$
Panagiotopoulos-Reid (PR) Two parameters: $k_{ij}, k_{ji}$ Three parameters: $k_{ij}, k_{ji}, I_j$	$a_{ij} = \sqrt{a_i a_j} (1 - k_{ij} + (k_{ij} - k_{ji}) x_i)$ $b_{ij} = \frac{1}{2} (b_i + b_j) (1 - \beta_{ij})$
General nonquadratic Two parameters: $\delta_i, \delta_j$	$a_{ij} = \sqrt{a_i a_j} (1 - k_{ij})$ $b_{ij} = 0.5 (b_i (1 - \beta_i) + b_j (1 - \beta_j))$

Three parameters: $\delta_i, \delta_j, \beta_j$	$\beta_i \neq 0$ for all solutes and $\beta_j \neq 0$ for all solvents
Kwak-Mansoori (KM) Three parameters: $k_{ij}, \beta_{ij}, I_{ij}$	$a_{ij} = \sqrt{a_i a_j} (1 - k_{ij})$ $b_{ij} = 0.5(b_i^{1/3} + b_j^{1/3})^3 (1 - \beta_{ij})$ $d_{ij} = 0.5(d_i^{1/3} + d_j^{1/3})^3 (1 - I_{ij})$
Kwak-Mansoori modification Three parameters: $k_{ij}, \beta_{ij}, I_{ij}$	$a_{ij} = \sqrt{a_i a_j} (1 - k_{ij})$ $b_{ij} = 0.5(b_i(1 - \beta_i) + b_j(1 - \beta_j))$ $d_{ij} = 0.5(d_i^{1/3} + d_j^{1/3})^3 (1 - I_{ij})$
Wong-sandler One parameter: $k_{ij}$ Two parameters: $k_{ij}, I_i$	$b_m = \sum \sum x_i x_j \left( b - \frac{a}{RT} \right)_{ij} / \left( 1 - \sum \frac{x_i a_i}{b_i RT} - A_{\infty}^E(x) / \Omega RT \right)$ $a_m = b_m \sum x_i a_i / b_i + A_{\infty}^E(x) / \Omega$ $(b - a/RT)_{ij} = (b_i + b_j) / 2 - (a_i a_j)^{0.5} (1 - k_{ij}) / RT$
Kurihara et al. (KTK) Three parameters $\eta_1, \eta_2, \eta_3$	$a = \sum \sum x_i x_j (a_i a_j)^{0.5} - (\tau - \phi) g_{RES}^E / \ln[(b - \phi) / (b - \tau)]$ $b = \sum \sum x_i x_j b_{ij}$ $b_{ij} = \frac{1}{2} (b_i + b_j)$ $g_{RES}^E = RT x_1 x_2 [\eta_1 + \eta_2 (x_1 - x_2) + \eta_3 (x_1 - x_2)^2]$

### 3.3 Natural Gas

As a fossil fuel, natural gas is preferred to other types because of energy efficiency. Indeed, it is a sustainable fossil fuel energy source with the lowest environmental impacts. Apart from an energy source, natural gas is also considered an industrial chemical for chemical and petrochemical feedstocks [62].

From a chemical composition point of view, natural gas can account for a varying number of alkanes, nitrogen, carbon dioxide, carbon disulfide, metallic substances, etc. Apart from dry (pure methane) and wet (containing condensate), natural gases are mainly classified into lean and rich categories according to the number of recoverable liquids [62], [63].

Relevant difficulties with storage and long-distance transporting, have provoked industries to develop liquified natural gas (LNG). Indeed, natural gas is cooled to about  $-160^\circ\text{C}$  at

atmospheric pressure, and the volume is decreased by 1/600 times. To further advance in LNG technology, it is required to study and measure the chemical composition and the phase behavior throughout the operations. Therefore, consistent samples from the process streams should be taken. So, it can be concluded that sampling is one of the most important steps of the LNG measuring sequence. In a better definition, the samples are taken as a representative of the process stream. On the other hand, different components with a wide range of thermodynamics' properties and the boil-off lead the sampling operation to the aging phenomena. Then, lighter gases of LNG leave the vaporizer, while heavier ones remain. So, the collected sample neither is a composition representative nor has the same properties as the process stream [63].

In the following, an appropriate sampling procedure is described and required thermodynamics' properties are explained.

## 3.4 Sampling requirement

Because of the importance of LNG sampling in the LNG industry, new samplers and sampling procedures have always been developed and revised continuously. While the discontinuous or the spot sampling systems have been dated except in failure mode or impurity analysis cases, ISO 8943 "*Refrigerated light hydrocarbon fluids — Sampling of liquefied natural gas — Continuous and intermittent methods*" [64] recommends intermittent or continuous sampling. For LNG streams, firstly collected liquid stream is vaporized and then sampling is accomplished for phase study as the main reason [65]. The continuous sampling system collects the gas from the vaporizer at a constant flow rate, and the intermittent system samples the process stream within a previously determined time interval.

Jiscoot [66] described the following requirement for an effective LNG sampling system:

- The LNG sampling system should satisfy the following standards
  - ISO 8943 [64]: 2007, Refrigerated light hydrocarbons fluids
  - ISO 10715-2013 [67]- Natural gas sampling guidelines
  - BS EN ISO 12838-2001 Installations and equipment for liquefied natural gas
  - API 14.1 (2006)- Collecting and Handling of Natural Gas Samples for Custody Transfer [68].
- The sampling system should be able to omit the probability of biased sampling while providing an averaged sample from the process stream automatically.
- The sampling system should be able to tolerate the pressure changes of the mainstream. In addition, within the stability of LNG in the liquid phase in the loading cycle, a suitable complete LNG batch should be taken.
- Regarding validation of producibility and redundancy, the sampling system should collect three samples based on ISO 8943:2007 [64].

- To be assured about the elimination of human errors, and the preparation of the representative sample, the sampling system should be automated.
- All the equipment, the facilities, and the interconnections should be purged following a sure procedure
- In the case of chromatographic analysis, the collected sample should be stable vaporized homogenous gas. In addition, the ability to extract samples throughout the batch is required.
- Simple maintenance is required.

## 3.5 The key components of an LNG sampling system

### 3.5.1 Sampling probe

The sampling probe is inserted into the process stream at the right angle. The installation point of the probe is the wherewith high degree of subcooling. It means, always the temperature at the sampling point should be less than the boiling point temperature of LNG. In addition, to preserve the sample from vaporizing or bubbling, subcooling should be kept. Then sufficient insulation is required. ISO 10715 recommends equipping the LNG sampling probe with a shut-off valve [63].

For taking a representative sample, vacuum insulated probes with specific characterizations have been recommended. Remotely cryogenic valves should be fitted to these kinds of probes. It is also better to assemble the probes to the vaporizer as a unit.

By considering all probable unloading conditions, the Interconnection between the liquid sampled and the vaporizer should be short, insulated, and slim as much as possible to fulfill the subcooled condition. Manner of calculating defined geometric conditions is provided by ISO 8943 [64].

### 3.5.2 Vaporizer and control devices

According to ISO 8943 [64], the vaporizer should be:

- *“The heat exchange capacity of the LNG sample vaporizer shall be sufficient to gasify the whole volume of LNG which is being withdrawn for sampling”*
- *“The sample vaporizer shall be so constructed that the heavier components of the LNG shall not remain in the vaporizer”*
- *“Where a compressor transferring vaporized LNG is provided, the maximum gasifying capacity (heat input) of the LNG sample vaporizer shall be greater than the capacity of the compressor”*

Eliminating fractionation is the main challenge of designing a vaporizer. Then, a high-temperature condition is required to vaporize even the heaviest component of sampled LNG immediately. Electrical-based or water-heated are the more commonly used vaporizer in sampling operations [62], [63].

Process control throughout the LNG vaporization is performed because of monitoring vaporization conditions and preserving the equipment. The following controllers are necessary throughout the vaporization operation [63].

- Check valve: at the inlet to the vaporizer to prevent flow back
- Restriction orifice: at the inlet to the vaporizer to succeed in flash vaporization
- Needle valve: to control the sampling flow
- Sample filter
- Bypass system: for emergency conditions and maintenance
- Temperature regulator, thermometer, thermostat: within the vaporizer
- Pressure regulator
- Mixing accumulator
- Safety instruments, etc.

#### 3.5.3 Sample holder and container

LNG sample holders are mainly divided into two types, including water seal and waterless with a capacity of 500-1000 liters. A constant pressure floating piston container is also available to accumulate a small volume of samples. Typically, constant pressure containers are accompanied by a gas compressor. It is worth saying that sample holders should have the ability to keep the representative sample mixed. More information about the features of sample containers and cleaning, filling, and purging is provided in ISO 8943 [63], [64].

## 3.6 Sampling condition

### 3.6.1 Sampling flow

Collected sample through the sampler is not considered unless establishing a full flow condition. Indeed, throughout the pressure or flow rate disturbances, the sampling process should be suspended. Then, flow monitoring instruments are required for loading and unloading parts of the process [63]. Figure 3.1 shows the acceptable and unacceptable flow rate for sampling.

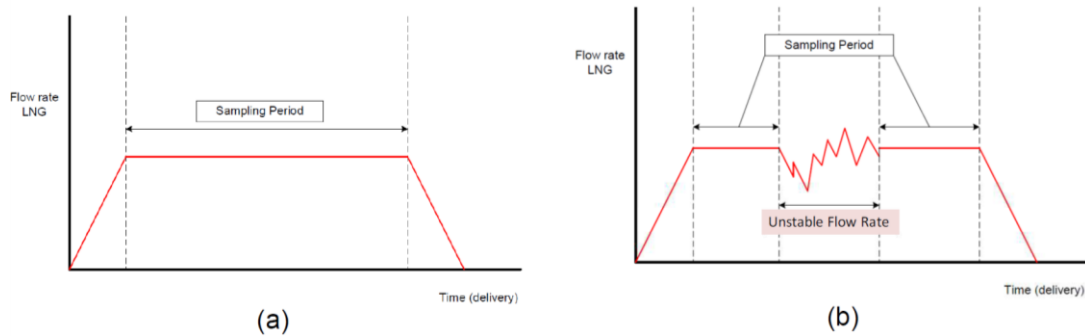


Figure 3.1: Schematic diagram of acceptable (a) and unacceptable (b) flow rates [63].

### 3.6.2 Inlet condition

The sampled LNG should go into the probe and the vaporizer under subcooled conditions. It means that knowing the boiling temperature of LNG is required to set the initial condition of sampling. In addition, it is known that the boiling point of a multicomponent mixture is a function of its fractional composition [35], [63].

By moving the sampled liquid LNG throughout the probe to the vaporizer, a small variation in pressure or heat transfer may lead the LNG into partial vaporization. To control this condition two important factors should be considered. Firstly, the degree of subcooling should be monitored continuously to keep the flow temperature less than the boiling point as much as possible (Figure 3.2). And then, insulation quality should be sufficient to deter the system from receiving heat.

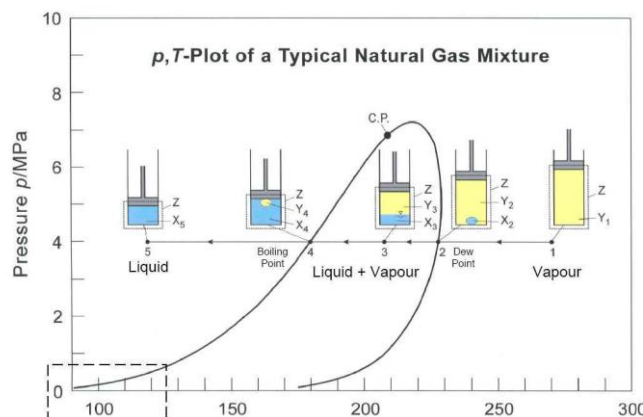


Figure 3.2: Schematic P-T diagram for a typical LNG [59].

To study how the LNG state is changing throughout passing the probe to the vaporizer inlet, a P-H (pressure-enthalpy) diagram can be helpful (Figure 3.3). for example, at the unloading LNG is at the subcooled point a state. Throughout passing the probe because of pressure disturbance or transferring heat, LNG will change to point b. now if the change of enthalpy is

less than the subcooling degree, the vaporizer inlet state is acceptable, otherwise, collected LNG would not be a representative sample [59].

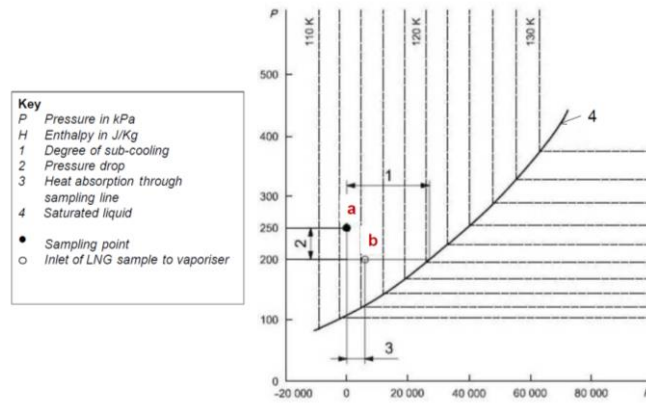


Figure 3.3: Schematic LNG pressure-enthalpy diagram [63].

### 3.6.3 Vaporization process

The vaporizer should vaporize the whole sampled LNG before sending it to the analyzer. In other words, all the collected components should be in the gaseous phase after vaporizer, and none of the heavier components should remain. For this step, studying the P-T diagram shows how the pressure and the temperature should be changed throughout the vaporizer. As is shown with a dotted line in Figure 3.4, changing the state of sampled LNG from liquid to supercritical gas without fractionation is desired [63].

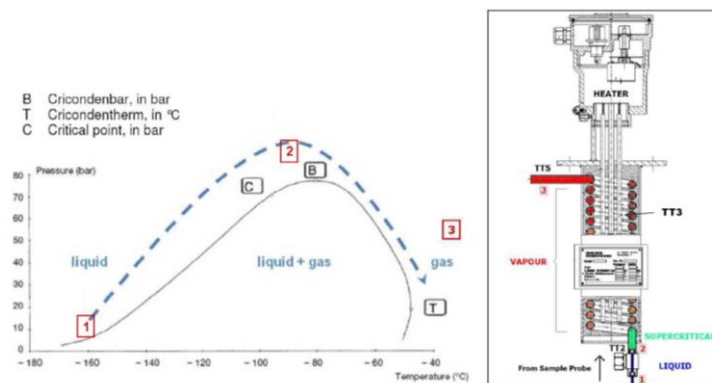


Figure 3.4: Schematic diagram of desired LNG vaporization path [59].

As an example, for a typical LNG, the following steps, can change the state of LNG without fractionation:

Before entering the vaporizer, restriction equipment like pressure relief valves should be considered to flash LNG into a supercritical state.

Higher pressure is required (from Fig 2-4 80 bar). Then with increasing the temperature there will not be an intersection with the two-phases area [63].

Flashed LNG goes into a heated environment at the outlet of the vaporizer to achieve predesign temperature.

### 3.7 Specification of the under-study LNG Sampling System

In this study, two parallel 24 in pipeline headers are considered for loading and unloading LNG with 3000-6000 m<sup>3</sup>/h flow rate at 0.5-3 and -161.5°C to -153 °C respectively.

An electrically based vaporizer is utilized to change the state of sampled LNG from liquid to gas with a flow rate of 1-2 L/h. In the following, the gaseous sample passes 10-30 m toward an instrument cabinet through an insulated tube with a 6-12 mm outer diameter. At the end of the sampling system, a gas chromatograph is enlisted to determine the heating value and analyze the composition of sampled gas online.

Layout and assembling of the facility are according to the following standards:

- Iso 8947:2007 – Refrigerated light hydrocarbon fuel – Sampling of liquified natural gas – continuous and intermittent methods
- GIIGNL: 2017 – LNG Custody Transfer Book

The following LNG composition and operation conditions are to be investigated (Table 3.3 for composition and Table 3.4 for operation conditions):

Table 3.3: Typical LNG composition.

Component	Mole % fraction
Nitrogen	0.0200
Carbon dioxide	0.0000
Methane	92.9800
Ethane	5.2000
Propane	1.3000
n-Butane	0.2300
iso-Butane	0.2500
n-Pentane	0.0100
Hexanes	0.0000

Table 3.4: Process design operation conditions.

Parameter	Unit	Min.	Normal	Max.
LNG transfer Flow	m <sup>3</sup> /h	3000	4000	6000



LNG pressure	barg	0.5	1.5	3
LNG temperature	°C	-161.5	-158	-153
Vaporizer regulator outlet pressure	barg		0.4	
Vaporizer outlet temperature	°C		40	
Ambient Temperature	°C	0	20	30

### 3.7.1 Probe design operation

The probe and interconnection tube to the vaporizer is made of the stainless-steel grade 316. The outer and inner diameters of the probe are 26.7 mm and 20.96 mm respectively. Subsample probe diameter is also 6 mm and 4 mm for outer and inner respectively. As it is shown in Figure 3.5 and 3.6, probe extract sample from the main process stream, and by-pass flow can be established using a dynamic pressure forced on the upstream pointing probe tips. In addition, a 6 mm subsample tubing probe is designed to sample LNG through the vaporizer.

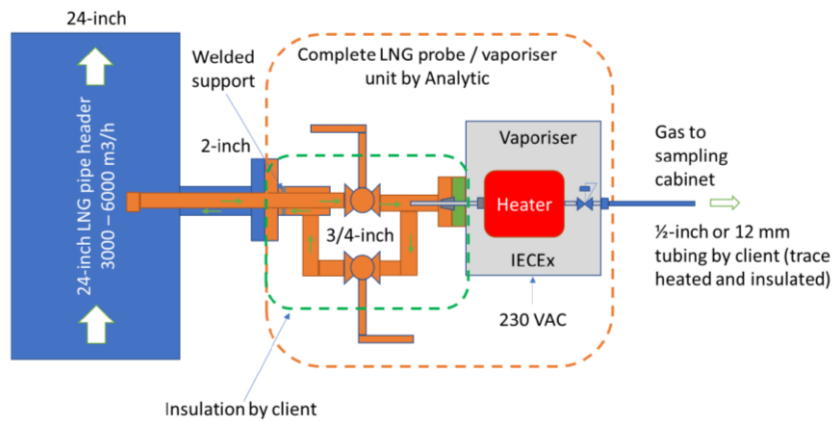


Figure 3.5: schematic diagram of LNG probe and vaporizer layout (With permission from Moreld Flux).

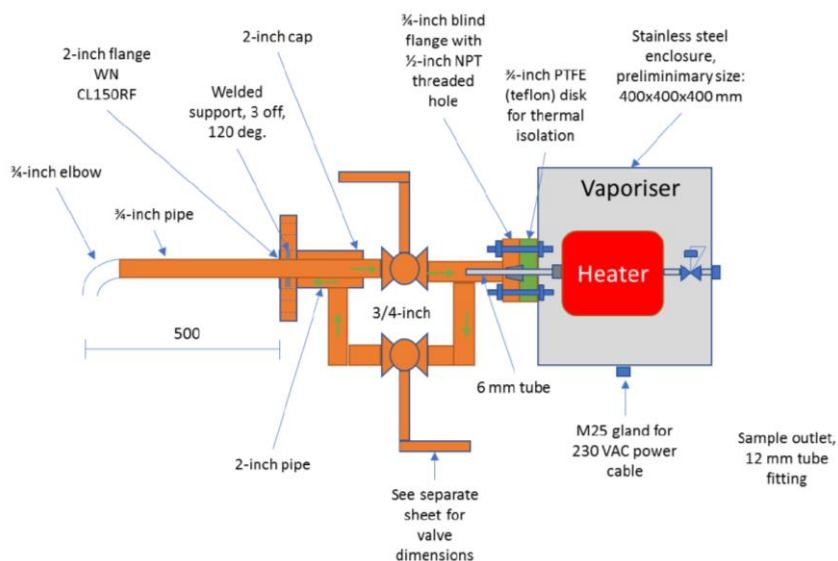


Figure 3.6: Detailed information on probe and vaporizer layout (With permission from Moreld Flux).

### 3.7.2 Vaporizer configuration

As a heater, a cylindrical cartridge heater is inserted into an aluminum block. Although the heater can produce 500-watt electrical heating power, thermal heat capacity depends on the maximum allowable surface temperature of the cartridge. Then, a PID controller is considered to not allow the cartridge reaches max. allowable temperature. the PID controller is tuned based on the available heat from the cartridge as a heat producer and LNG flow rate as a heat receiver.

The base case flow passes between the cartridge and aluminum block in annuls. While relevant standards require the cartridge to be surrounded with an additional metal block. Although this configuration may reduce the heating efficiency, it is assured that sampled LNG is vaporized sufficiently even with 50% efficiency of the designed cartridge. Figure 3.7 provides more information regarding vaporizer configurations.

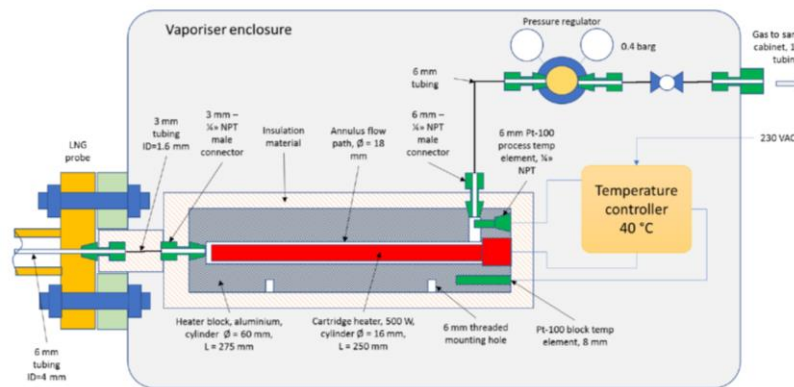


Figure 3.7: Schematic diagram of vaporizer configuration details (With permission from Moreld Flux).

The vaporizer is equipped with three thermocouples and a Coriolis flow meter. To measure the temperature and flow rate the following LabVIEW program is developed (Figure 3.8).

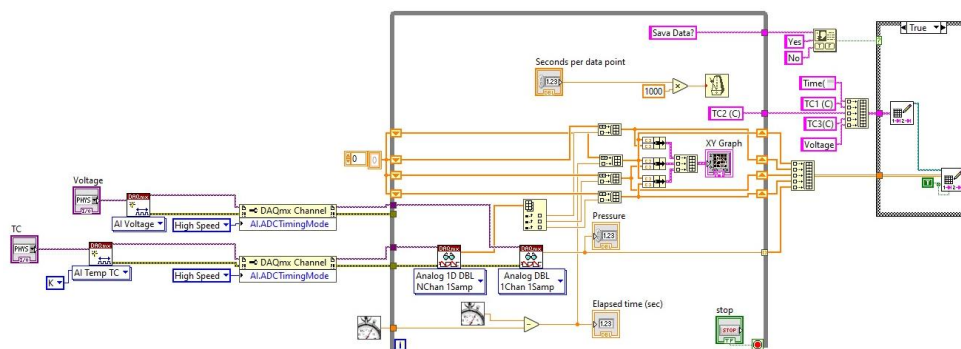


Figure 3.8: Schematic block diagram of the developed LabVIEW program for measuring the temperature and flow rate throughout the vaporizer.

### 3.7.3 Post heating

For this study, a post-heating facility is predicted to be assured about the temperature of fluid after vaporizer, schematically shown in Figure 3.9. Therefore, a vertical helical coil is emerged in a water bath with constant temperature and the fluid is flowing through the pipe. Entrance temperature of the fluid flow, flow velocity, water bath temperature, and thermodynamic properties are known, and it is to calculate the required pipe length based on the exit flow temperature. therefore, inside, and outside heat transfer coefficients should be calculated based on the Nusselt number correlations.

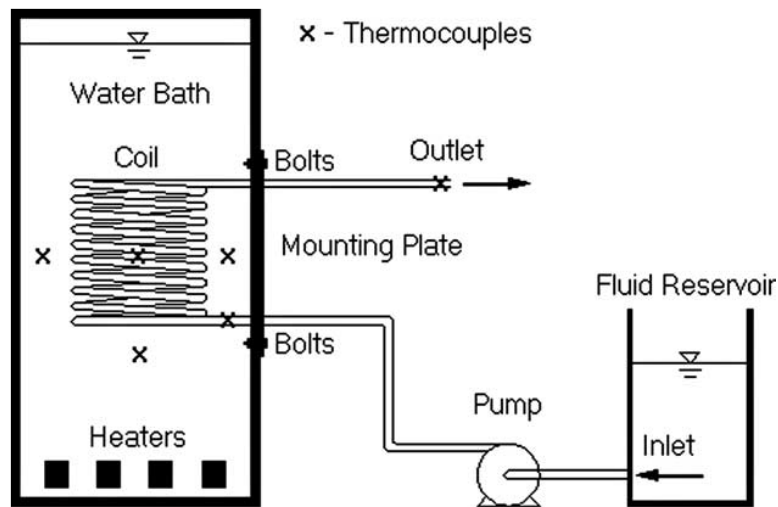


Figure 3.9: schematic diagram of vertical helical coil tube immersed in a water bath [69].

Regarding the vertically helical coiled inside convection heat transfer coefficient, Rogers, and Mayhew [70] developed following Nusselt number correlation, Equation (3.32).

$$Re = \frac{\rho u D}{\mu} \quad (3.30)$$

$$Pr = \frac{c_p \mu}{k} \quad (3.31)$$

$$Nu = 0.021 Re^{0.85} Pr^{0.4} \left(\frac{r_i}{R}\right)^{0.1} \quad (3.32)$$

$$h = \frac{Nu \cdot k}{D} \quad (3.33)$$

Nu = Nusselt Number

Re = Reynolds Number

Pr = Prandtl Number

$r_i$  = Inside Radius [m]

R = Helical Coil Radius [m]

$\rho$  = density [kg/m<sup>3</sup>]

u = velocity [m/s]

$\mu$  = viscosity [N.s/m<sup>2</sup>]

$c_p$  = Specific heat [j/kg. K]

$k$  = Thermal conductivity [W/m. K]

By considering Equation (3.30) to (3.33) inside convection heat transfer coefficient can be obtained. All the thermodynamic properties are evaluated at the film temperature  $T_f$ , Equation (3.34).

$$T_f = T_{wi} + \frac{T_{in} + T_{out}}{2} \quad (3.34)$$

$T_{wi}$  = inside wall temperature

Free convection is the main heat transfer coefficient between the outside of the helical coil and the surrounding bath. To calculate the Nusselt number in the case of free convection, the Rayleigh number (Equation (3.35)) should be calculated first.

$$Ra = \frac{g\beta(T_s - T_\infty)L^3}{\nu\alpha} \quad (3.35)$$

Ra = Rayleigh number

$g$  = gravitational acceleration [m<sup>2</sup>/s]

$\beta$  = thermal expansion coefficient [1/K]

$T_s$  = pipe outside wall temperature [K]

$T_\infty$  = surrounding temperature [K]

$L$  = characteristics length [m]

$\nu$  = kinematic viscosity [N.m/kg]

$\alpha$  = thermal diffusivity [m/s<sup>2</sup>]

Although there are different definitions for characteristics length like the overall length, the diameter of the coil, etc., **normalized length is utilized in this study**. To calculate normalized length, firstly helical coil should be considered as a continuous cylinder, then  $L_n$  would be the division of the outer surface area of the imagined cylinder to the total tube length [69]. Regarding the outside heat transfer coefficient, different correlations have been developed for the Nu number, which is mainly the power function of the Ra number.

$$Nu = a(Ra)^b \quad (3.36)$$

For applying normalized length, Devanahalli et al. [69] suggested the Equation (3.37) correlation

$$Nu = 2.0487(Ra)^{0.1768} \quad (3.37)$$

Nevertheless, because of the unknown length of the tube, an iteration approach is applied to calculate the free convection heat transfer coefficient.

The total amount of transferred heat can be calculated based on the change of internal energy of flowing N2 throughout the pipe.

$$\dot{q} = \dot{m}c_p(T_{out} - T_{in}) \quad (3.38)$$

$$\dot{m} = \rho u A_{in} \quad (3.39)$$

In another view, this amount of heat is equal to heat transfer between fluids and surfaces. In addition, the heat conduction between the inside and outside surface of the tube should also be the same. Then,  $\dot{q}$  can also be rewritten as follow:

$$\dot{q} = \bar{h}_i(2\pi r_i L)(T_{wi} - \frac{T_{in} + T_{out}}{2}) \quad (3.40)$$

$$\dot{q} = \bar{h}_o(2\pi r_o L)(T_{bath} - T_{wo}) \quad (3.41)$$

$$\dot{q} = 2\pi k L \ln(\frac{r_{out}}{r_{in}})(T_{wo} - T_{wi}) \quad (3.42)$$

Apart from L and  $\bar{h}_o$ , all other variables are known. Equation (3.38), (3.40), and (3.41) are inserted into Equation (3.42) and with an initial guess for  $\bar{h}_o$ , iteration is started. Each iteration will give a value for L. then Ra number, in following Nu number, and finally  $\bar{h}_o$  can be calculated. Iteration will be continued until a reliable convergence on  $\bar{h}_o$ . The schematic diagram of the prediction flow chart is shown in Figure 3.10.

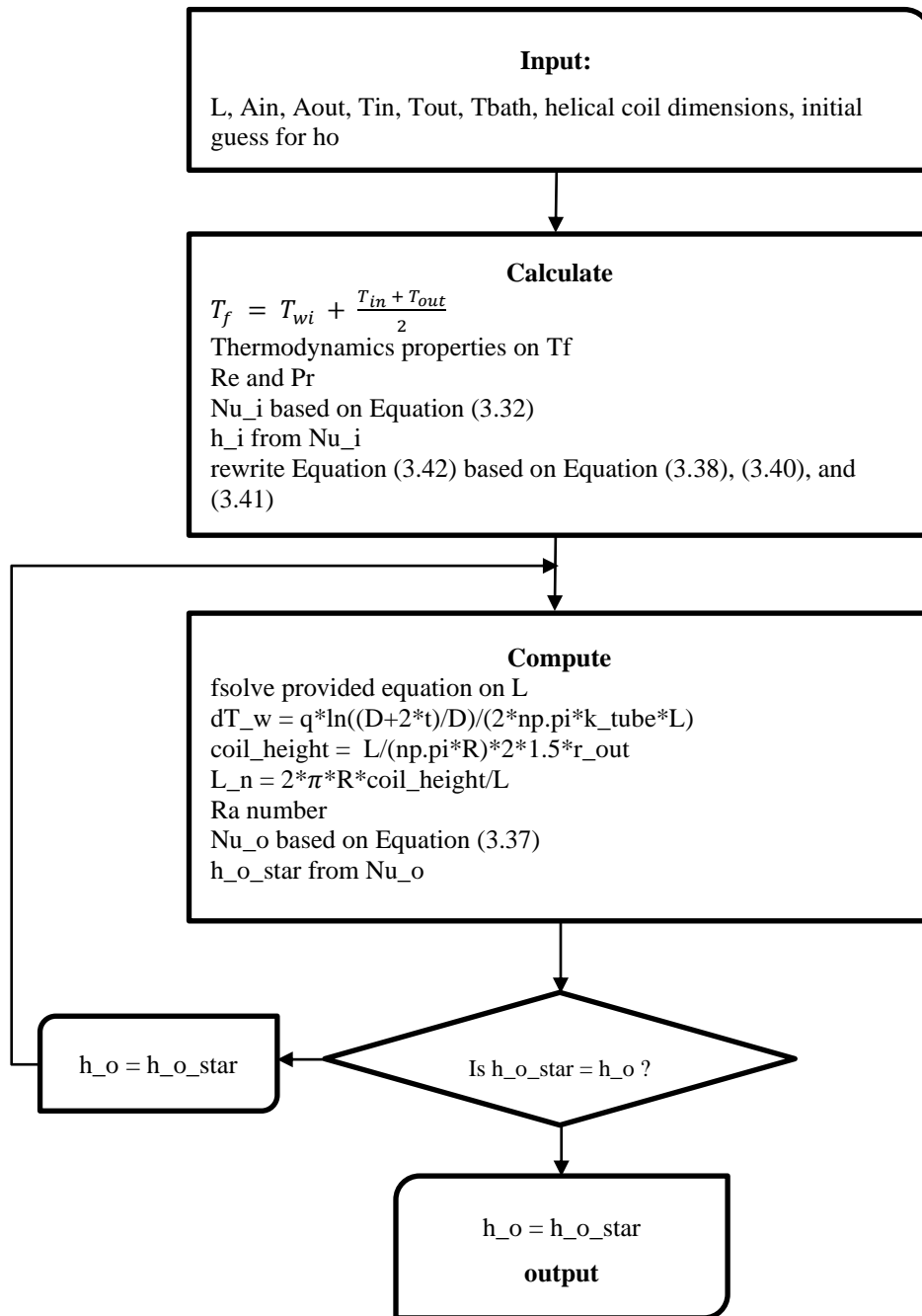


Figure 3.10: Suggested Algorithm for calculating required length for helical coil heat exchanger.

### 3.8 Experiment procedure

In this part we are going to describe a liquified nitrogen sampling procedure for accurate measuring and complying safety principle.

### 3 Material and Methodology

First, the probe should be connected at the sampling point with right angle. ISO 10715 recommends installing probe at a point with at least 20 pipe diameters downstream from a flow disturbance like elbow, etc. in case of horizontal process stream, the probe should be inserted into one-tired of the pipe diameter upper from the center.

Regardless type of sampling, the samples should be taken at constant flow rate. It means, the measurements throughout the initial period of starting the process and the final period of stopping the process should not be included. Moreover, the measurements should be ignored temporarily, in the case of occurrence a considerable change in flow rate or pressure.

The temperature should be measured where the flow is fully developed thermally. In this case, LN<sub>2</sub> is to study in three different mass flow rate, including 0.5, 1, and 2 kg/s. by calculating Reynolds number, fully developed length can be obtained (refer to Principles of Heat and Mass Transfer, Incropera). For an instance, in turbulent flow by considering following approximation:

$$10 \leq \frac{x_{fd,T}}{D} \leq 60 \quad (3.43)$$

Before vaporizer:  $D = \frac{1}{8} \text{ in}$   $x_{fd,T} = 7.5 \text{ in}$

After vaporizer:  $D = \frac{1}{4} \text{ in}$   $x_{fd,T} = 8.6 \text{ in}$

Thermally fully developed region for each velocity should be calculated and the maximum should be considered in laying out the connecting pipes and thermocouples. Therefore, the first thermocouple should be located at least 7.5 in (in the case of turbulent flow) far from the sampling point. And first thermocouple after vaporizer should be 8.6 in (in the case of turbulent flow) far from vaporizer outlet. In addition, ISO 8943 presents the Equation (3.44) to calculate the maximum allowable distance from the probe to the vaporizer:

$$L = \frac{W \times \Delta H}{q} \quad (3.44)$$

W = sampling mass flow rate [kg/h]

$\Delta H$  = degree of subcooling of sample at probe inlet [J/kg]

q = heat input [J/m.h]

*note: Annex (A) of ISO 8943(2007) described how to calculate the degree of sub-cooling.*

Prior to the vaporizer, the LN<sub>2</sub> flow should be kept at sub-cooled state. While LN<sub>2</sub> is leaving container into the pipeline, pressure decreases. Therefore, by considering the magnitude of the pressure, always the temperature at the pipeline prior to the vaporizer should be kept under the saturation temperature. A qualified insulation for probe and sampling line to the vaporizer is then required. If thermocouple before the vaporizer detects an abrupt change in temperature, the measured values should be ignored insofar as establishing a flow with temperature less than LN<sub>2</sub> saturation temperature.

### 3 Material and Methodology

At the vaporizer outlet the temperature of gaseous nitrogen should be more than **60 °C**, to be assured about completed vaporization of LN<sub>2</sub>.

Before starting the sampling process, all the facilities and the interconnections should be purged with gaseous nitrogen to remove contamination from last operation or air. ISO 10715 (Naturgass Retningslinjer for prøvetaking) provides a procedure for purging the facilities and the interconnection prior to sampling. Based on this standard, purging should be performed slowly and for at least 1 min. in addition, as it is shown in Figure 3.11, it is possible to identify the required purging time according to flow rate, pipeline diameter and interconnection distance. Nevertheless, purging time can be calculated based on the volume of the facilities, purging flowrate, and considering a safety factor.

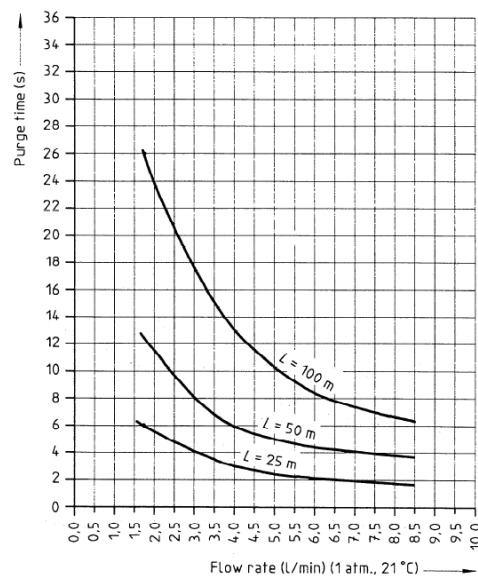


Figure 3.11: Identifying purge time as function of flow rate, interconnection diameter, and long of pipeline (inner diameter 3 mm) (EN ISO 10715:2000).

Figure 3.12 shows the P&ID of the rig is to be studied. For purging following procedure is recommended:

1. Close all the valve
2. Open valve V-1 and then open the valve prior to flowmeter.
3. Open the end valve and let purging for at least for 1 min.
4. Close the end valve, then close the valve prior to the flowmeter, then open the by-pass valve and open the end valve again and let purging for at least 1 min.

Now system is purged.

5. Open the prior valve to the flow meter and clos the by-pass valve and start LN<sub>2</sub> flowing.
6. Purging by LN<sub>2</sub> should be continued for at least 1 min since appearing LN<sub>2</sub> at the end valve



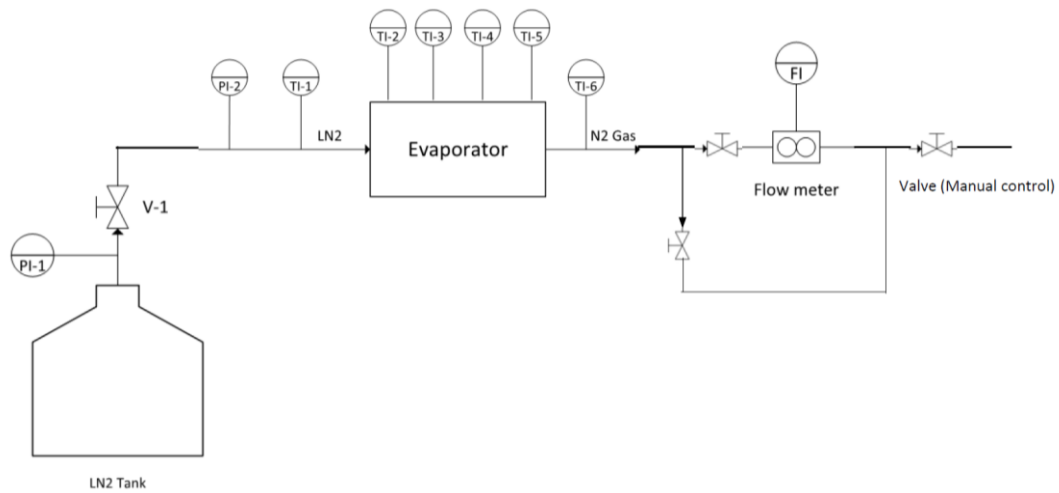


Figure 3.12: P&ID of installed rig.

Right after purging with gaseous nitrogen, LN<sub>2</sub> should be passed through the system with the same period of purging time. In following the vaporizer will go into service and measurement recording will not be started as far as establishing a constant flowrate.

LN<sub>2</sub> should not be trapped between two valves inside the pipeline. So that, for starting up the sampling process, the furthest valve to the LN<sub>2</sub> container should be opened sooner, and regarding stopping the process, the closest valve to the LN<sub>2</sub> container should be closed sooner.

This study is indeed a sampling with controlled rate method, and a needle valve is applied to control the sample flowrate. Annex (E) of ISO 10715 provides a procedure for this type of sampling.

## 4 Results and Discussion

The result of this study is divided into three parts. Firstly, a multicomponent gas mixture is modeled as a real gas, using different EoS and mixing rules. Then the prepared model is validated by comparing the results with performed experimental studies. In the following heat transfer from the under-study LNG, the sampler is modeled mathematically and thermodynamically. And finally, it is recommended to validate the developed models and prepared procedure by performing future experiments on the sampler using LN<sub>2</sub>.

### 4.1 Modeling EoS to calculate fluid phase equilibrium

To describe the homogeneity or inhomogeneity behavior of a fluid, interfacial properties and phase equilibrium of fluid should be calculated. These two physical properties play a crucial role in designing a process and operations.

According to the equation of state, Phasepy has been developed as a python package to calculate the fluid phase properties. In this package phase equilibrium is modeled by utilizing  $\phi - \phi$  and  $\phi - \gamma$  approaches, where  $\phi$  is the fugacity coefficient and  $\gamma$  is the activity coefficient.

Phasepy can model the fugacity coefficient as a perfect gas, virial gas, or EoS fluid. However, the activity coefficient is modeled by conventional approaches like Redlich-Kister expansion, modified UNIFAC, etc.

By extending Cubic EoS groups to mixing rules, Phasepy evaluates the Vapor-Liquid, Liquid-Liquid, and Vapor-Liquid-Liquid equilibrium. Generally, in a continuous approach, combining cubic EoS (accounts for Van der Waals, Peng-Robinson, Redlich-Kwong, and their derivatives) and mixing rules (e.g., Quadratic, Modified Huron-Vidal, Wang-Sandler) can model phase equilibrium [71].

#### 4.1.1 Phasepy Package

Phasepy has been developed on a structure based on Figure 4.1, to reduce the required code for end-user. Firstly, an appropriate model is selected based on pure or multi-component fluid. Then, the selected model computes the stability and equilibrium. Finally,  $\Phi - \Phi$  continuous approach is utilized to study the interfacial behavior using square gradient theory (SGT). As a theoretical approach, SGT is linked to an EoS and predict directly the spinodal boundary using a single van der Waals loop [71], [72].

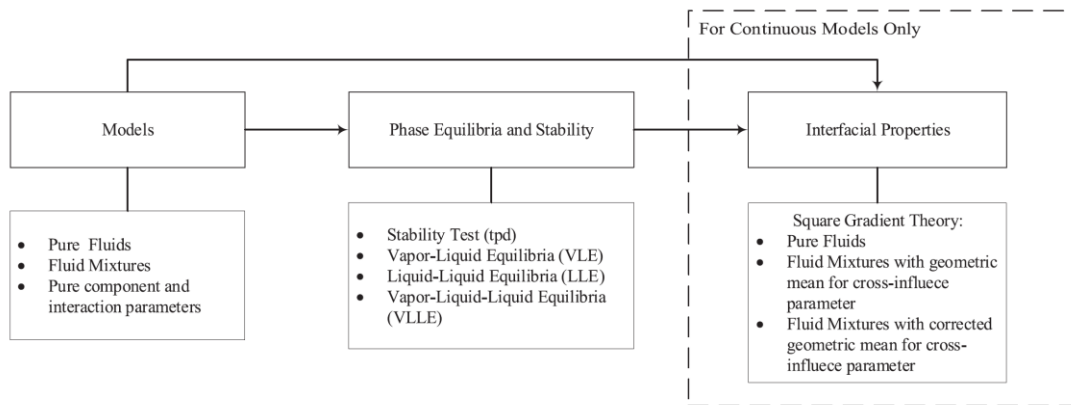


Figure 4.1: Phasepy structure [71].

In the beginning, the pure components should be defined. The *Component* function of Phasepy defines pure component based on critical pressure  $P_c$ , critical Temperature  $T_c$ , critical compressibility factor  $Z_c$ , critical molar volume  $v_c$ , and acentric factor  $\omega$ . Moreover, relevant data to coefficient parameters for vapor pressure, group contribution for SGT, and influence parameters can also be provided by this function.

```
>>> propane = component(name = 'propane', Tc = 369.8, Pc = 42.48, Zc = 0.276, Vc = 200, w = 0.152, GC = {'CH3': 2, 'CH2': 1}, Mw = 44.097)
```

In the following, an equation of state should be selected to model phase equilibrium for the defined components. Throughout this study, the generic cubic EoS, including two well-known EoS, Peng-Robinson, Soave/Redlich/Kwong are studied. On the other hand, calculated isofugacity based on Segura and Wisniak is employed to compute vapor pressures.

After defining the EoS for the program, the function *eos.psat* is run to output the equilibrium pressure and molar volumes of the phases. Finally, an appropriate approach should be selected. The  $\phi - \gamma$  approach models the vapor phase deviation  $\phi$ , in a virial expansion. And the second virial is anticipated with ideal gas behavior or Tsonopoulos correlations. In addition, liquid phase deviations  $\gamma$  are modeled with a predictive modified-UNIFAC model, RK expansion, Wilson model, or NRTL model [71].

By using another approach, all phases are modeled with the same EoS. Classical cubic EoS are defined in Phasepy, including van der Waals *vdweos*, Redlich-Kwong *rkeos*, Redlich-Kwong-Soave *rkseos*, Peng-Robinson *preos*, and Peng-Robinson-Stryjek-Vera *prsv eos*. In addition, Wong-Sandler, Quadratic and Modified-Huron-Vidal model is also available in Phasepy as a mixing rule. Among the defined mixing models and EoS, the Author has recommended UNIFAC and *prsv eos* respectively. Throughout the program EoS and mixing rules are defined as:

For example:

```
#Setting EoS with UNIFAC
```

```

>>> mix.unifac()
>>> eos = prsveos(mix,'mhv_unifac')
#Setting EoS with qmr
>>> kij = np.array([...], ..., [...])
>>> mix.kijcubic(Kij)
>>> eos = prsveos(mix,'qmr')

```

Briefly, the required information for two different approaches  $\phi - \phi$  and  $\phi - \gamma$  are presented in Table 4.1.

Table 4.1: Required information for type of modeling  $\phi - \phi$  and  $\phi - \gamma$  [71].

Type of modeling	Models	Component definition	Interaction
Discontinuous model $\phi - \gamma$	$\phi$ models: ideal gas, Abott Van Ness $\gamma$ models: NRTL, Wilson, Redlich-Kister, modified-UNIFAC	Critical temperature Critical pressure Critical compressibility factor Acentric factor Antoine parameters	Activity coefficient models need specific interaction parameters
Continuous model $\phi - \phi$	VdW, PR, PR, PRSV, RK, RKS,	Critical temperature Critical pressure Acentric factor Volume translation Influence parameter	Specific activity coefficient models WS and MHV need a correction factor $k_{ij}$ for QMR and WS

### Bubble point and dew point calculation

Based on Rachford-Rice mass balance, Equation (4.1), the isothermal-isobaric calculation is performed for vapor-liquid equilibrium.

$$FO = \sum_{i=1}^c (x_i^\beta - x_i^\alpha) \frac{z_i(K_i-1)}{1 + \psi(K_i-1)} \quad (4.1)$$

Where,

$$K_i = \frac{x_i^\beta}{x_i^\alpha} = \frac{\phi_i^\beta}{\phi_i^\alpha} \quad (4.2)$$

Here,  $K_i$  refers equilibrium constant and  $\psi$  shows the fraction of phase  $\beta$ . Priorly,  $\psi$  is known and it should be set 0 and 1 for bubble and dew point calculation respectively (Equation (4.3)).

$$FO = \sum_{i=1}^c x_i(K_i - 1) = \sum_{i=1}^c y_i - 1 \quad (4.3)$$

To solve this correlation, an inner loop Accelerated Successive Substitution should be utilized to update the phase composition. In addition, Pressure and Temperature are updated in an outer

loop based on the quasi-Newton method. Phasepy has used SciPy optimization manners to remedy the situation in case of slow convergence.

Figure 4.2 shows the general algorithm to calculate the saturation points. In the case of calculating bubble P, firstly fluid composition and temperature are known, then a primary guess for pressure and gaseous composition should be defined for the program. Now, given that the pressure is an iterative variable, the function returns the equilibrium state and gaseous composition straightforwardly.

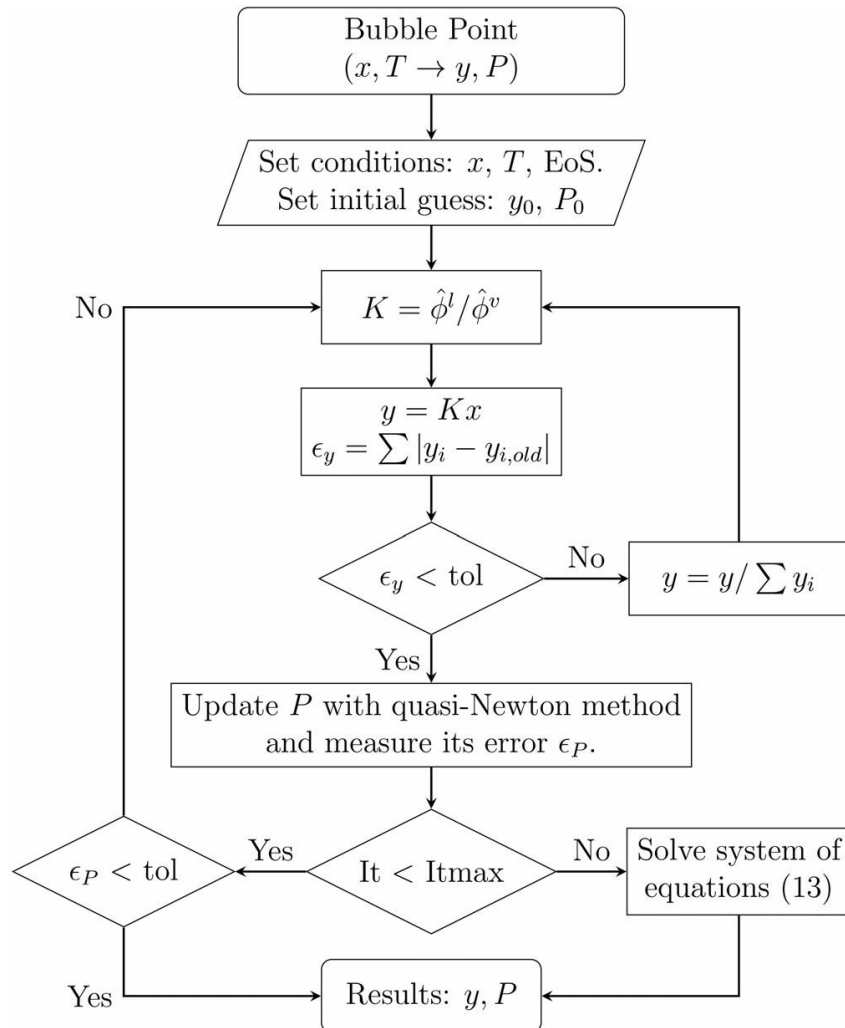


Figure 4.2: Suggested algorithm in Phasepy to calculate the saturation points.

Code example:

```
>>> x = np.array([...])
```

```
>>> T = 250 #k
```

#Initial guess from tpd minimization

```
>>> y0 = np.array([...])
```

```
>>> P0 = 1 #initial guess for pressure in bar
```

```
>>> bubblePy(y_guess = y0, P_guess = P0, X = x, T = T, model = eos)
```

### Phase Equilibrium

To evaluate how much the developed model in predicting phase equilibrium is reliable three two-component mixtures at two different pressure and two four-component mixtures are studied and outputs are compared with the experimental results; a example of python code scripts is provided in Appendix A.

Knudsen et al. [73] investigated the most appropriate mixing rule, including the Huron-Vidal rule, the MHV-model, the Schwarzenuber - Galivel-Solastouk - Renon rule, and the density-dependent local composition rule, for SRK EoS. The authors showed that the Huron-Vidal rule and modified Huron-Vidal rule can be used as the best mixing rule. On the other hand, Pedersen et al. [74] also suggested that when the system is only containing hydrocarbons and sour gas simple QMR can be adequate. Therefore, for binary mixtures, Modified Huron Vidal mixing rule and Quadratic Mixing Rule are compared in three different systems.

Marlus et al. [75] investigated a binary mixture of Benzene and Cyclohexane at two different pressure 101.5 and 40 kPa. Tables 4.2 and 4.3 depict the experimentally measured values for gaseous mole fraction and liquid mole fraction at 40 and 101.3 kPa respectively. In addition, T-x,y diagrams are also drawn in Figure 4.3, and 4.4. In this case, SRK is used as EoS, and two mixing rules, the quadratic mixing rule, and the Modified Huron Vidal mixing rule are compared.

Table 4.2: Benzene (1) + Cyclohexane (2) 40kPa.

T[K]	Cal. T[K]		P[kPa]	Exp. liquid mole fraction		Exp. gaseous mole fraction		Cal. gaseous mole fraction			
	QMR	MHV		x <sub>1</sub>	x <sub>2</sub>	y <sub>1</sub>	y <sub>2</sub>	QMR		MHV-Wilson	
								y <sub>1</sub>	y <sub>2</sub>	y <sub>1</sub>	y <sub>2</sub>
325.75	325.58	325.58	40	0.000	1.000	0.000	1.000	0.000	1.000	0.000	1.000
324.30	324.39	324.32	40	0.112	0.888	0.125	0.875	0.146	0.854	0.147	0.853
323.65	323.67	323.60	40	0.208	0.792	0.238	0.762	0.250	0.750	0.250	0.750
323.50	323.50	323.43	40	0.237	0.763	0.262	0.738	0.278	0.722	0.278	0.722
322.95	322.91	322.87	40	0.388	0.612	0.423	0.577	0.413	0.587	0.411	0.589
322.85	322.82	322.80	40	0.432	0.568	0.454	0.546	0.449	0.551	0.447	0.553
322.90	322.88	322.90	40	0.637	0.363	0.616	0.384	0.614	0.386	0.612	0.388
323.10	323.09	323.13	40	0.708	0.292	0.672	0.328	0.673	0.327	0.672	0.328
323.20	323.15	323.19	40	0.724	0.276	0.687	0.313	0.687	0.313	0.686	0.314
323.55	323.58	323.63	40	0.807	0.193	0.765	0.235	0.765	0.235	0.764	0.236
325.55	325.56	325.56	40	1.000	0.000	1.000	0.000	1.000	0.000	1.000	0.000

Table 4.3: Benzene (1) + Cyclohexane (2) 101.5kPa.

T[K]	Cal. T[K]		P[kPa]	Exp. liquid mole fraction		Exp. gaseous mole fraction		Cal. gaseous mole fraction			
	QMR	MHV		$x_1$	$x_2$	$y_1$	$y_2$	QMR		MHV-Wilson	
								$y_1$	$y_2$	$y_1$	$y_2$
353.80	353.71	353.71	101.3	0.000	1.000	0.000	1.000	0.000	1.000	0.000	1.000
352.55	352.36	352.36	101.3	0.125	0.875	0.144	0.856	0.155	0.845	0.155	0.845
352.50	352.30	352.29	101.3	0.132	0.868	0.154	0.846	0.163	0.837	0.163	0.837
351.85	351.70	351.69	101.3	0.210	0.790	0.235	0.765	0.246	0.754	0.246	0.754
351.65	351.58	351.57	101.3	0.229	0.771	0.252	0.748	0.265	0.735	0.265	0.735
351.30	351.30	351.29	101.3	0.278	0.722	0.293	0.707	0.312	0.688	0.312	0.688
351.20	351.14	351.14	101.3	0.310	0.690	0.332	0.668	0.342	0.658	0.342	0.658
350.75	350.79	350.78	101.3	0.412	0.588	0.428	0.572	0.433	0.567	0.433	0.567
350.55	350.62	350.62	101.3	0.552	0.448	0.549	0.451	0.551	0.449	0.551	0.449
350.60	350.63	350.63	101.3	0.579	0.421	0.565	0.435	0.573	0.427	0.573	0.427
350.75	350.72	350.72	101.3	0.645	0.355	0.624	0.376	0.629	0.371	0.629	0.371
350.90	350.88	350.88	101.3	0.706	0.294	0.687	0.313	0.682	0.318	0.682	0.318
351.20	351.08	351.08	101.3	0.758	0.242	0.726	0.274	0.729	0.271	0.729	0.271
351.40	351.32	351.31	101.3	0.803	0.197	0.772	0.228	0.772	0.228	0.772	0.228
351.60	351.54	351.54	101.3	0.839	0.161	0.808	0.192	0.808	0.192	0.808	0.192
352.05	351.96	351.96	101.3	0.893	0.107	0.868	0.132	0.866	0.134	0.866	0.134
353.25	353.14	353.14	101.3	1.000	0.000	1.000	0.000	1.000	0.000	1.000	0.000

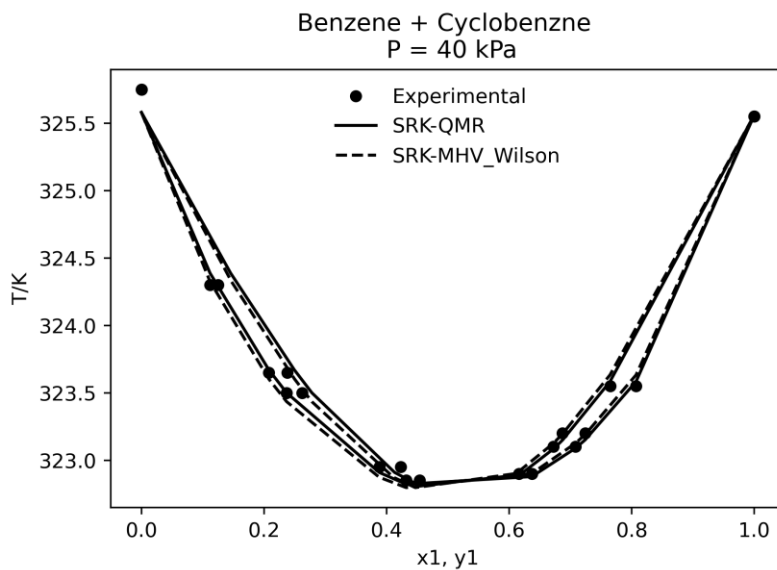


Figure 4.3: T-x,y diagram for Benzene (1) + Cyclohexane (2) at 40kPa.

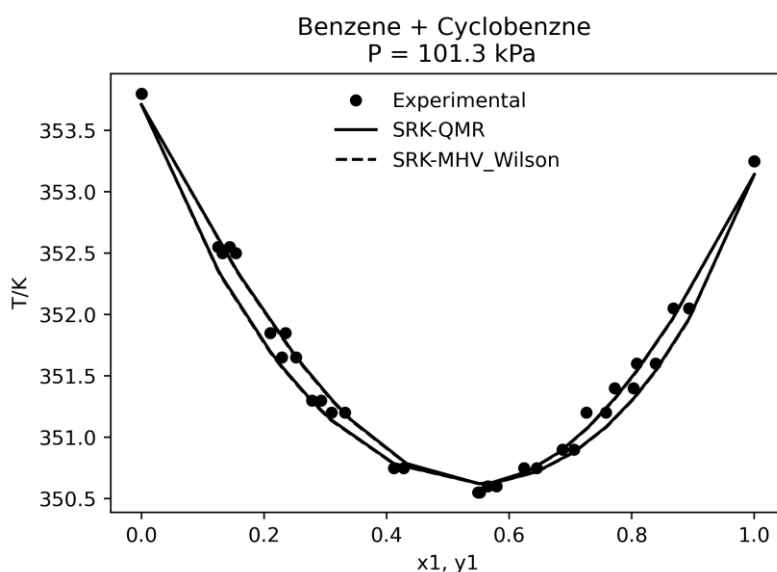


Figure 4.4: T-x,y diagram for Benzene (1) + Cyclohexane (2) at 101.3kPa.

Marlus et al. [75] studied a binary mixture of Benzene and Chlorobenzene at pressure 101.5 and 40 kPa. Tables 4.4 and 4.5 show the experimentally measured values for gaseous and liquid mole fractions at the pressure of 40 and 101.3 kPa respectively. In addition, T-x,y diagrams are also drawn in Figure 4.5. In this case, SRK is used as EoS, and two mixing rules, the quadratic mixing rule, and the Modified Huron Vidal mixing rule are compared.

Table 4.4: Benzene (1) + Chlorobenzene (2) 40 kPa.

T[K]	Cal. T[K]		P[kPa]	Exp. liquid mole fraction		Exp. gaseous mole fraction		Cal. gaseous mole fraction			
	QMR	MHV		x <sub>1</sub>	x <sub>2</sub>	y <sub>1</sub>	y <sub>2</sub>	QMR		MHV-Wilson	
								y <sub>1</sub>	y <sub>2</sub>	y <sub>1</sub>	y <sub>2</sub>
373.45	373.52	373.52	40	0.000	1.000	0.000	1.000	0.000	1.000	0.000	1.000
365.35	364.75	364.51	40	0.090	0.910	0.307	0.693	0.319	0.681	0.324	0.676
362.50	360.39	360.21	40	0.143	0.857	0.405	0.595	0.449	0.551	0.451	0.549
357.45	356.45	356.35	40	0.197	0.803	0.535	0.465	0.551	0.449	0.551	0.449
351.60	351.47	351.50	40	0.275	0.725	0.660	0.340	0.662	0.338	0.660	0.340
346.05	345.91	346.05	40	0.378	0.622	0.759	0.241	0.765	0.235	0.762	0.238
342.20	342.04	342.22	40	0.462	0.538	0.825	0.175	0.825	0.175	0.823	0.177
339.40	339.03	339.20	40	0.536	0.464	0.863	0.137	0.866	0.134	0.865	0.135
337.05	336.84	336.99	40	0.595	0.405	0.892	0.108	0.893	0.107	0.892	0.108
334.55	334.13	334.25	40	0.675	0.325	0.922	0.078	0.923	0.077	0.923	0.077
333.95	333.49	333.61	40	0.695	0.305	0.926	0.074	0.930	0.070	0.930	0.070
330.20	329.91	329.97	40	0.817	0.183	0.963	0.037	0.964	0.036	0.964	0.036
328.30	327.73	327.76	40	0.900	0.100	0.980	0.020	0.982	0.018	0.982	0.018
325.75	325.33	325.33	40	1.000	0.000	1.000	0.000	1.000	0.000	1.000	0.000



Table 4.5: Benzene (1) + Chlorobenzene (2) 101.3 kPa.

T[K]	Cal. T[K]		P[kPa]	Exp. liquid mole fraction		Exp. gaseous mole fraction		Cal. gaseous mole fraction			
	QMR	MHV		x <sub>1</sub>	x <sub>2</sub>	y <sub>1</sub>	y <sub>2</sub>	QMR		MHV-Wilson	
								y <sub>1</sub>	y <sub>2</sub>	y <sub>1</sub>	y <sub>2</sub>
404.75	404.70	404.70	101.3	0.000	1.000	0.000	1.000	0.000	1.000	0.000	1.000
397.10	396.14	396.47	101.3	0.090	0.910	0.259	0.741	0.278	0.722	0.271	0.729
388.95	387.93	388.41	101.3	0.193	0.807	0.483	0.517	0.492	0.508	0.486	0.514
382.65	382.12	382.61	101.3	0.279	0.721	0.612	0.388	0.618	0.382	0.614	0.386
376.90	375.65	376.07	101.3	0.391	0.609	0.717	0.283	0.736	0.264	0.734	0.266
372.65	372.06	372.43	101.3	0.462	0.538	0.782	0.218	0.792	0.208	0.791	0.209
369.15	368.12	368.40	101.3	0.549	0.451	0.830	0.170	0.846	0.154	0.847	0.153
367.25	366.00	366.24	101.3	0.600	0.400	0.856	0.144	0.873	0.127	0.874	0.126
363.65	361.84	361.99	101.3	0.710	0.290	0.900	0.100	0.920	0.080	0.921	0.079
360.90	358.77	358.85	101.3	0.801	0.199	0.935	0.065	0.950	0.050	0.952	0.048
357.10	356.20	356.24	101.3	0.884	0.116	0.967	0.033	0.974	0.026	0.974	0.026
356.45	355.09	355.11	101.3	0.922	0.078	0.974	0.026	0.983	0.017	0.983	0.017
355.05	353.68	353.69	101.3	0.972	0.028	0.985	0.015	0.994	0.006	0.994	0.006
353.25	352.92	352.92	101.3	1.000	0.000	1.000	0.000	1.000	0.000	1.000	0.000

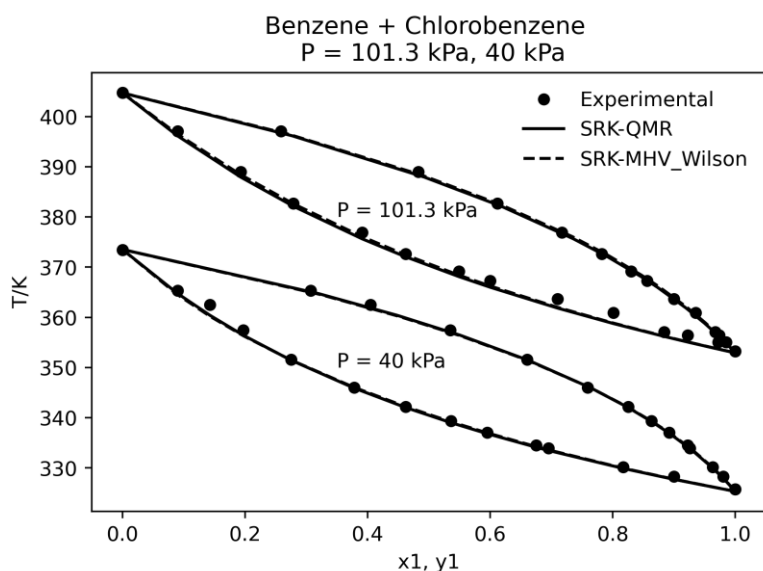


Figure 4.5: T-x,y diagram for Benzene (1) + Chlorobenzene (2) at P = 40 kPa, and P = 101.3kPa.

Marlus et al. [75] studied a binary mixture of Cyclohexane and Chlorobenzene at the pressure of 101.5 and 40 kPa. Tables 4.6 and 4.7 present the experimentally measured values for gaseous and liquid mole fractions at the pressure of 40 and 101.3 kPa respectively. In addition, T-x,y

## 4 Results and Discussion

diagrams are also drawn in Figure 4.6. In this case, SRK is used as EoS, and two mixing rules, the quadratic mixing rule, and the Modified Huron Vidal mixing rule are compared.

Table 4.6: Cyclohexane (1) + Chlorobenzene (2) 40 kPa.

T[K]	Cal. T[K]		P[kPa]	Exp. liquid mole fraction		Exp. gaseous mole fraction		Cal. gaseous mole fraction			
				x <sub>1</sub>	x <sub>2</sub>	y <sub>1</sub>	y <sub>2</sub>	QMR		MHV-Wilson	
	QMR	MHV						y <sub>1</sub>	y <sub>2</sub>	y <sub>1</sub>	y <sub>2</sub>
373.45	373.52	373.52	40	0.000	1.000	0.000	1.000	0.000	1.000	0.000	1.000
369.25	369.47	367.90	40	0.021	0.979	0.160	0.840	0.142	0.858	0.185	0.815
362.45	363.16	360.85	40	0.060	0.940	0.351	0.649	0.333	0.667	0.381	0.619
348.25	347.01	347.65	40	0.228	0.772	0.640	0.360	0.686	0.314	0.665	0.335
344.95	344.21	345.46	40	0.277	0.723	0.690	0.310	0.732	0.268	0.704	0.296
340.55	339.86	341.74	40	0.376	0.624	0.773	0.227	0.796	0.204	0.768	0.232
337.25	337.16	339.12	40	0.457	0.543	0.826	0.174	0.833	0.167	0.811	0.189
334.35	334.38	336.11	40	0.560	0.440	0.869	0.131	0.870	0.130	0.857	0.143
330.35	331.98	333.27	40	0.666	0.334	0.923	0.077	0.902	0.098	0.899	0.101
328.70	329.67	330.45	40	0.780	0.220	0.944	0.056	0.934	0.066	0.938	0.062
328.10	328.79	329.37	40	0.826	0.174	0.953	0.047	0.947	0.053	0.952	0.048
326.65	327.03	327.27	40	0.919	0.081	0.979	0.021	0.974	0.026	0.979	0.021
325.95	325.52	325.52	40	1.000	0.000	1.000	0.000	1.000	0.000	1.000	0.000

Table 4.7: Cyclohexane (1) + Chlorobenzene (2) 40 kPa.

T[K]	Cal. T[K]		P[kPa]	Exp. liquid mole fraction		Exp. gaseous mole fraction		Cal. gaseous mole fraction			
				x <sub>1</sub>	x <sub>2</sub>	y <sub>1</sub>	y <sub>2</sub>	QMR		MHV-Wilson	
	QMR	MHV						y <sub>1</sub>	y <sub>2</sub>	y <sub>1</sub>	y <sub>2</sub>
404.75	404.70	404.70	101.3	0.000	1.000	0.000	1.000	0.000	1.000	0.000	1.000
391.35	392.06	391.29	101.3	0.105	0.895	0.362	0.638	0.364	0.636	0.378	0.622
378.75	378.43	377.26	101.3	0.280	0.720	0.638	0.362	0.651	0.349	0.663	0.337
372.55	373.30	372.12	101.3	0.375	0.625	0.760	0.240	0.736	0.264	0.746	0.254
369.60	369.61	368.48	101.3	0.458	0.542	0.810	0.190	0.792	0.208	0.798	0.202
365.75	364.43	363.52	101.3	0.600	0.400	0.850	0.150	0.863	0.137	0.865	0.135
362.35	361.52	360.81	101.3	0.694	0.306	0.892	0.108	0.900	0.100	0.900	0.100
360.95	359.18	358.67	101.3	0.777	0.223	0.914	0.086	0.930	0.070	0.928	0.072
359.35	357.45	357.11	101.3	0.842	0.158	0.928	0.072	0.951	0.049	0.948	0.052
356.05	354.65	354.56	101.3	0.953	0.047	0.940	0.060	0.986	0.014	0.984	0.016
353.80	353.50	353.50	101.3	1.000	0.000	1.000	0.000	1.000	0.000	1.000	0.000

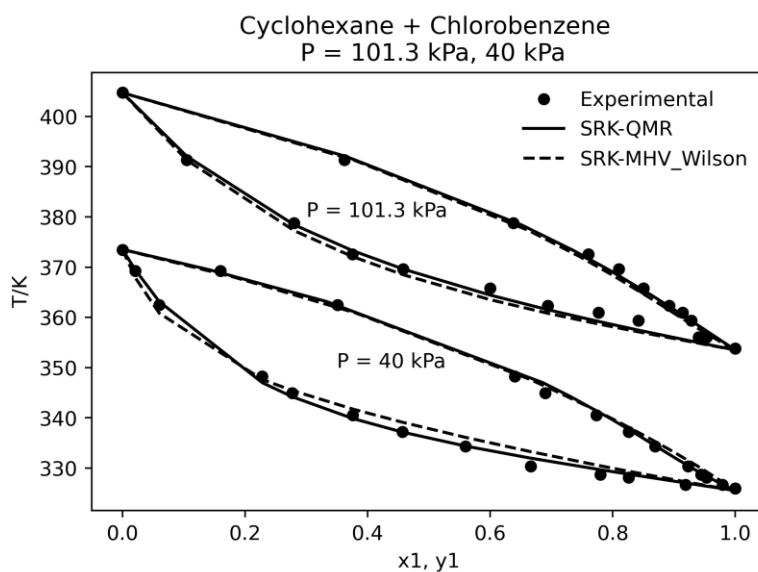


Figure 4.6: T-x,y diagram for Cyclohexane (1) + Chlorobenzene (2) at P = 40 kPa, and P = 101.3kPa.

To study the consistency of EoS and mixing rules for the abovementioned binary mixtures, average absolute relative deviation (AARD), Equation (4.4), and absolute maximum deviation (AMD), Equation (4.5), are calculated.

$$AARD = \frac{1}{n} \sum_{i=1}^n \frac{|Exp_i - Cal_i|}{Exp_i} \times 100 \quad (4.4)$$

$$AMD = \text{Max}(|Exp_i - Cal_i|) \quad i = 1, 2, \dots, n \quad (4.5)$$

For the described three different binary mixtures at two different pressures, values of AARD and AMD are depicted in Table 4.8.

Table 4.8: Calculated AARD and AMD for binary mixtures at P = 40 and 101.3 kPa.

Mixture	P [kPa]	EoS	Mix. rule	AARD (%)	AMD
<b>Benzene + Cyclohexane</b>	40	SRK	QMR	2.87	0.020
			MHV	3.09	0.021
	101.3	SRK	QMR	2.49	0.019
			MHV	2.26	0.019
<b>Benzene + Chlorobenzene</b>	40	SRK	QMR	1.42	0.043
			MHV	1.55	0.046
	101.3	SRK	QMR	1.73	0.019
			MHV	1.43	0.021

<b>Cyclohexane + Chlorobenzene</b>	40	SRK	QMR	2.93	0.045
			MHV	2.88	0.030
	101.3	SRK	QMR	1.77	0.045
			MHV	2.06	0.043

As it is shown, at a pressure of 40 kPa, SRK-QMR is the better model to predict the equilibrium of the Benzene (1) + Cyclohexane (2) mixture. However, at pressure 101.3 kPa, SRK-QMR and SRK-MHV-Wilson are so closed, and SRK-MHV-Wilson is the more appropriate model to predict the equilibrium of mixture.

In the case of the Benzene + Chlorobenzene mixture, in lower pressure, SRK-QMR is the better model and experimental results are perfectly predicted. However, at Pressure 101.3 kPa SRK-MHV\_Wilson is the better model to predict the system.

In the case of Cyclohexane + Chlorobenzene mixture, in lower pressure, SRK-MHV\_Wilson is the better model to be fitted with the experimental results. Moreover, at Pressure – 101.3 kPa the SRK-QMR can provide more accurate results.

For all these binary mixtures, Marlus et al. [75] proved the thermodynamic consistency of experimental results by applying the area test [76], the point-to-point test of Van Ness-Fredenslund [77], and based on Wilsak and Philip analysis [78]. It means, the results of this article possess adequate quality to evaluate the accuracy of Phasepy in calculating the phase equilibrium of binary mixtures. On the other hand, small values for AARD and AMD in calculating the phase equilibrium show that Phasepy can be considered a reliable thermodynamics' package.

Thomas et al. [79] experimentally studies the phase equilibrium of LNG. The authors indeed performed experiments on two different four components' mixtures, and then tried to model the behaviors using PR EoS. This study is to model these two mixtures and then compare PR EoS and SRK EoS. In addition, as a mixing rule, QMR is utilized.

First mixture account for CH<sub>4</sub>, C<sub>2</sub>H<sub>6</sub>, C<sub>3</sub>H<sub>8</sub>, and i-C<sub>4</sub>H<sub>10</sub>. Firstly, at the different pressure and temperature, it is tried to predict the gaseous and liquid mole fraction according to the initial mole fraction, Table 4.10. As it is shown in Table 4.11, the developed model based on SRK EoS predicts the mole fractions with the consistent R<sup>2</sup>. Figure 4.7 shows the P-x,y diagram for CH<sub>4</sub> mole fraction according to experimental results and developed models output in Table 4.12.

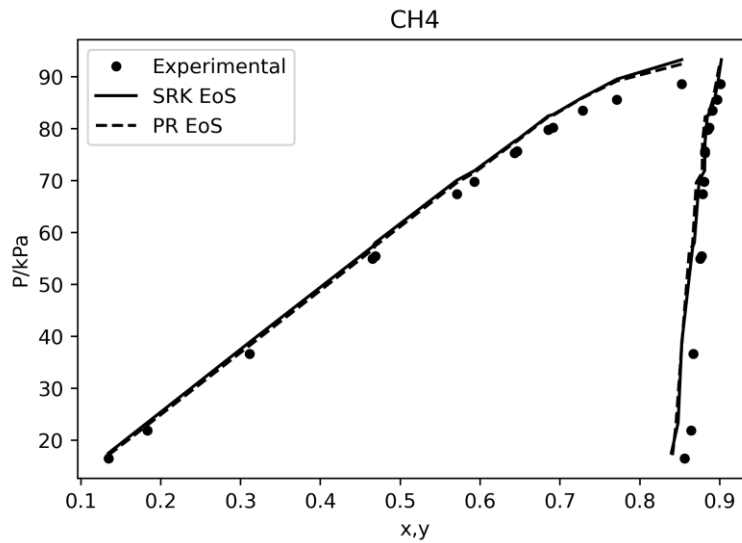


Figure 4.7: P-x,y diagram for CH4 in CH4, C2H6, C3H8, and i-C4H10 mixture.

The second mixture accounts for CH4, C2H6, C3H8, and n-C4H10. By changing pressure and temperature, gaseous and liquid mole fractions are predicted using SRK EoS and according to the initial mole fraction, as shown in Table 4.13, and Table 4.14 shows R2 for these predictions. Figure 4.8 and Table 4.15 also depict the P-x,y diagram and results respectively for CH4 mole fraction based on PR and SRK EoS.

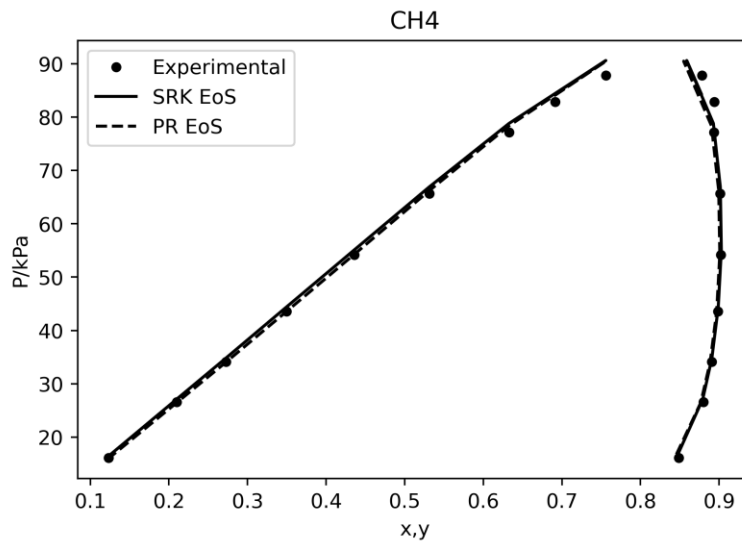


Figure 4.8. P-x,y diagram for CH4 in CH4, C2H6, C3H8, and i-C4H10 mixture.

As it is shown in Fig 3-7 and according to data of 3-12, SRK is a better EoS for modeling this mixture.

To compare the SRK EoS and PR EoS, AARD (Equation (4.4)) and AMD (Equation (4.5)) are again calculated.

Table 4.9: Calculated AARD and AMD for binary mixtures at  $T = 243.60$  K.

Mixture	T [K]	EoS	Mix. rule	AARD (%)	AMD [ $x_i$ ]
CH <sub>4</sub> , C <sub>2</sub> H <sub>6</sub> , C <sub>3</sub> H <sub>8</sub> , and n-C <sub>4</sub> H <sub>10</sub>	243.60	SRK	QMR	0.79	0.029
		PR		0.83	0.032
CH <sub>4</sub> , C <sub>2</sub> H <sub>6</sub> , C <sub>3</sub> H <sub>8</sub> , and i-C <sub>4</sub> H <sub>10</sub>	243.60	SRK	QMR	0.30	0.019
		PR		0.53	0.023

As it is shown in Figure 4.7 and Table 4.9, PR and SRK EoS both, are an adequate choice for modeling the CH<sub>4</sub>, C<sub>2</sub>H<sub>6</sub>, C<sub>3</sub>H<sub>8</sub>, and i-C<sub>4</sub>H<sub>10</sub> mixture. Although Thomas et al. [79] did not investigate the SRK EoS, based on these results, SRK-QMR model is the better model in comparison with PR-QMR. In addition, this study shows that for CH<sub>4</sub>, C<sub>2</sub>H<sub>6</sub>, C<sub>3</sub>H<sub>8</sub>, and n-C<sub>4</sub>H<sub>10</sub> mixture, SRK-QMR model provide more accurate output rather than PR-QMR model. Although Thomas et al. [79] compared PR EoS the multi-parameter EOS of the Groupe Européen de Recherches Gazières (GERG) [80], and showed that the PR EoS is a better alternative.

#### 4.1.2 SRK modeling

It is also tried to model SRK EoS in combination with linear mixing rule for parameter  $b$  and quadratic mixing rule for parameter  $\alpha$ .

$$b = \sum x_i b_i \quad (4.6)$$

$$\alpha = \sum_i \sum_j x_i x_j \alpha_{ij} \quad (4.7)$$

$$\alpha_{ij} = (\alpha_i \alpha_j)^{1/2} \quad (4.8)$$

$$\alpha_{ij} = \alpha_{ji} \quad (4.9)$$

These mixing rules can be utilized for gaseous and liquid mixtures both.  $\alpha$  and  $b$  are indeed two positive constants related to a particular species. In a better word,  $b_i$  is for species  $i$  and  $\alpha$  shows the interaction between two species. It is worth saying that evaluating mixture parameters based on the parameter for pure substances solely is known as van der Waals prescriptions. In addition,  $\alpha$  for a pure species is a function of temperature. In the case of SRK EoS:

$$\alpha_{SRK}(T_r, \omega) = \left[ 1 + (0.48 + 1.574\omega - 0.176\omega^2)(1 - T_r^{1/2}) \right]^2 \quad (4.10)$$

Where:

$T_r$  = Reduced Temperature  $T/T_c$

$\omega$  = specific parameter to a chemical species

To calculate the mixture parameters, the following Equations (4.11) to (4.14) are applied

$$\alpha^l = x_1^2 \alpha_1 + 2x_1 x_2 \sqrt{\alpha_1 \alpha_2} + x_2^2 \alpha_2 \quad (4.11)$$

$$b^l = x_1 b_1 + x_2 b_2$$

$$\bar{q}_1^l = q^l \left( \frac{2x_1 \alpha_1 + 2x_2 \sqrt{\alpha_1 \alpha_2}}{\alpha^l} - \frac{b_1}{b^l} \right) \quad (4.12)$$

$$\bar{q}_2^l = q^l \left( \frac{2x_2 \alpha_2 + 2x_1 \sqrt{\alpha_1 \alpha_2}}{\alpha^l} - \frac{b_2}{b^l} \right) \quad (4.13)$$

$$q^l = \frac{\alpha^l}{b^l RT} \quad (4.14)$$

These Equations can also be applied to liquid by replacing  $x$  with  $y$ . Then by applying vapor or liquid related parameters and considering  $\varepsilon = 1$  and  $\sigma = 1$  for the SRK EoS. compressibility factor ( $Z$ ) and  $I$  can be calculated by Equation (4.15) and (4.16) respectively:

$$Z = \beta + Z(Z + \beta) \left( \frac{1 + \beta - Z}{q\beta} \right) \quad (4.15)$$

$$I = \frac{1}{\sigma - \varepsilon} \ln \left( \frac{Z + \sigma\beta}{Z + \varepsilon\beta} \right) \quad (4.16)$$

$$\beta = \frac{bP}{RT} \quad (4.17)$$

By knowing  $Z$  and  $I$ , the fugacity coefficient can also be calculated with Equation (4.18):

$$\ln \Phi = \frac{b_i}{b} (Z - 1) - \ln(Z - \beta) - \bar{q}_i I \quad (4.18)$$

now by knowing  $K_i = \frac{\Phi_i^l}{\phi_i^v}$ , the constraint  $\sum y_i = 1$  should be imposed.

If  $\sum K_i x_i \neq 1$ , a new value for  $y_i$  should be calculated throughout the normalizing Equation (4.19)

$$y_i = \frac{K_i x_i}{\sum_i^n K_i x_i} \text{ and } y_n = 1 - \sum_1^{n-1} y_i \quad (4.19)$$

Now new values for  $y$  would reevaluate new values for  $K$  and  $\Phi$ , then this iteration is continued by leading  $\sum K_i x_i$  into unit. In case of no convergence of  $\sum K_i x_i$ , the value for pressure should

also be changed. If  $\sum K_i x_i < 1$ , P should be decreased, and in case of  $\sum K_i x_i > 1$ , P should be reduced.

The aforementioned algorithm is applied to the results of an experimental study performed by SAGE et al. [81]. The authors tried to measure the bubble pressure of the methane (1)/n-butane (2) mixture. The performed algorithm is completely fitted with these experimental results, as shown in Figure 4.9 (Python code scripts is provided in Appendix C).

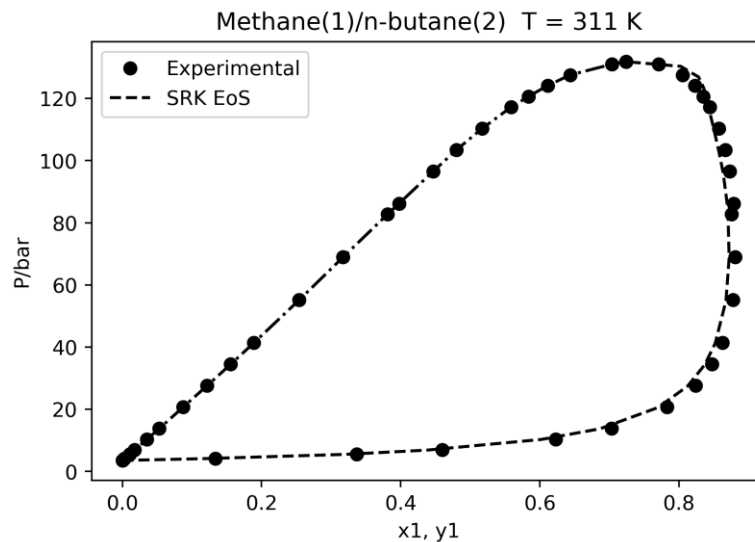


Figure 4.9: P-x,y diagram for methane(1)/n-butane (2) mixture at T = 311K, experiment and SRK EoS.

To evaluate the accuracy of developed algorithm in this case, AARD and AMD are also calculated. The developed model for calculating the bubble points based on the SRK EoS accounts for **AARD = 0.54%** and **AMD = 0.031** (difference in mole fraction of Methane) in comparison with experimental results.

## 4.2 LN<sub>2</sub> behavior throughout the Vaporizer

The model on the vaporizer is developed to evaluate the performance of heater at three different mass flow rates. Mass flow rate of 0.5, 1, and 2 Kg/h are studied.

Figures 4.10, 4.11, and 4.12 present the calculated temperature, heat rate and mole fraction of vapour along the heater for mass flow rate of 0.5 kg/hr of LN<sub>2</sub>. Figure 4.12 shows the liquid is fully evaporated at approximately 10 mm. Based on the Figure 4.10 the flow is going out from the vaporizer in superheated state with the temperature of 370 k. it is worth saying that the heat transfer rate is modelled as laminar in the superheated vapour.



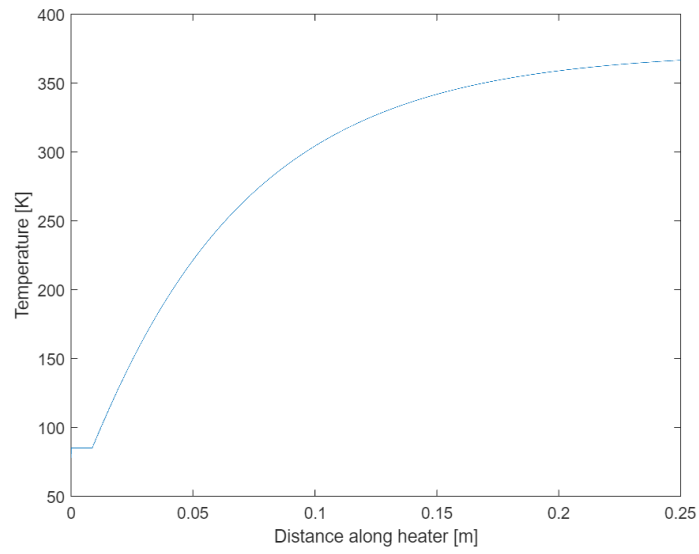


Figure 4.10: Calculated temperature along vaporizer at LN<sub>2</sub> flow rate of 0.5 kg/hr.

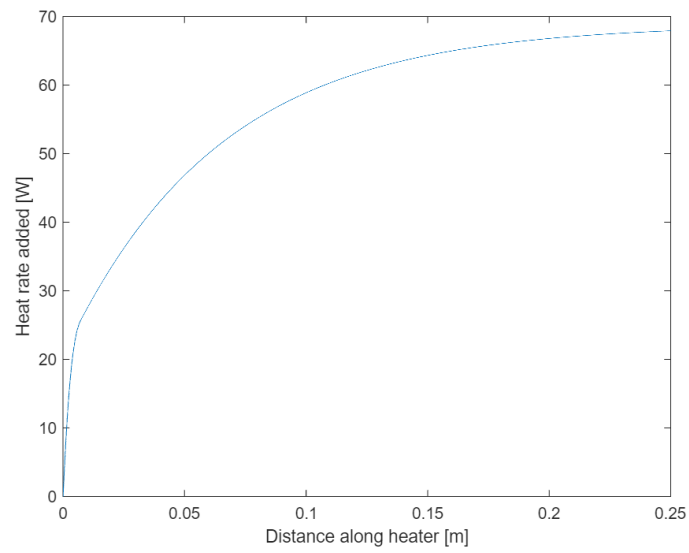


Figure 4.11: Calculated cumulative heat rate along vaporizer at LN<sub>2</sub> flow rate of 0.5 kg/hr.

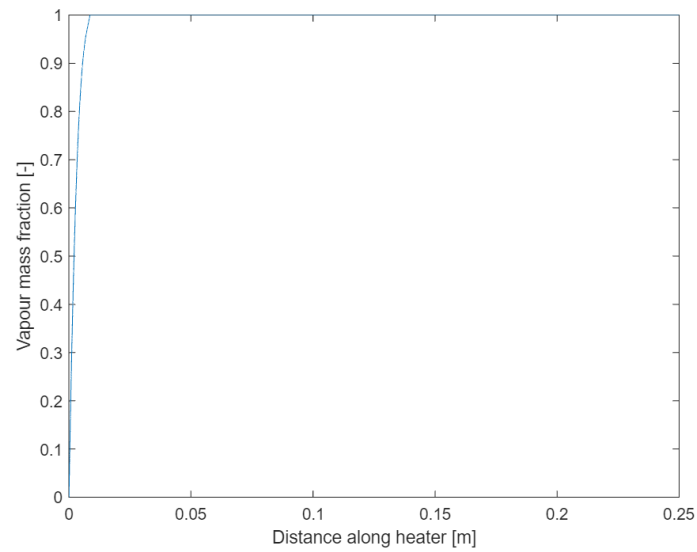


Figure 4.12: Calculated mole fraction of vaporizer at LN<sub>2</sub> flow rate of 0.5 kg/hr.

Figures 4.13, 4.14, and 4.15 depict the calculated temperature, heat rate and mole fraction of vapour along the heater for mass flow rate of 1 kg/hr of LNG. Figure 4.15 shows the liquid is fully evaporated at approximately 25 mm. Based on the Figure 4.13 the flow is going out from the vaporizer in superheated state with the temperature of between 320 and 330 k. it is worth saying that the heat transfer rate is modelled as laminar in the superheated vapour, although the calculated  $Re$  number says that the flow at the outlet of heater should be in early transition.

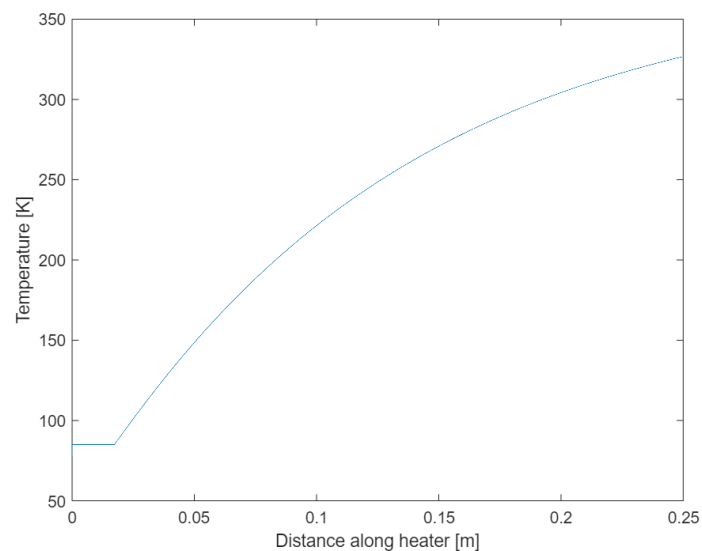


Figure 4.13: Calculated temperature along vaporizer at LN<sub>2</sub> flow rate of 1 kg/hr.

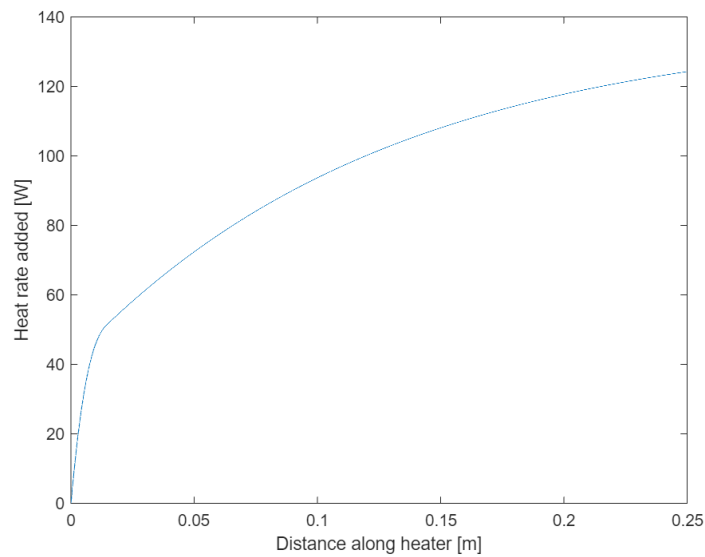


Figure 4.14: Calculated cumulative heat rate along vaporizer at LN<sub>2</sub> flow rate of 1 kg/hr.

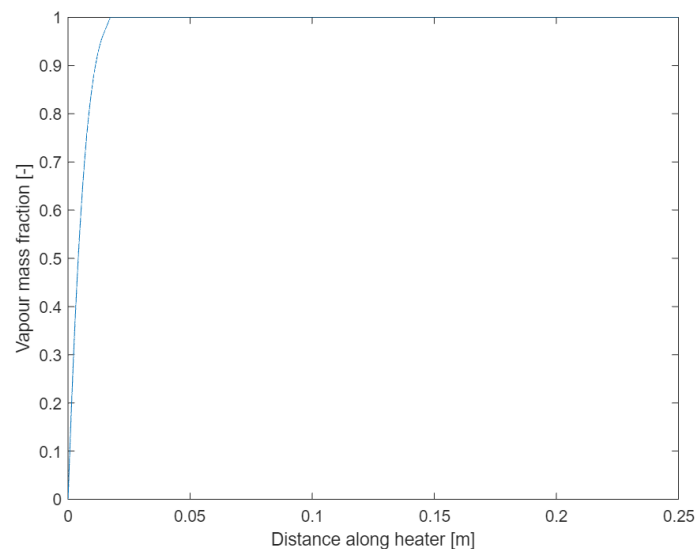


Figure 4.15: Calculated mole fraction of vaporizer at LN<sub>2</sub> flow rate of 1 kg/hr.

Figures 4.16, 4.17, and 4.18 show the calculated temperature, heat rate and mole fraction of vapour along the heater for mass flow rate of 2 kg/hr of LNG. Figure 4.18 depicts the liquid is fully evaporated at approximately 35 mm from the inlet. While, Because of probability of accruing liquid hold-up it is not desirable. Based on the Figure 4.17 the flow is going out from the vaporizer with the temperature of between 240 and 250 k, which it is not applicable for the flowmeter after vaporizer. Then a post heating facility is required.

## 4 Results and Discussion

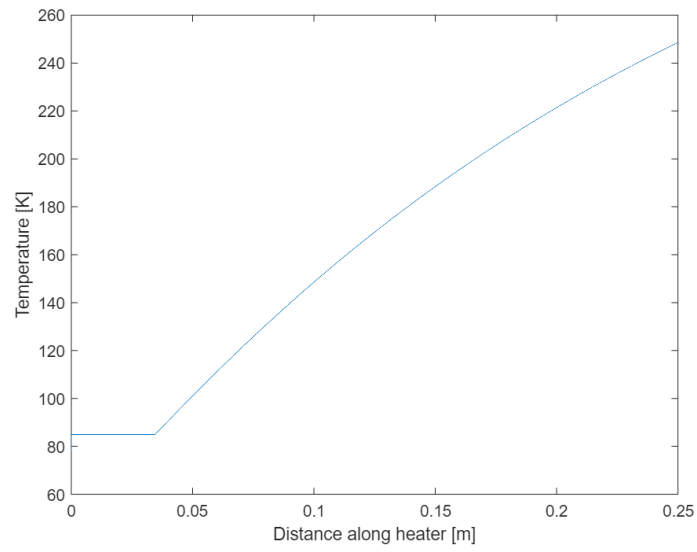


Figure 4.16: Calculated temperature along vaporizer at LN<sub>2</sub> flow rate of 2 kg/hr.

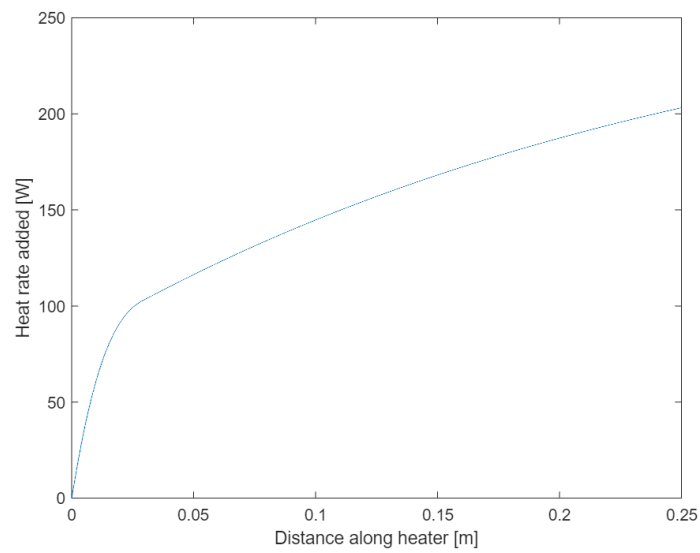


Figure 4.17: Calculated cumulative heat rate along vaporizer at LN<sub>2</sub> flow rate of 2 kg/hr.

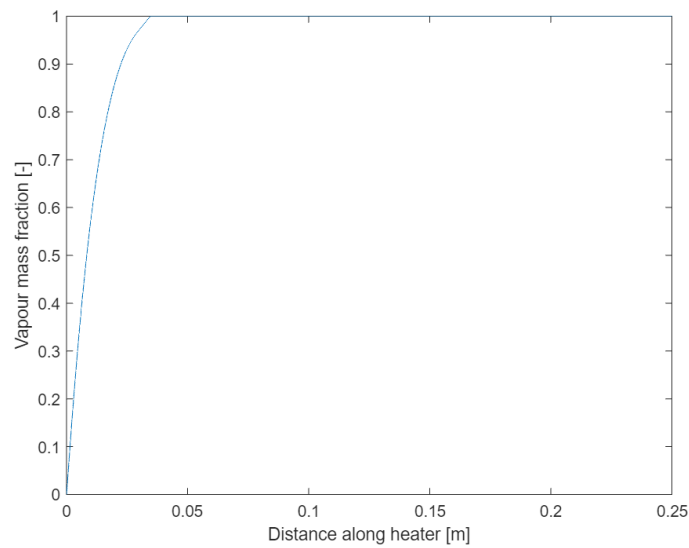


Figure 4.18: Calculated mole fraction of vaporizer at LN<sub>2</sub> flow rate of 2 kg/hr.

By comparing the vapor mass fraction and Temperature diagrams, it is obvious that while the liquid Nitrogen is evaporating, temperature is constant, and where the LN<sub>2</sub> is fully evaporated the temperature starts increasing. In addition, the added heat by this distance divided by mass flow rate should represent the specific heat of LN<sub>2</sub> ( $h_{fg}$ ) at the condition of vaporizing. And the second part of added heat diagrams represents the required heat for increasing the temperature of N<sub>2</sub>.

### 4.3 Post heating

Mainly helical tubes are preferred to straight tubes because of better heat transfer. To design a fluid-to-fluid helical heat exchanger, it is required to know the mechanisms of heat transfer on each side of the tube. Type of the flow inside the tube, properties of the surrounding bath, and direction of immersion, vertically or horizontally are the most effective variables that should be considered throughout studying the heat transfer phenomenon.

Performing the algorithm based on the Figure 3.10, provides following results, shown in Figure 4.19, for mas flow rate of 2 Kg/h. It is obvious that by increasing the initial flow velocity, the required pipe length increases. In addition, by increasing the initial temperature, the output target temperature is obtained within less pipe length. The model is developed for the case that a helically coiled stainless steel with inside diameter of ¼ in is immersed into water bath with temperature of 340 K and it is desired to have the outlet temperature of 280 K. Program code scripts is provided in Appendix B.

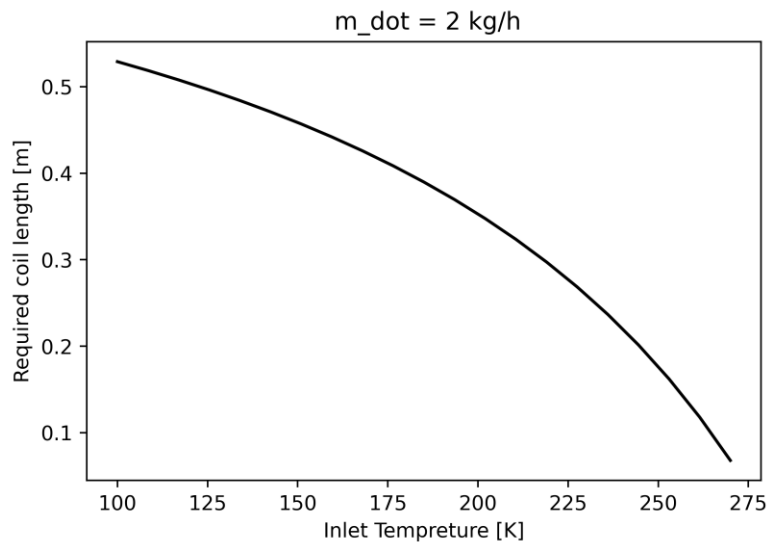


Figure 4.19: the change of required helical pipe length with changing initial flow temperature.

It is worth saying that the effect of pressure drop is not considered for the defined algorithm.

#### 4.4 Future Experimental necessity

Provided model on behaviour of LN<sub>2</sub> throughout the vaporizer, developed model for post heating facility, prepared LabVIEW program for measuring the temperature and flowrate, and prepared procedure for accurate sampling experiments need to be validated. The predicted future experiments should evaluate the aforementioned models and procedure.

Table 4.10: CH<sub>4</sub>+C<sub>2</sub>H<sub>6</sub>+C<sub>3</sub>H<sub>8</sub>+i-C<sub>4</sub>H<sub>10</sub> SRK EoS.

T[K]	P[bar]	Exp. liquid mole fraction				Cal. liquid mole fraction				Exp. gaseous mole fraction				Cal. gaseous mole fraction			
		x <sub>1</sub>	x <sub>2</sub>	x <sub>3</sub>	x <sub>4</sub>	x <sub>1</sub>	x <sub>2</sub>	x <sub>3</sub>	x <sub>4</sub>	y <sub>1</sub>	y <sub>2</sub>	y <sub>3</sub>	y <sub>4</sub>	y <sub>1</sub>	y <sub>2</sub>	y <sub>3</sub>	y <sub>4</sub>
203.26	35.13	0.5903	0.1887	0.1075	0.1135	0.5660	0.1984	0.1140	0.1217	0.9588	0.0350	0.0047	0.0015	0.9622	0.0328	0.0037	0.0012
213.40	40.31	0.5481	0.1978	0.122	0.1321	0.5254	0.2055	0.1285	0.1406	0.9433	0.0466	0.0072	0.0029	0.9465	0.0447	0.0064	0.0024
223.50	47.76	0.5406	0.1908	0.1274	0.1413	0.5200	0.1982	0.1323	0.1495	0.9249	0.0583	0.0115	0.0053	0.9298	0.0556	0.0101	0.0045
223.51	45.38	0.5150	0.2005	0.1341	0.1504	0.4928	0.2058	0.1412	0.1603	0.9258	0.0585	0.0108	0.0049	0.9288	0.0567	0.0101	0.0044
233.56	50.37	0.4875	0.1983	0.1449	0.1693	0.4675	0.2006	0.1514	0.1805	0.9073	0.0698	0.0153	0.0077	0.9096	0.0680	0.0150	0.0075
243.61	55.28	0.4661	0.1923	0.1529	0.1887	0.4479	0.1921	0.1587	0.2013	0.8865	0.0802	0.0213	0.0121	0.8891	0.0779	0.0210	0.0121
243.72	58.63	0.4905	0.1829	0.1458	0.1807	0.4756	0.1874	0.1493	0.1877	0.8850	0.0789	0.0222	0.0138	0.8892	0.0771	0.0212	0.0125
253.61	60.16	0.4488	0.1836	0.1581	0.2095	0.4337	0.1817	0.1625	0.2220	0.8648	0.0890	0.0281	0.0181	0.8673	0.0862	0.0279	0.0186
263.57	65.02	0.4360	0.1737	0.1599	0.2304	0.4242	0.1708	0.1629	0.2421	0.8418	0.0963	0.0355	0.0264	0.8440	0.0929	0.0355	0.0276
273.49	69.87	0.4281	0.1641	0.1586	0.2492	0.4187	0.1600	0.1603	0.2610	0.8119	0.1030	0.0449	0.0402	0.8188	0.0983	0.0433	0.0396

Table 4.11: R<sup>2</sup> between calculated mole fraction based on SRK EoS and experimental results for. CH<sub>4</sub>+C<sub>2</sub>H<sub>6</sub>+C<sub>3</sub>H<sub>8</sub>+i-C<sub>4</sub>H<sub>10</sub> mixture.

Experimental vs Computational								
	x <sub>1</sub>	x <sub>2</sub>	x <sub>3</sub>	x <sub>4</sub>	y <sub>1</sub>	y <sub>2</sub>	y <sub>3</sub>	y <sub>4</sub>
R <sup>2</sup>	0.95	0.99	0.98	0.98	0.99	0.99	0.99	0.99

## 4 Results and Discussion

Table 4.12: Calculated gaseous mole fraction for CH<sub>4</sub>+C<sub>2</sub>H<sub>6</sub>+C<sub>3</sub>H<sub>8</sub>+i-C<sub>4</sub>H<sub>10</sub> mixture.

T[K]	P[bar]	Cal. P[bar]	Exp. liquid mole fraction				Exp. liquid mole fraction				Cal. gaseous mole fraction PR				Cal. gaseous mole fraction SRK			
			x <sub>1</sub>	x <sub>2</sub>	x <sub>3</sub>	x <sub>4</sub>	x <sub>1</sub>	x <sub>2</sub>	x <sub>3</sub>	x <sub>4</sub>	y <sub>1</sub>	y <sub>2</sub>	y <sub>3</sub>	y <sub>4</sub>	y <sub>1</sub>	y <sub>2</sub>	y <sub>3</sub>	y <sub>4</sub>
243.60	54.98	56.67	0.4652	0.1931	0.1539	0.1878	0.8852	0.0807	0.0218	0.0123	0.8855	0.0800	0.0219	0.0126	0.8876	0.0790	0.0212	0.0120
243.60	69.81	71.53	0.5929	0.1624	0.1116	0.133	0.8813	0.0783	0.0242	0.0163	0.8818	0.0776	0.0241	0.0165	0.8844	0.0764	0.0233	0.0157
243.60	75.63	77.59	0.6462	0.1418	0.0962	0.1158	0.887	0.0722	0.0237	0.0171	0.8780	0.0752	0.0265	0.0202	0.8810	0.0740	0.0256	0.0192
243.60	75.31	77.33	0.6432	0.1422	0.0971	0.1176	0.8786	0.0751	0.0262	0.02	0.8786	0.0749	0.0264	0.0201	0.8816	0.0737	0.0255	0.0191
243.60	80.19	82.54	0.6913	0.1245	0.0831	0.1013	0.8804	0.0713	0.0266	0.0216	0.8706	0.0745	0.0297	0.0253	0.8742	0.0731	0.0286	0.0239
243.60	83.45	85.91	0.7283	0.1113	0.0722	0.0882	0.8757	0.0704	0.0287	0.0252	0.8620	0.0747	0.0328	0.0305	0.8661	0.0733	0.0315	0.0288
243.60	85.59	89.16	0.7712	0.0979	0.0597	0.0713	0.8668	0.0714	0.0316	0.0302	0.8408	0.0792	0.0393	0.0407	0.8394	0.0796	0.0397	0.0412
243.60	88.56	92.42	0.8524	0.0745	0.0361	0.037	0.8558	0.0733	0.0352	0.0327	0.8524	0.0745	0.0361	0.0370	0.8524	0.0744	0.0360	0.0369
243.60	79.78	82.27	0.6854	0.1169	0.0857	0.112	0.8816	0.0667	0.0275	0.0242	0.8785	0.0676	0.0285	0.0255	0.8818	0.0664	0.0275	0.0241
243.60	67.39	69.59	0.5707	0.1414	0.1216	0.1662	0.8969	0.0639	0.0226	0.0166	0.8959	0.0638	0.0231	0.0173	0.8982	0.0629	0.0223	0.0164
243.60	55.44	57.41	0.4686	0.1576	0.1547	0.2194	0.9008	0.0648	0.0209	0.0135	0.9000	0.0643	0.0214	0.0143	0.9020	0.0635	0.0208	0.0136
243.60	36.67	38.23	0.3112	0.1684	0.2075	0.3129	0.891	0.0727	0.023	0.0133	0.8920	0.0714	0.0230	0.0136	0.8940	0.0705	0.0223	0.01306
243.60	21.89	22.94	0.1834	0.157	0.2513	0.4083	0.8642	0.0879	0.0309	0.017	0.8658	0.0864	0.0304	0.0173	0.8682	0.0854	0.0297	0.0166
243.60	16.51	17.14	0.1345	0.1426	0.2665	0.4556	0.8772	0.0975	0.0375	0.0207	0.8452	0.0961	0.0373	0.0215	0.8478	0.0950	0.0364	0.0206



Table 4.13: CH<sub>4</sub>+C<sub>2</sub>H<sub>6</sub>+C<sub>3</sub>H<sub>8</sub>+n-C<sub>4</sub>H<sub>10</sub> SRK EoS.

T[K]	P[bar]	Exp. liquid mole fraction				Cal. liquid mole fraction				Exp. gaseous mole fraction				Cal. gaseous mole fraction			
		x <sub>1</sub>	x <sub>2</sub>	x <sub>3</sub>	x <sub>4</sub>	x <sub>1</sub>	x <sub>2</sub>	x <sub>3</sub>	x <sub>4</sub>	y <sub>1</sub>	y <sub>2</sub>	y <sub>3</sub>	y <sub>4</sub>	y <sub>1</sub>	y <sub>2</sub>	y <sub>3</sub>	y <sub>4</sub>
203.24	38.82	0.648	0.1794	0.0861	0.0866	0.6321	0.1857	0.0880	0.0941	0.9595	0.0350	0.0042	0.0013	0.9627	0.0331	0.0034	0.0008
213.35	45.76	0.6186	0.1881	0.0952	0.0981	0.6010	0.1944	0.0978	0.1069	0.9449	0.0467	0.0066	0.0018	0.9463	0.0460	0.0060	0.0018
223.45	52.55	0.5854	0.1944	0.1062	0.1141	0.5725	0.1987	0.1073	0.1215	0.9244	0.0619	0.0104	0.0034	0.9271	0.0598	0.0097	0.0034
233.44	56.87	0.5371	0.2024	0.1217	0.1388	0.5265	0.2050	0.1223	0.1462	0.9042	0.0753	0.0150	0.0056	0.9060	0.0738	0.0144	0.0058
233.48	59.36	0.5595	0.1947	0.1141	0.1317	0.5504	0.1979	0.1151	0.1366	0.9039	0.0745	0.0154	0.0062	0.9061	0.0732	0.0146	0.0062
243.49	63.15	0.5164	0.1986	0.1288	0.1562	0.5080	0.1996	0.1285	0.1639	0.8834	0.0869	0.0207	0.0090	0.8842	0.0859	0.0202	0.0098
243.51	65.83	0.5389	0.1931	0.1223	0.1457	0.5307	0.1941	0.1215	0.1537	0.8826	0.0864	0.0210	0.0099	0.8837	0.0854	0.0205	0.0103
243.51	63.80	0.5149	0.1989	0.1294	0.1568	0.5134	0.1983	0.1268	0.1614	0.8830	0.0869	0.0208	0.0094	0.8840	0.0858	0.0203	0.0099
253.52	72.23	0.5213	0.1878	0.1268	0.1641	0.5163	0.1875	0.1253	0.1709	0.8591	0.0970	0.0281	0.0159	0.8603	0.0960	0.0273	0.0164
263.46	78.20	0.5056	0.1807	0.1292	0.1844	0.5045	0.1798	0.1269	0.1888	0.8341	0.1060	0.0357	0.0242	0.8361	0.1046	0.0346	0.0247
273.41	84.21	0.4975	0.1727	0.1282	0.2014	0.4981	0.1712	0.1256	0.2051	0.8076	0.1131	0.0437	0.0357	0.8103	0.1115	0.0421	0.0361
248.14	79.16	0.6183	0.1205	0.1234	0.1378	0.6106	0.1691	0.0975	0.1228	0.8858	0.0632	0.0322	0.0322	0.8654	0.0913	0.0263	0.0170
238.14	72.94	0.6519	0.1229	0.1145	0.1107	0.6403	0.1661	0.0889	0.1048	0.9035	0.0585	0.0258	0.0258	0.8905	0.0789	0.0196	0.0110
228.17	66.09	0.6885	0.1234	0.1022	0.0859	0.6740	0.1588	0.0789	0.0883	0.9223	0.0513	0.0513	0.0189	0.9151	0.0646	0.0136	0.0067
218.17	58.76	0.7289	0.118	0.0866	0.0665	0.7139	0.1459	0.0675	0.0727	0.9428	0.0409	0.0409	0.0123	0.9384	0.0492	0.0087	0.0037
208.19	50.77	0.7721	0.1075	0.0700	0.0504	0.7548	0.1291	0.0565	0.0595	0.9609	0.0303	0.0303	0.0071	0.9590	0.0343	0.0050	0.0018
233.16	69.36	0.6691	0.1265	0.1093	0.095	0.6541	0.1639	0.0847	0.0972	0.9132	0.0557	0.0557	0.0221	0.9031	0.0719	0.0164	0.0086

Table 4.14: R2 between calculated mole fraction based on SRK EoS and experimental results for. CH4+C2H6+C3H8+n-C4H10 mixture.

Experimental vs Computational								
	x <sub>1</sub>	x <sub>2</sub>	x <sub>3</sub>	x <sub>4</sub>	y <sub>1</sub>	y <sub>2</sub>	y <sub>3</sub>	y <sub>4</sub>
R <sup>2</sup>	0.95	0.99	0.98	0.98	0.99	0.91	0.94	0.91

Table 4.15: Calculated gaseous mole fraction for CH4+C2H6+C3H8+n-C4H10 mixture.

T[K]	P[bar]	Cal. P[bar]	Exp. liquid mole fraction				Exp. liquid mole fraction				Cal. gaseous mole fraction PR				Cal. gaseous mole fraction SRK			
			x <sub>1</sub>	x <sub>2</sub>	x <sub>3</sub>	x <sub>4</sub>	x <sub>1</sub>	x <sub>2</sub>	x <sub>3</sub>	x <sub>4</sub>	y <sub>1</sub>	y <sub>2</sub>	y <sub>3</sub>	y <sub>4</sub>	y <sub>1</sub>	y <sub>2</sub>	y <sub>3</sub>	y <sub>4</sub>
243.60	82.88	84.14	0.6916	0.1271	0.0794	0.1017	0.8938	0.0688	0.0222	0.0152	0.8743	0.0761	0.0280	0.0215	0.8773	0.0750	0.0271	0.0205
243.60	87.79	90.49	0.7559	0.1041	0.0611	0.0789	0.8783	0.0698	0.0275	0.0244	0.8550	0.0778	0.0341	0.0332	0.8587	0.0765	0.0330	0.0316
243.60	77.14	78.37	0.6327	0.1334	0.0962	0.1377	0.8932	0.0673	0.0231	0.0163	0.8903	0.0684	0.0241	0.0173	0.8927	0.0674	0.0233	0.0164
243.60	65.66	66.20	0.5312	0.1533	0.1264	0.1891	0.9012	0.0699	0.0205	0.0115	0.8995	0.0671	0.0210	0.0124	0.9015	0.0661	0.0204	0.0118
243.60	54.18	54.26	0.4358	0.1663	0.1554	0.2425	0.9024	0.0686	0.0196	0.0094	0.9009	0.0687	0.0201	0.0103	0.9028	0.0677	0.0195	0.0098
243.60	43.56	43.55	0.3495	0.1717	0.182	0.2968	0.8986	0.0723	0.0204	0.0086	0.8969	0.0725	0.0209	0.0097	0.8989	0.0715	0.0202	0.0092
243.60	34.11	34.04	0.2725	0.1701	0.206	0.3514	0.8908	0.0777	0.0225	0.0089	0.8886	0.0785	0.0230	0.0100	0.8908	0.0773	0.0223	0.0095
243.60	26.57	26.48	0.2101	0.1621	0.2241	0.4037	0.8801	0.0841	0.0256	0.0102	0.8767	0.0858	0.0264	0.0112	0.8792	0.0844	0.0256	0.0106
243.60	16.09	15.98	0.1230	0.138	0.2477	0.4912	0.8489	0.1002	0.0360	0.0149	0.8432	0.1040	0.0372	0.0156	0.8465	0.1024	0.0362	0.0148

## 5 Conclusion

To identify the characteristics of a batch or continuous process stream, monitor the process, and control the quality, sampling techniques are employed. The nature of sampled materials and operation conditions make a sampling technique the priority for a process. By selecting the most appropriate sampling technique and considering uncertainty and probability of human error within the sampling, a representative sample can be collected. Moreover, representative sampling is required if it is to make a reliable decision about the process. Among the investigated sampling techniques, the grab sampling technique has attracted more attention because of simplicity, though in the case of higher accuracy, other sampling techniques are preferred.

Knowing the interfacial properties and fluid phase equilibria are required to study the fluid behavior. In addition, thermodynamic models enable scientists to investigate the feasibility of an operation and process. However, finding an appropriate thermodynamic model and algorithm for computing the phase equilibria and interfacial properties is challenging. Although these days some commercial software has been developed to solve these difficulties, there are still some restrictions, including licenses fee, limitations in manipulating the defined process, and a lack of square gradient theory (SGT) for interfacial descriptions. Therefore, scientists have been provoked to apply alternative solutions like homemade programs.

Phasepy is a scientifically defined open-source package in python for computational thermodynamics. This package has been developed based on the most popular and reliable theories to calculate the interfacial properties and phase equilibria. The simplicity and accuracy of Phasepy enable studies to compare different EoS, mixing rules, etc.

This study tries to evaluate how much the developed methods based on Phasepy can predict the behavior of multicomponent mixtures. In this way, four binary mixtures and two four-components LNG mixtures are modeled. Then the developed models are validated based on the performed experimental results. The results depict that Phasepy could be a solution for thermodynamic modeling, if an appropriate EoS, mixing rule, and activity coefficient model were selected. In this study, PR and SRK as the EoS and QMR and MHV as the mixing rule are applied.

A model is also developed in this study based on the SRK EoS. The output of the developed model is compared with the experimental results of a study on Methane + n-pentane mixture, SAGE et al. [81]. The outputs are fitted with experimental results with **AARD = 0.54%** and **AMD = 0.031** (difference in mole fraction of Methane). Apart from SEK EoS, calculating the compressibility factor ( $Z$ ) is also modeled based on van der Waals EoS, RK EoS, and PR EoS.

## 5 Conclusion

Moreld Flux is in the process of manufacturing a system sampling of LNG. The vaporizer part of the system is modeled for calculating insulation requirement, heating requirement, pressure drop, and finally instrument performance. Therefore, some experiments should be performed to validate the developed model. In this regard, for accurate experiments, a sampling procedure is prepared based on the literature studies and the requirement of ISO 8943: 2007 (“Refrigerated light hydrocarbon fluids — Sampling of liquefied natural gas — Continuous and intermittent methods”), and BS EN ISO 12838-2001 (“Installations and equipment for liquefied natural gas- suitability testing of LNG sampling systems” (section 8)). To collect the required information, the vaporizer is to be equipped with 3 thermocouples and a Coriolis flow meter. Then, to measure the real-time temperatures and the flow rate LabVIEW programming is developed to sense the temperature using National Instrument modules, including NI 9207 and NI 9211.

The modeling outputs show that in the case of a 2 kg/h flow rate, the vaporizer can increase the temperature of the fluid to 250 K maximumly, while the temperature of the fluid should be higher before entering the Coriolis flow meter. Therefore, a post-heating part needs to be installed. In this way, by considering the performance and applicability of the helical coil heat exchanger, a model is developed to calculate the required length of the tube which is immersed into a water bath in a helically coiled shape. Tube dimensions, bath temperature, inlet temperature into post heater, and preferred outlet temperature are the variables of the model.

# References

- [1] Ø. Wilhelmsen *et al.*, “Thermodynamic Modeling with Equations of State: Present Challenges with Established Methods,” *Industrial and Engineering Chemistry Research*, vol. 56, no. 13. 2017. doi: 10.1021/acs.iecr.7b00317.
- [2] B. Jung *et al.*, “Prediction Model of LNG Weathering Using Net Mass and Heat Transfer,” *SSRN Electronic Journal*, 2021, doi: 10.2139/ssrn.3918139.
- [3] K. Shin, S. Son, J. Moon, Y. Jo, J. S.-I. Kwon, and S. Hwang, “Dynamic modeling and predictive control of boil-off gas generation during LNG loading,” *Computers & Chemical Engineering*, vol. 160, p. 107698, Apr. 2022, doi: 10.1016/j.compchemeng.2022.107698.
- [4] T. Dumas, “Environmental problem solving using gas and liquid chromatography,” *Pesticide Biochemistry and Physiology*, vol. 18, no. 2, 1982, doi: 10.1016/0048-3575(82)90115-8.
- [5] Lee Machemer, “Sampling of process streams,” Jan. 22, 2022. <https://www.processingmagazine.com/process-control-automation/article/21124299/sampling-of-process-streams> (accessed Feb. 05, 2022).
- [6] Seth Martin, Billy Terry, and Padraic O’Neil, “Closed Loop Sampling Systems,” *Safe-Reliable Sampling Made Easy for All Applications*, Feb. 03, 2022.
- [7] E. W. McAllister, *Pipeline Rules of Thumb Handbook*. 2005. doi: 10.1016/B978-0-7506-7852-0.X5000-X.
- [8] S. Deshmukh, R. Bandyopadhyay, N. Bhattacharyya, R. A. Pandey, and A. Jana, “Application of electronic nose for industrial odors and gaseous emissions measurement and monitoring - An overview,” *Talanta*, vol. 144. 2015. doi: 10.1016/j.talanta.2015.06.050.
- [9] M. B. Cristóvão, A. Bento-Silva, M. R. Bronze, J. G. Crespo, and V. J. Pereira, “Detection of anticancer drugs in wastewater effluents: Grab versus passive sampling,” *Science of the Total Environment*, vol. 786, 2021, doi: 10.1016/j.scitotenv.2021.147477.
- [10] M. Bernard *et al.*, “Combination of passive and grab sampling strategies improves the assessment of pesticide occurrence and contamination levels in a large-scale watershed,” *Science of the Total Environment*, vol. 651, 2019, doi: 10.1016/j.scitotenv.2018.09.202.
- [11] L. Gobelius, C. Persson, K. Wiberg, and L. Ahrens, “Calibration and application of passive sampling for per- and polyfluoroalkyl substances in a drinking water treatment plant,” *Journal of Hazardous Materials*, vol. 362, 2019, doi: 10.1016/j.jhazmat.2018.09.005.
- [12] S. L. Kaserzon *et al.*, “Development and calibration of a passive sampler for perfluorinated alkyl carboxylates and sulfonates in water,” *Environmental Science and Technology*, vol. 46, no. 9, 2012, doi: 10.1021/es300593a.

## References

- [13] A. Charriau, S. Lissalde, G. Poulhier, N. Mazzella, R. Buzier, and G. Guibaud, "Overview of the Chemcatcher® for the passive sampling of various pollutants in aquatic environments Part A: Principles, calibration, preparation and analysis of the sampler," *Talanta*, vol. 148, 2016. doi: 10.1016/j.talanta.2015.06.064.
- [14] J. K. Kingston, R. Greenwood, G. A. Mills, G. M. Morrison, and L. B. Persson, "Development of a novel passive sampling system for the time-averaged measurement of a range of organic pollutants in aquatic environments," *Journal of Environmental Monitoring*, vol. 2, no. 5, 2000, doi: 10.1039/b003532g.
- [15] C. Li *et al.*, "Diffusive gradients in thin films: devices, materials and applications," *Environmental Chemistry Letters*, vol. 17, no. 2, 2019. doi: 10.1007/s10311-018-00839-9.
- [16] W. Guo *et al.*, "In situ measurement of estrogenic activity in various aquatic systems using organic diffusive gradients in thin-film coupled with ERE-CALUX bioassay," *Environment International*, vol. 127, 2019, doi: 10.1016/j.envint.2019.03.027.
- [17] C. Berho *et al.*, "Estimating 42 pesticide sampling rates by POCIS and POCIS-MIP samplers for groundwater monitoring: a pilot-scale calibration," *Environmental Science and Pollution Research*, vol. 27, no. 15, 2020, doi: 10.1007/s11356-020-08385-0.
- [18] L. Wang, R. Liu, X. Liu, and H. Gao, "Sampling rate of polar organic chemical integrative sampler (POCIS): Influence factors and calibration methods," *Applied Sciences (Switzerland)*, vol. 10, no. 16, 2020. doi: 10.3390/app10165548.
- [19] K. Godlewska, P. Stepnowski, and M. Paszkiewicz, "Pollutant analysis using passive samplers: principles, sorbents, calibration and applications. A review," *Environmental Chemistry Letters*, vol. 19, no. 1, 2021. doi: 10.1007/s10311-020-01079-6.
- [20] K. Godlewska, P. Stepnowski, and M. Paszkiewicz, "Application of the Polar Organic Chemical Integrative Sampler for Isolation of Environmental Micropollutants—A Review," *Critical Reviews in Analytical Chemistry*, vol. 50, no. 1, 2020. doi: 10.1080/10408347.2019.1565983.
- [21] R. G. Ross, "Refrigeration systems for achieving cryogenic temperatures," in *Low Temperature Materials and Mechanisms*, 2016. doi: 10.1201/9781315371962.
- [22] B. A. Berven, P. T. Perdue, J. B. Kark, and M. O. Gibson, "Use of a cryogenic sampler to measure radioactive gas concentrations in the main off-gas system at a high-flux isotope reactor," United States, 1982. [Online]. Available: [http://inis.iaea.org/search/search.aspx?orig\\_q=RN:14729082](http://inis.iaea.org/search/search.aspx?orig_q=RN:14729082)
- [23] "Cryogenic gas sampler." Google Patents, Mar. 10, 1964.
- [24] J. P. Pellerin, "Cryogenic liquid sampler." Google Patents, Nov. 19, 2019.
- [25] M. Heidari, A. Bahrami, A. R. Ghiasvand, M. Rafiei Emam, F. G. Shahna, and A. R. Soltanian, "Graphene packed needle trap device as a novel field sampler for determination of perchloroethylene in the air of dry cleaning establishments," *Talanta*, vol. 131, 2015, doi: 10.1016/j.talanta.2014.07.043.
- [26] N. Heidari, A. Ghiasvand, and S. Abdolhosseini, "Amino-silica/graphene oxide nanocomposite coated cotton as an efficient sorbent for needle trap device," *Analytica Chimica Acta*, vol. 975, 2017, doi: 10.1016/j.aca.2017.04.031.

## References

- [27] P. Trefz, S. Kischkel, D. Hein, E. S. James, J. K. Schubert, and W. Miekisch, "Needle trap micro-extraction for VOC analysis: Effects of packing materials and desorption parameters," *Journal of Chromatography A*, vol. 1219, 2012, doi: 10.1016/j.chroma.2011.10.077.
- [28] A. Wang, F. Fang, and J. Pawliszyn, "Sampling and determination of volatile organic compounds with needle trap devices," in *Journal of Chromatography A*, 2005, vol. 1072, no. 1. doi: 10.1016/j.chroma.2004.12.064.
- [29] J. M. Warren and J. Pawliszyn, "Development and evaluation of needle trap device geometry and packing methods for automated and manual analysis," *Journal of Chromatography A*, vol. 1218, no. 50, 2011, doi: 10.1016/j.chroma.2011.10.017.
- [30] H. Li, C. Bi, X. Li, and Y. Xu, "A needle trap device method for sampling and analysis of semi-volatile organic compounds in air," *Chemosphere*, vol. 250, 2020, doi: 10.1016/j.chemosphere.2020.126284.
- [31] E. Schaller, S. Zenhäusern, T. Zesiger, J. O. Bosset, and F. Escher, "Use of preconcentration techniques applied to a MS-based 'electronic nose,'" *Analisis*, vol. 28, no. 8, 2000, doi: 10.1051/analisis:2000145.
- [32] J. L. Wang, S. W. Chen, and C. Chew, "Automated gas chromatography with cryogenic/sorbent trap for the measurement of volatile organic compounds in the atmosphere," *Journal of Chromatography A*, vol. 863, no. 2, 1999, doi: 10.1016/S0021-9673(99)00965-6.
- [33] W. R. Parrish, J. M. Arvidson, and J. F. LaBrecque, "Development and evaluation of an LNG sampling measurement system," National Bureau of Standards, Boulder, CO (USA). Thermophysical Properties Div., 1978.
- [34] C. Borgnakke and R. E. Sonntag, "Fundamentals of thermodynamics, 8th edition," *University of Michigan, Willey*. 2013.
- [35] J. M. Smith, H. C. van Ness, M. M. Abbot, and M. T. . Swihart, *Introduction to Chemical Engineering Thermodynamics Eight Edition*. 2018.
- [36] D. S. H. Wong and S. I. Sandler, "A theoretically correct mixing rule for cubic equations of state," *AIChE Journal*, vol. 38, no. 5. 1992. doi: 10.1002/aic.690380505.
- [37] J. O. Valderrama, "The state of the cubic equations of state," *Industrial and Engineering Chemistry Research*, vol. 42, no. 8. 2003. doi: 10.1021/ie020447b.
- [38] G. M. Wilson, "Vapor-Liquid Equilibrium. XI. A New Expression for the Excess Free Energy of Mixing," *J Am Chem Soc*, vol. 86, no. 2, 1964, doi: 10.1021/ja01056a002.
- [39] O. Redlich and J. N. S. Kwong, "On the thermodynamics of solutions. V. An equation of state. Fugacities of gaseous solutions," *Chemical Reviews*, vol. 44, no. 1, 1949, doi: 10.1021/cr60137a013.
- [40] H. E. Barner, R. L. Pigford, and W. C. Schreiner, "A Modified Redlich-Kwong Equation of State," 1966.
- [41] G. Soave, "Equilibrium constants from a modified Redlich-Kwong equation of state," *Chemical Engineering Science*, vol. 27, no. 6, 1972, doi: 10.1016/0009-2509(72)80096-4.

## References

- [42] E. Usdin and J. C. McAuliffe, "A one parameter family of equations of state," *Chemical Engineering Science*, vol. 31, no. 11, 1976, doi: 10.1016/0009-2509(76)87030-3.
- [43] G. S. Soave, "APPLICATION OF A CUBIC EQUATION OF STATE TO VAPOUR-LIQUID EQUILIBRIA OF SYSTEMS CONTAINING POLAR COMPOUNDS.," *Institution of Chemical Engineers Symposium Series*, vol. 1, no. 56, 1979.
- [44] G. Heyen, "CUBIC EQUATION OF STATE WITH EXTENDED RANGE OF APPLICATION.," 1983.
- [45] L. Raimondi, "A modified Redlich-Kwong equation of state for vapour-liquid equilibrium calculations," *Chemical Engineering Science*, vol. 35, no. 6, 1980, doi: 10.1016/0009-2509(80)85119-0.
- [46] T. Ishikawa, W. K. Chung, and B. C. -Y Lu, "A cubic perturbed, hard sphere equation of state for thermodynamic properties and vapor-liquid equilibrium calculations," *AIChE Journal*, vol. 26, no. 3, 1980, doi: 10.1002/aic.690260307.
- [47] P. M. Mathias, "A Versatile Phase Equilibrium Equation of State," *Industrial and Engineering Chemistry Process Design and Development*, vol. 22, no. 3, 1983, doi: 10.1021/i200022a008.
- [48] P. M. Mathias and T. W. Copeman, "Extension of the Peng-Robinson equation of state to complex mixtures: Evaluation of the various forms of the local composition concept," *Fluid Phase Equilibria*, vol. 13, no. C, 1983, doi: 10.1016/0378-3812(83)80084-3.
- [49] S. A. Newman, "Chemical engineering thermodynamics," Ann Arbor Science Publishers, Ann Arbor, MI, 1983.
- [50] Y. Adachi and B. C. -Y Lu, "Simplest equation of state for vapor-liquid equilibrium calculation: A modification of the van der waals equation," *AIChE Journal*, vol. 30, no. 6, 1984, doi: 10.1002/aic.690300619.
- [51] R. M. Gibbons and A. P. Laughton, "An equation of state for polar and non-polar substances and mixtures," *Journal of the Chemical Society, Faraday Transactions 2: Molecular and Chemical Physics*, vol. 80, no. 9, 1984, doi: 10.1039/F29848001019.
- [52] V. N. Kabadi and R. P. Danner, "A Modified Soave-Redlich-Kwong Equation of State for Water-Hydrocarbon Phase Equilibria," *Industrial and Engineering Chemistry Process Design and Development*, vol. 24, no. 3, 1985, doi: 10.1021/i200030a004.
- [53] R. Stryjek and J. H. Vera, "PRSV: An improved peng—Robinson equation of state for pure compounds and mixtures," *The Canadian Journal of Chemical Engineering*, vol. 64, no. 2, 1986, doi: 10.1002/cjce.5450640224.
- [54] Y. Adachi and H. Sugie, "A new mixing rule-modified conventional mixing rule," *Fluid Phase Equilibria*, vol. 28, no. 2, 1986, doi: 10.1016/0378-3812(86)85072-5.
- [55] Y. Du and T. M. Guo, "Prediction of hydrate formation for systems containing methanol," *Chemical Engineering Science*, vol. 45, no. 4, 1990, doi: 10.1016/0009-2509(90)85011-2.



## References

- [56] K. Nasrifar and M. Moshfeghian, "A new cubic equation of state for simple fluids: Pure and mixture," *Fluid Phase Equilibria*, vol. 190, no. 1–2, 2001, doi: 10.1016/S0378-3812(01)00592-1.
- [57] M. S. Graboski and T. E. Daubert, "A Modified Soave Equation of State for Phase Equilibrium Calculations. 1. Hydrocarbon Systems," *Industrial and Engineering Chemistry Process Design and Development*, vol. 17, no. 4, 1978, doi: 10.1021/i260068a009.
- [58] T. Arai and H. Nishiumi, "CORRELATION OF THE BINARY INTERACTION PARAMETER OF THE PENG-ROBINSON EQUATION OF STATE.," *Hosei Daigaku Kogakubu kenkyu shuho*, no. 23, 1987.
- [59] A. Benito, "Accurate determination of LNG quality unloaded in Receiving Terminals: An Innovative Approach," in *International Gas Union World Gas Conference Papers*, 2009, vol. 6.
- [60] A. Z. Panagiotopoulos and R. C. Reid, "NEW MIXING RULE FOR CUBIC EQUATIONS OF STATE FOR HIGHLY POLAR, ASYMMETRIC SYSTEMS.," 1986. doi: 10.1021/bk-1986-0300.ch028.
- [61] H. Orbey and S. I. Sandler, *Modelling Vapor-Liquid Equilibria. Cubic equation of state and their mixing rules*. 1998.
- [62] S. Mokhatab, W. A. Poe, and J. Y. Mak, *Handbook of natural gas transmission and processing: Principles and practices*. 2018. doi: 10.1016/C2017-0-03889-2.
- [63] A. Kenbar, "Assessment of LNG sampling systems and recommendations," 2013.
- [64] ISO 8943:2007, "Refrigerated light hydrocarbon fluids — Sampling of liquefied natural gas — Continuous and intermittent methods." International Organization for Standardization, 2007. Accessed: Mar. 01, 2022. [Online]. Available: <https://www.iso.org/standard/41508.html>
- [65] GIIGNL Technical Study Group, "LNG Custody Transfer Handbook," *Information Paper No. 1*, vol. 5, 2015.
- [66] Mark Jiskoot, "IsoFraction automatic LNG sampling and GC sample conditioning system," 2021. <https://www.sensiaglobal.com/Measurement/Sampling/JISKOOT-LPG-Sampling-Systems> (accessed Mar. 01, 2022).
- [67] ISO 10715, "Natural gas — Sampling guidelines." International Organization for Standardization, 1997. Accessed: Mar. 01, 2022. [Online]. Available: <https://www.iso.org/standard/18803.html>
- [68] "Chapter 14 - Natural gas fluids measurement, Section 1 - Collecting and handling of natural gas samples for custody transfer, fifth edition," *API MPMS - Manual of Petroleum Measurement Standards*, no. JUNE E. 2001.
- [69] D. G. Prabhanjan, T. J. Rennie, and G. S. V. Raghavan, "Natural convection heat transfer from helical coiled tubes," *International Journal of Thermal Sciences*, vol. 43, no. 4, 2004, doi: 10.1016/j.ijthermalsci.2003.08.005.
- [70] G. F. C. Rogers and Y. R. Mayhew, "Heat transfer and pressure loss in helically coiled tubes with turbulent flow," *International Journal of Heat and Mass Transfer*, vol. 7, no. 11, 1964, doi: 10.1016/0017-9310(64)90062-6.

## References

- [71] G. Chaparro and A. Mejía, “Phasepy: A Python based framework for fluid phase equilibria and interfacial properties computation,” *Journal of Computational Chemistry*, vol. 41, no. 29, 2020, doi: 10.1002/jcc.26405.
- [72] A. Mejía, E. A. Müller, and G. Chaparro Maldonado, “SGTPy: A Python Code for Calculating the Interfacial Properties of Fluids Based on the Square Gradient Theory Using the SAFT-VR Mie Equation of State,” *Journal of Chemical Information and Modeling*, vol. 61, no. 3, 2021, doi: 10.1021/acs.jcim.0c01324.
- [73] K. Knudsen, E. H. Stenby, and A. Fredenslund, “A comprehensive comparison of mixing rules for calculation of phase equilibria in complex systems,” *Fluid Phase Equilibria*, vol. 82, no. C, 1993, doi: 10.1016/0378-3812(93)87159-X.
- [74] S. Valiollahi, B. Kavianpour, S. Raeissi, and M. Moshfeghian, “A new Peng-Robinson modification to enhance dew point estimations of natural gases,” *Journal of Natural Gas Science and Engineering*, vol. 34, 2016, doi: 10.1016/j.jngse.2016.07.049.
- [75] M. P. Rolemberg and M. A. Krahenbuhl, “Vapor-liquid equilibria of binary and ternary mixtures of benzene, cyclohexane, and chlorobenzene at 40.0 kPa and 101.3 kPa,” *Journal of Chemical and Engineering Data*, vol. 46, no. 2, 2001, doi: 10.1021/je000059l.
- [76] J. Wisniak, “The Herington Test for Thermodynamic Consistency,” *Industrial and Engineering Chemistry Research*, vol. 33, no. 1, 1994, doi: 10.1021/ie00025a025.
- [77] H. Renon, “Vapor-liquid equilibria using UNIFAC. A group contribution method,” *Fluid Phase Equilibria*, vol. 1, no. 4, 1977, doi: 10.1016/0378-3812(77)80014-9.
- [78] P. L. Jackson and R. A. Wilsak, “Thermodynamic consistency tests based on the Gibbs-Duhem equation applied to isothermal, binary vapor-liquid equilibrium data: data evaluation and model testing,” *Fluid Phase Equilibria*, vol. 103, no. 2, 1995, doi: 10.1016/0378-3812(94)02581-K.
- [79] T. J. Hughes *et al.*, “High pressure multi-component vapor-liquid equilibrium data and model predictions for the LNG industry,” *Journal of Chemical Thermodynamics*, vol. 113, 2017, doi: 10.1016/j.jct.2017.05.023.
- [80] O. Kunz and W. Wagner, “The GERG-2008 wide-range equation of state for natural gases and other mixtures: An expansion of GERG-2004,” *Journal of Chemical and Engineering Data*, vol. 57, no. 11, 2012, doi: 10.1021/je300655b.
- [81] B. H. Sage and W. N. Lacey, “Phase Equilibria in Hydrocarbon Systems,” *Industrial and Engineering Chemistry*, vol. 28, no. 1, 1936, doi: 10.1021/ie50313a025.

# Appendices

## Appendix A: Phasepy Modelling

As an example the phase equilibrium of binary mixture of Cyclohexane(1) + Chlorobenzene(2)

```

7
8 from __future__ import division, print_function, absolute_import
9
10 import numpy as np
11 from phasepy import mixture, component, preos, prsveos
12 from phasepy import rkseos, rkeos
13 from phasepy.equilibrium import bubblePy, bubbleTy
14 from phasepy.equilibrium import dewPx, dewTx
15 import matplotlib.pyplot as plt
16
17
18 DATA = [[84.161, 553.5, 40.73, 309.0, 0.271, 0.212],
19          [112.558, 632.4, 45.2, 308., 0.265, 0.250]]
20
21
22 DATA = np.array(DATA)
23
24
25 Xexp = np.array([[0.000, 0.021, 0.060, 0.228, 0.277, 0.376, 0.457, 0.560,
26                  0.666, 0.780, 0.826, 0.919, 1.000],
27                 [1 - 0.000, 1 - 0.021, 1 - 0.060, 1 - 0.228, 1 - 0.277, 1 - 0.376, 1 - 0.457,
28                  1 - 0.560,
29                  1 - 0.666, 1 - 0.780, 1 - 0.826, 1 - 0.919, 0.000]])
30
31
32 Yexp = np.array([[0.000, 0.160, 0.351, 0.640, 0.690, 0.773, 0.826, 0.869,
33                  0.923, 0.944, 0.953, 0.979, 1.000],
34                 [1 - 0.000, 1 - 0.160, 1 - 0.351, 1 - 0.640, 1 - 0.690, 1 - 0.773, 1 - 0.826,
35                  1 - 0.869,
36                  1 - 0.923, 1 - 0.944, 1 - 0.953, 1 - 0.979, 0.000]])
37
38
39 Texp = np.array([373.45, 369.25, 362.45, 348.25, 344.95, 340.55, 337.25, 334.35, 330.35,
40                  328.70, 328.10, 326.65, 325.95])
41
42 Pexp = np.array([0.4, 0.4, 0.4, 0.4, 0.4, 0.4, 0.4, 0.4, 0.4, 0.4, 0.4, 0.4, 0.4])
43
44
45 datavle = (Xexp, Yexp, Texp, Pexp)
46
47
48 javad = [('Benzene'), ('CycLohexane')]
49
50 row = 0
51 phasepy_components = []
52
53 compositions = []
54 for i in range(len(Texp)):
55     compositions.append([])
56
57 for name in javad:
58     comp = component(name=name, Tc=DATA[row, 1], Pc=DATA[row, 2], Vc=DATA[row, 3],
59                     Zc=DATA[row, 4], w=DATA[row, 5], Mw=DATA[row, 0])
60
61     phasepy_components.append(comp)
62     if row == 1:
63         # Create th mixture as 2 components are done already
64         mix = mixture(phasepy_components[0], phasepy_components[1])
65     elif row > 1:
66         # Add to the existing mixture
67         mix.add_component(phasepy_components[-1])
68
69     row += 1
70
71
72 # KIJ interaction coefficients
73 # Methane, Nitrogen CO2 Ethane Propane Isobutane Butane Isopentane Pentane Hexane
74 KIJ = [[0.00000, 0.03895],
75         [0.03895, 0.00000]]
76
77 KIJ = np.array(KIJ)
78 mix.kij_cubic(KIJ)
79 eos_KIJ = rkseos(mix, mixrule='qmr')
80
81
82 A = np.array([[0, 469.54],
83               [-100.25, 0]])
84
85 mix.wilson(A)
86 eos_wilson = rkseos(mix, 'mhv1_wilson')
87
88 for i in range(len(Texp)):
89     for fraction in Xexp:
90         compositions[i].append(fraction[i])
91
92
93
94 from phasepy.fit import fit_kij
95
96 mixkij = mix.copy()
97 fit_kij((-0.18, -0.05), rkseos, mixkij, datavle)
98
99

```

```

100 Molar_density = np.zeros(len(Texp))
101 Z = np.zeros(len(Texp))
102 Sr = np.zeros(len(Texp))
103 Hr = np.zeros(len(Texp))
104 Cvr = np.zeros(len(Texp))
105 Cpr = np.zeros(len(Texp))
106
107
108 for i in range(len(Texp)):
109     T = Texp[i]
110     P = Pexp[i]
111     x = np.array(compositions[i])
112     # Molar_density[i] = 1e3*eos.density(x, T, P, 'V')
113     # Z[i] = eos.Zmix(x, T, P)[0]
114     # Sr[i] = eos.EntropyR(x, T, P, 'L')
115     # Hr[i] = eos.EnthalpyR(x, T, P, 'V')
116     # Cvr[i] = eos.CvR(x, T, P, 'V')
117     # Cpr[i] = eos.CpR(x, T, P, 'V')
118
119
120
121 Ykij = np.zeros_like(Yexp)
122 Tkij = np.zeros_like(Pexp)
123 Ywilson = np.zeros_like(Yexp)
124 Twilson = np.zeros_like(Pexp)
125
126 n = len(Pexp)
127
128 for i in range(n):
129     Ykij[:,i],Tkij[i] = bubbleTy(Yexp[:,i],Texp[i],Xexp[:,i],Pexp[i],eos_KIJ)
130     Ywilson[:,i],Twilson[i] = bubbleTy(Yexp[:,i],Texp[i],Xexp[:,i],Pexp[i],eos_wilson)
131
132
133 import matplotlib.pyplot as plt
134
135 plt.plot(Xexp[0], Texp, 'k.', mew = 3.0)
136 plt.plot(Xexp[0], Tkij, 'k-')
137 plt.plot(Xexp[0], Twilson, 'k--')
138 plt.legend(['Experimental', 'SRK-QMR', 'SRK-MHV_Wilson'], frameon=False)
139 plt.plot(Yexp[0], Texp, 'k.', mew = 3.0)
140 plt.plot(Ykij[0], Tkij, 'k-')
141 plt.plot(Ywilson[0], Twilson, 'k--')
142 plt.xlabel('x,y')
143 plt.ylabel('T/K')
144
145 DATA = [[84.161 , 553.5 , 40.73 , 308.0 , 0.273, 0.210],
146          [112.558, 632.4 , 45.2 , 308. , 0.265 , 0.250]]
147
148
149 DATA = np.array(DATA)
150
151
152 Xexp = np.array([[0.000, 0.105, 0.280, 0.375,0.458, 0.600, 0.694, 0.777,
153                 0.842, 0.953, 1.000],
154                 [ 1 - 0.000, 1 - 0.105, 1 - 0.280, 1 - 0.375, 1 - 0.458, 1 - 0.600,
155                 1 - 0.694, 1 - 0.777,
156                 1 - 0.842, 1 - 0.953, 0.000]])
157
158
159 Yexp = np.array([[0.000, 0.362, 0.638, 0.760, 0.810, 0.850, 0.892, 0.914,
160                 0.928, 0.940, 1.000],
161                 [ 1 - 0.000, 1 - 0.362, 1 - 0.638, 1 - 0.760, 1 - 0.810, 1 - 0.850,
162                 1 - 0.892, 1 - 0.914,
163                 1 - 0.928, 1 - 0.940, 0.000]])
164
165
166 Texp = np.array([404.75, 391.35, 378.75, 372.55, 369.60, 365.75, 362.35, 360.95,
167                 359.35, 356.05, 353.80])
168
169 Pexp = np.array([1.013, 1.013, 1.013,1.013,1.013,1.013,1.013,1.013,1.013,1.013,
170                 1.013])
171
172 datavle = (Xexp, Yexp, Texp, Pexp)
173
174 javad = [('Benzene'), ('Cyclohexane')]
175
176 row = 0
177 phasepy_components = []
178
179 compositions = []
180 for i in range(len(Texp)):
181     compositions.append([])
182
183 for name in javad:
184     comp = component(name=name, Tc=DATA[row, 1], Pc=DATA[row, 2], Vc=DATA[row, 3],
185                     Zc=DATA[row, 4], w=DATA[row, 5], Mw=DATA[row, 0])
186
187     phasepy_components.append(comp)
188     if row == 1:
189         # Create th mixture as 2 components are done already
190         mix = mixture(phasepy_components[0], phasepy_components[1])
191     elif row > 1:
192         # Add to the existing mixture
193         mix.add_component(phasepy_components[-1])
194
195     row += 1

```

```

196 |
197 | # KIJ interaction coefficients
198 | # Methane, Nitrogen CO2 Ethane Propane Isobutane Butane Isopentane Pentane Hexane
199 | KIJ = [[0.00000, 0.02095],
200 |        [0.02095, 0.00000]]
201 |
202 |
203 | KIJ = np.array(KIJ)
204 | mix.kij_cubic(KIJ)
205 | eos_KIJ = rkseos(mix, mixrule='qmr')
206 |
207 | A = np.array([[0, -60.114],
208 |              [245.36, 0]])
209 |
210 | mix.wilson(A)
211 | eos_wilson = rkseos(mix, 'mhv1_wilson')
212 |
213 | for i in range(len(Texp)):
214 |     for fraction in Xexp:
215 |         compositions[i].append(fraction[i])
216 |
217 |
218 |
219 | from phasepy.fit import fit_kij
220 |
221 | mixkij = mix.copy()
222 | fit_kij((-0.18, -0.05), rkseos, mixkij, datavle)
223 |
224 |
225 | Molar_density = np.zeros(len(Texp))
226 | Z = np.zeros(len(Texp))
227 | Sr = np.zeros(len(Texp))
228 | Hr = np.zeros(len(Texp))
229 | Cvr = np.zeros(len(Texp))
230 | Cpr = np.zeros(len(Texp))
231 |
232 |
233 | for i in range(len(Texp)):
234 |     T = Texp[i]
235 |     P = Pexp[i]
236 |     x = np.array(compositions[i])
237 |     # Molar_density[i] = 1e3*eos.density(x, T, P, 'V')
238 |     # Z[i] = eos.Zmix(x, T, P)[0]
239 |     # Sr[i] = eos.EntropyR(x, T, P, 'L')
240 |     # Hr[i] = eos.EnthalpyR(x, T, P, 'V')
241 |     # Cvr[i] = eos.CVR(x, T, P, 'V')
242 |     # Cpr[i] = eos.CpR(x, T, P, 'V')
243 |
244 |
245 |
246 |
247 | Ykij = np.zeros_like(Yexp)
248 | Tkiij = np.zeros_like(Pexp)
249 | Ywilson = np.zeros_like(Yexp)
250 | Twilson = np.zeros_like(Pexp)
251 |
252 | n = len(Pexp)
253 |
254 | for i in range(n):
255 |     Ykij[:,i],Tkiij[i] = bubbleTy(Yexp[:,i],Texp[i],Xexp[:,i],Pexp[i],eos_KIJ)
256 |     Ywilson[:,i],Twilson[i] = bubbleTy(Yexp[:,i],Texp[i],Xexp[:,i],Pexp[i],eos_wilson)
257 |
258 |
259 | import matplotlib.pyplot as plt
260 | plt.plot(Xexp[0], Texp, 'k.', mew = 3.0)
261 | plt.plot(Xexp[0], Tkiij, 'k-')
262 | plt.plot(Xexp[0], Twilson, 'k--')
263 | plt.legend( ['Experimental', 'SRK-QMR', 'SRK-MHV_Wilson'], frameon=False)
264 | plt.plot(Yexp[0], Texp, 'k.', mew = 3.0)
265 | plt.plot( Ykij[0], Tkiij, 'k-')
266 | plt.plot(Ywilson[0], Twilson, 'k--')
267 | plt.xlabel('X,Y')
268 | plt.ylabel('T/K')
269 | plt.grid('on')
270 | plt.text(0.30, 380, 'P = 101.3 kPa', fontsize = 10,
271 |         )
272 | plt.text(0.35, 350, 'P = 40 kPa', fontsize = 10,
273 |         )
274 | plt.title('Cyclohexane + Chlorobenzene \n P = 101.3 kPa, 40 kPa')
275 | plt.savefig(r'C:\Users\marym\Desktop\master thesis\thermodynamic article\3rd\Results\CH+CB+40+10')
276 |

```

## Appendix B: Post heating code scripts

Developed model for calculating the required tube length in post heating facility.

```

6  """
7  import numpy as np
8
9  from scipy.optimize import fsolve
10
11 #pipe dimention
12 r_in = 0.00635/2
13 A_in = np.pi*r_in**2
14 r_out = 0.00639/2
15 A_out = np.pi*r_out**2
16 t= r_out - r_in
17 R = 0.1
18 D = 0.00635
19 k_tube = 45
20
21 #bath config
22 alpha = 0.162*10**-6
23 beta = 210*10**-6
24 nu = 3.862*10**-7
25 g = 9.81
26 k_w = 0.598
27
28 #N2 properties
29 c_p_N2 = 1.04 * 10**3
30 ru_N2 = 1.237
31 u = 8.59
32 ru = ru_N2
33 k= 23.76 * 10**-3
34 mu = 16.48 * 10**-6
35 cp = c_p_N2
36 m_dot = ru_N2 * u * A_in
37
38 T_in = 170
39 T_bath = 340
40 T_out = 280
41
42 q = m_dot*cp*(T_out - T_in)
43
44 #inside properties
45 Pr = cp*mu/k
46 Re = ru*u*D/mu
47 Nu_i = 0.021 * Re**0.85 * Pr**0.4 * (r_in/R)**0.1
48 h_i = Nu_i*k/D
49
50 h_o = 10000
51
52 def L(L):
53
54     return m_dot*cp*(T_out - T_in) - 2*np.pi*k_tube*L*np.log(r_out/r_in)*(
55         (T_bath - m_dot*cp*(T_out - T_in)/(h_o*2*np.pi*r_out*L))-(m_dot*cp*(T_o
56             (h_i*2*np.pi*
57
58 repeat = True
59 while repeat:
60
61     Length = fsolve(L, 1)
62     dT_w = q*np.log((D+2*t)/D)/(2*np.pi*45*Length)
63     coil_height = Length/(np.pi*R)*2*1.5*r_out
64     n_L = 2*np.pi*R*coil_height/Length
65     T_w = T_bath - m_dot*cp*(T_out - T_in)/(h_o*2*np.pi*r_out*Length)
66     Ra = g * beta * (T_bath - T_w - dT_w)*n_L**3/(nu * alpha)
67     Nu_o = 2.0487*Ra**0.1768
68     h_o_star = Nu_o*k_w/(D+2*t)
69
70
71     if abs(h_o_star - h_o) < 0.1:
72         h_o = h_o_star
73         repeat = False
74     else:
75         h_o = h_o_star
76         print('no')
77
78 print(Length)
79

```

## Appendix C: SRK EoS

Calculating bubble point of a binary mixture using SRK or PR as the EoS and QMR

```

7
8 import numpy as np
9 import matplotlib.pyplot as plt
10
11
12 T = 310.93 #K
13 R = 83.14
14
15 Pc = [45.99, 37.96] #bar
16 Tc = [190.6, 425.1] #k
17
18 omega = [0.012, 0.200]
19
20
21
22 def EoS(x,T,y,P, Tc, Pc, omega):
23
24     import numpy as np
25     from scipy.optimize import fsolve
26
27     Pr = np.zeros(len(Pc))
28     Tr = np.zeros(len(Pc))
29     for i in range(len(Tc)):
30         # Pr[i] = P/Pc[i]
31         Tr[i] = T/Tc[i]
32
33     #SRK
34     Sai = 0.42748
35     alpha_Tr = np.zeros(len(Tc))
36     for i in range(len(Tc)):
37         alpha_Tr[i] = (1+(0.480 + 1.574*omega[i] - 0.176*omega[i]**2)*(1-Tr[i])**0
38     OMEGA = 0.08664
39     sigma = 1
40     epsilon = 0
41
42
43
44     # PR
45     # Sai = 0.45724
46     # alpha_Tr = np.zeros(len(Tc))
47     # for i in range(len(Tc)):
48     #     alpha_Tr[i] = (1+(0.37464 + 1.54226*omega[i] - 0.26992*omega[i]**2)*(1-
49     # OMEGA = 0.07780
50     # sigma = 1 + 2**-.5
51     # epsilon = 1 - 2**-.5
52
53
54
55
56     a_i = np.zeros(len(Tc))
57     for i in range(len(Tc)):
58         a_i[i] = alpha_Tr[i]*Sai**2*Tc[i]**2/Pc[i]
59
60     b_i = np.zeros(len(Tc))
61     for i in range(len(Tc)):
62         b_i[i] = OMEGA*R*Tc[i]/Pc[i]
63
64
65     aij = np.zeros([len(y), len(y)])
66     for i in range(len(a_i)):
67         for j in range(len(a_i)):
68             aij[i,j] = (a_i[i]*a_i[j])**0.5
69
70
71     b = 0
72     for i in range(len(x)):
73         b = b + x[i]*b_i[i]
74
75     beta = b*P/R/T
76
77     a = 0
78     for i in range(len(x)):
79         for j in range(len(x)):
80             a = x[i]*x[j]*aij[i,j] + a
81
82     q = a/(b*R*T)
83
84
85
86     def Z_1(z):
87         return z - (beta + (z + epsilon*beta)*(z + sigma*beta)*((1+beta-z)/(q*bet
88
89     initial_guess = beta
90     Z_1 = fsolve(Z_1, initial_guess)
91
92     I_1 = 1/(sigma - epsilon)*np.log((Z_1 + sigma*beta)/(Z_1 + epsilon*beta))
93
94
95     q_bar = np.zeros(len(x))
96     Phi_1 = np.zeros(len(x))
97
98     for i in range(len(x)):
99         c = 0
100         for j in range(len(x)):
101             c = 2*x[j]*aij[i,j] + c
102         q_bar[i] = q*(c/a - b_i[i]/b)

```



```

103     Phi_l[i] = np.exp(b_i[i]/b *(Z_l - 1) - np.log(Z_l - beta) - q_bar[i]*I_l
104
105
106
107
108
109     b = 0
110     for i in range(len(y)):
111         b = b + y[i]*b_i[i]
112
113     beta = b*R/R/T
114
115     a = 0
116     for i in range(len(y)):
117         for j in range(len(y)):
118             a = y[i]*y[j]*aij[i,j] + a
119
120     q = a/(b*R*T)
121
122
123
124     def Z_v(z):
125         return z - (1 + beta -q*beta*((z-beta)/((z+epsilon*beta)*(z + sigma*beta)
126
127     initial_guess = 1
128     Z_v = fsolve(Z_v, initial_guess)
129
130     I_v = 1/(sigma - epsilon)*np.log((Z_v + sigma*beta)/(Z_v + epsilon*beta))
131
132
133     q_bar = np.zeros(len(y))
134     Phi_v = np.zeros(len(y))
135
136     for i in range(len(y)):
137         c = 0
138         for j in range(len(y)):
139             c = 2*y[j]*aij[i,j] + c
140         q_bar[i] = q*(c/a - b_i[i]/b)
141         Phi_v[i] = np.exp(b_i[i]/b *(Z_v - 1) - np.log(Z_v - beta) - q_bar[i]*I_v
142
143     K = Phi_l/Phi_v
144
145
146     return K
147
148     T = 310.93     #K
149     R = 83.14
150
151     Pc = [45.99, 37.96] #bar
152     Tc = [190.6, 425.1] #k
153
154     omega = [0.012, 0.200] #eccentric factor
155
156     Pexp = np.array([51.62, 60, 80, 100, 150, 200, 300, 400, 500, 600, 800,
157                    1000, 1200, 1250, 1400, 1500, 1600, 1700, 1750, 1800, 1850,
158                    1900, 1912])
159
160     Pexp = Pexp/14.504
161
162     X = np.array([0, 0.0008, 0.0029, 0.0049, 0.0100, 0.0152, 0.0257, 0.0368, 0.0484,
163                0.0604, 0.0859, 0.1136, 0.1452, 0.1540, 0.1821, 0.2030, 0.2279,
164                0.2589, 0.2790, 0.3024, 0.3325, 0.3954, 0.4195])
165
166     B = np.zeros(len(X))
167     for i in range(len(X)):
168         B[i] = 3.625*X[i]/(2.625*X[i] + 1)
169
170
171     Xexp = np.zeros([len(X), 2])
172     for i in range(len(X)):
173         Xexp[i,0] = B[i]
174         Xexp[i,1] = 1 - B[i]
175
176     Y = np.array([0, 0.0408, 0.1230, 0.1901, 0.3128, 0.3948, 0.4985, 0.5636, 0.6050,
177                0.6335, 0.6640, 0.6712, 0.66, 0.6664, 0.6550, 0.6418, 0.6232,
178                0.5990, 0.5825, 0.5616, 0.5330, 0.4815, 0.4195])
179
180     B = np.zeros(len(X))
181     for i in range(len(X)):
182         B[i] = 3.625*Y[i]/(2.625*Y[i] + 1)
183
184     Yexp = np.zeros([len(X), 2])
185     for i in range(len(X)):
186         Yexp[i,0] = B[i]
187         Yexp[i,1] = 1 - B[i]
188
189     ww = np.copy(Yexp)
190
191     Ycal = np.zeros([len(X), len(Tc)])
192     Pcal = np.zeros(len(X))
193
194     K = np.zeros([len(X), len(Tc)])
195
196     for t in range(len(Yexp)):
197

```

```

198 P = Pexp[t]
199 y = Yexp[t]
200 x = Xexp[t]
201
202 K[t] = EoS(x,T,y,P, Tc, Pc, omega)
203 i = 0
204 while i < 10:
205     if K[t,0]*x[0] + K[t,1]*x[1] != 1:
206         e = K[t,0]*x[0]/(K[t,0]*x[0] + K[t,1] * x[1])
207         y = [e, 1-e]
208         K[t] = EoS(x,T,y,P, Tc, Pc, omega)
209         Ycal[t] = y
210         Pcal[t] = P
211
212     i = i + 1
213
214 for z in range(len(Yexp)):
215     P = Pexp[z]
216     y = Yexp[z]
217     x = Xexp[z]
218     j = 0
219     while j < 10:
220
221         if K[z,0]*x[0] + K[z,1]*x[1] > 1:
222             P = P + 0.1336*P
223             # e = K[z,0]*x[0]/(K[z,0]*x[0] + K[z,1] * x[1])
224             # y = [e, 1-e]
225             K[z] = EoS(x,T,y,P, Tc, Pc, omega)
226             # Ycal[z] = y
227             Pcal[z] = P
228         elif K[z,0]*x[0] + K[z,1]*x[1] < 1:
229             P = P - 0.156*P
230             # e = K[z,0]*x[0]/(K[z,0]*x[0] + K[z,1] * x[1])
231             # y = [e, 1-e]
232             K[z] = EoS(x,T,y,P, Tc, Pc, omega)
233             # Ycal[z] = y
234             Pcal[z] = P
235         j = j + 1
236
237
238 plt.plot(Yexp[:,0], Pexp, 'ko')
239 plt.plot(Ycal[:,0], Pcal, 'k--')
240 plt.legend(['Experimental', 'SRK EoS'])
241 plt.plot(Xexp[:,0], Pexp, 'k-.o')
242 plt.xlabel('x1,y1')
243 plt.ylabel('P/bar')
244 plt.grid('on')
245 plt.xlabel('x1, y1')
246 plt.ylabel('P/bar')
247 plt.title('Methane(1)/n-butane(2) T = 311 K')
248 plt.savefig(r'C:\Users\marym\Desktop\master thesis\thermodynamic article\CH4+n-C4

```

## Appendix D: Project Description



Faculty of Technology, Natural Sciences and Maritime Sciences, Campus Porsgrunn

## FMH606 Master's Thesis

**Title:** Performance evaluation of an LNG analyser by mathematical modelling and experiments in a pilot rig.

**USN supervisor:** Sumudu Karunaratne (main supervisor) and Knut Vågsæther (co-supervisor)

**External partner:** Moreld Flux

### Task background:

Analytic is in the process of designing a standardised instrumentation system for sampling and analysis of liquified natural gas (LNG). The instrument consists of a sampling probe and an LNG vaporizer. LNG samples are collected through the sampling prob from LNG main header. Then the sample is sent into the vaporizer to produce an LNG vapour before sending it into the GC for further analysis. The critical design aspects that affect the instrument performance are the insulation requirement for the LNG sampling section, pressure drop and the heating requirement of the LNG vaporizer.

### Task description:

- Literature study of different sampling techniques from process streams.
- Evaluate different EOS (Equations of states) for the bubble point temperature calculation. (Aspen HYSYS can be used as a tool).
- Perform experiments in a pilot-rig and compare the results with simulations.

**Student category:** PT and EET students.

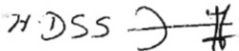
**Is the task suitable for online students (not present at the campus)?** :No

**Practical arrangements:** -

### Supervision:

As a general rule, the student is entitled to 15-20 hours of supervision. This includes necessary time for the supervisor to prepare for supervision meetings (reading material to be discussed, etc).

### Signatures:

Supervisor (date and signature):  16/05/2022

Student (write clearly in all capitalized letters): JAVAD TAVAKOLIFARADONBE

Student (date and signature):

  
16,05, 2022